DECELLULARIZED PRECISION CUT LUNG SLICES AS A MODEL TO STUDY IN VITRO LUNG REGENERATION

Inauguraldissertation

zur Erlangung des Grades eines Doktors der Medizin

des Fachbereichs Medizin

der Justus-Liebig-Universität Gießen

vorgelegt von Yannik Dittmer,
aus Speyer

Gießen, 2022

Aus dem Fachbereich Medizin der Justus-Liebig-Universität Gießen

Arbeitsgruppe Lungenfibrose

Gutachter: Prof. Dr. Andreas Günther

Gutachter/in: Prof. Dr. Savai

Prüfungsvorsitz: Prof. Dr. Huttner

Prüfungsmitglied: Prof. Dr. Wudy

Tag der Disputation: 11.10.2022

Table of Contents

1. Introduction

Each day, the human lung is flooded by up to 12.000 liters of air and circulated by the entire cardiac output - as much as 6000 liters of blood daily [18]. To meet the continuous demand for oxygen of the human body, the lung is highly optimized for performing its crucial task of gas exchange. It is built in the form of a dichotomous tree, with each airway branching into two daughter branches during development, for an average of 23 generations [31]. They are divided into conducting airways (generations 0-15) and acinar airways (generations 16-23), which end in alveolar sacs where the gas exchange happens [65]. This results in an average surface area of about 130 m², the largest surface area of any organ in the human body [44][86]. In order to reliably deliver oxygen into the bloodstream, despite being continuously exposed to outside stressors, more than 40 different cell types work together to ensure sufficient gas exchange [88].

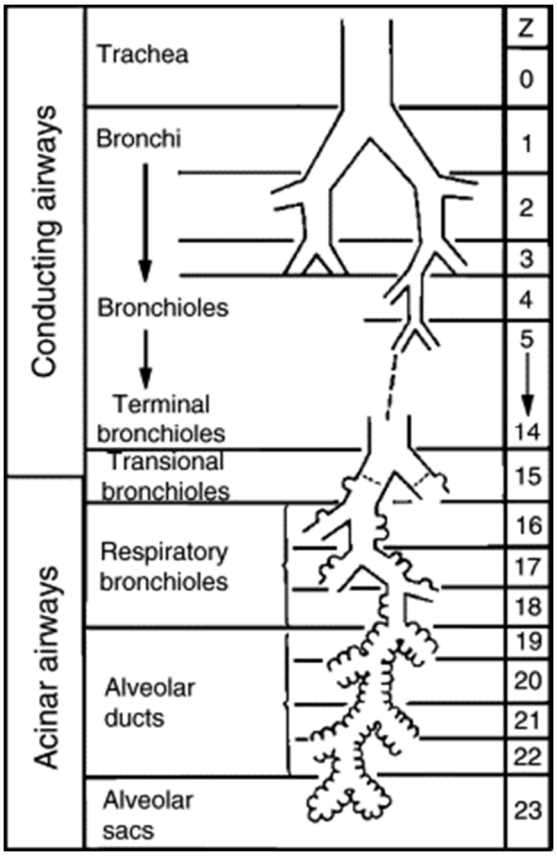

Figure 1. Model of the human airway system assigned to generations of symmetric branching from trachea (generation 0) to acinar airways (generations 15–23), ending in alveolar sacs. Modified after Weibel (1963) [31].

1.1. The alveolar compartment

The alveolar region (lung parenchyma) accounts for approximately 90% of the lungs total volume [65]. It contains both the alveolar structure, consisting of countless, air-filled alveoli separated by thin septa, and a dense capillary network. The most recent estimates put the number of individual alveoli in the lung at about 400 million [128]. It is designed to meet the functional requirements of continuous gas exchange: An intricate connective tissue-framework alongside the surfactant system provides a huge surface area, whilst keeping the diffusion barrier exceedingly thin at about 2µm [44]. Additionally, it provides functional reserves able to be rapidly recruited during increased demand and also possesses a variety of adaptive mechanisms, designed to ensure compensation for sudden loss of capacity brought on by disease or external insult [18, 65].

1.1.1. Morphology/histology of the alveolar compartment

The tissue forming the blood-air-barrier is made from two different, continuous cell layers. There is an endothelium facing the capillary lumen and a layer of epithelial cells facing the alveolar lumen. They are given structural stability and flexibility by an extremely thin layer of extracellular matrix deposited in the interstitial space located in between them [108]. The epithelium itself consists mainly of two types of epithelial cells arranged in an interspersed mosaic. The vast majority of the lungs surface (>95%), and therefore the blood-gas-barrier, is covered by alveolar epithelial cells type I (AECI) [203]. AECI are highly specialized, extremely thin, squamous cells meant to facilitate passive gas diffusion. They also take part in keeping the fluid balance in the lung and its innate immune response [155]. An individual AECI may take part in the covering of the surface of several alveoli. AECI are thought to be derived from alveolar epithelial cells type II (AECII) by differentiation [195]. Recent research suggests that AECI may retain some plasticity after differentiation, and may even be able to convert back into AECII under specific circumstances [74, 203].

The AECII is a cuboidal cell, often found in “corners” of the alveolar space and is responsible for keeping the homeostasis of the lung. It is about twice as numerous as AECI in the alveolar space, yet only covers a fraction of the surface covered by AECI [25]. The functions performed by AECII include stabilization of the airway epithelial barrier, production of surfactant, immune defense, and response to airway injury and regeneration [171]. Therefore, they possess an abundance of mitochondria and ribosomes,

and have an extensive endoplasmatic reticulum and Golgi apparatus [25]. Additionally they serve as a stem-cell reservoir and are able to proliferate and subsequently differentiate in response to injury or growth factor release [11, 59].

The interstitial space, located between the alveolar epithelium and the capillary endothelium, contains a network of intertwined collagen fibers and elastic fibers, alongside a heterogenous population of fibroblasts [167]. One subpopulation of fibroblasts produces and maintains extracellular matrix (ECM) and confers structural support. Myofibroblasts possess contractile properties, whereas lipofibroblasts support and nourish AECIIs. Together they provide an intricate network of connective tissue which supports the capillary net, the alveolar epithelium and maintain the structural integrity of the lung [78, 108]. The extracellular matrix composition is also thought to be a modulator of cellular behavior: Depending on matrix composition and content of key matrix proteins, such as laminin, fibronectin and collagen, the ECM may induce AECII transdifferentiation and fibroblast recruitment and activation [70]. Another important function of the ECM is to store and control the release of various growth factors, like TGF-ß. [120]

Against the backdrop of the continuous exposure of the alveolar space to pathogens, allergens and pollutants, the alveolar macrophages play a crucial role in sustaining homeostasis [102]. They fight off microbial invasions, clear up cell debris, and surfactant by phagocytosis, and modulate AECII function through growth factors and chemokines [102].

1.1.2. Alveolar physiology: Gas exchange and the surfactant system

Surfactant, or surface active agent, is a lipoprotein complex consisting of mainly phospholipids (80%), neutral lipids (10%) and surfactant proteins (10%), which lines the alveolar compartment [121]. Due to its amphiphilic properties, it highly reduces surface tension at the air/liquid interface and thereby prevents alveolar collapse at the end of expiration. The hydrophobic surfactant proteins B and C (SP-B, SP-C) fulfill integral functions related to alveolar stability, promotion of lipid adsorption in the air/liquid interface and stabilization of the monolayer lipid film, as well as the binding and fusion of membranes [14, 187]. Additionally, surfactant protein A (SP-A) and surfactant protein D (SP-D), play an important role in the innate host defense of the lung, both by opsonizing pathogens and modulating the immune response, as well as by direct anti-microbial

effects. [109, 199–201]. Pulmonary surfactant is mainly synthesized and assembled in AECII, where it is stored in lamellar bodies (LB) and secreted into the alveolus. At the same time, these highly specialized, lysosomal-related organelles represent the main place of surfactant protein B and C processing. Secretion of surfactant may be regulated by both chemotactic and mechanical signals. [32, 113]. There is a constant turnover in the surfactant metabolism, with degraded, protein-poor surfactant aggregates being removed from the air space by macrophages and AECII. Both the protein and lipid parts are largely recycled and re-secreted by AECII [121, 132].

Gas exchange is the core function necessary to maintain life. After a historic debate about the oxygen uptake mechanism, passive diffusion was shown to solely account for gas exchange in the human lung [65, 108]. Thus, net oxygen uptake is determined by three main factors. The permeability of the blood-air-barrier, which is mainly dictated by the distance between the two compartments participating in the diffusion process [154]; the rate of capillary blood flow, providing means of convective gas transfer into the circulation, and finally the difference in the O2 partial pressure between the alveolar space and the bloodstream as the driving force of gas diffusion [65, 154]. The discharge of CO2 follows the same principles in reversed order.

1.1.3. Lung regeneration: Injury and repair in the alveolar compartment and the regenerative capacity of lung epithelial cells and the stem cell compartment

During its early fetal development, the lung draws from both endodermal and mesodermal cell lineages, which are engaging in highly precise crosstalk to establish the exceedingly complex structure of the lung, combining more than 40 different cell types [15, 19]. Growth and maturation of the respiratory tract continue until the arrest of body growth, therefore establishing a linear correlation between lung size and body mass [19]. Based on the very slow rate of tissue turnover at steady state, compared to continuously renewing organs such as skin or gut, the lung was historically thought to possess only limited regenerative capacity [51]. However, the lung possesses the ability to respond robustly to injury or insult and quickly replace damaged or deceased cells. This capability is thought to be provided by the presence of several populations of resident progenitor cells [92, 97].

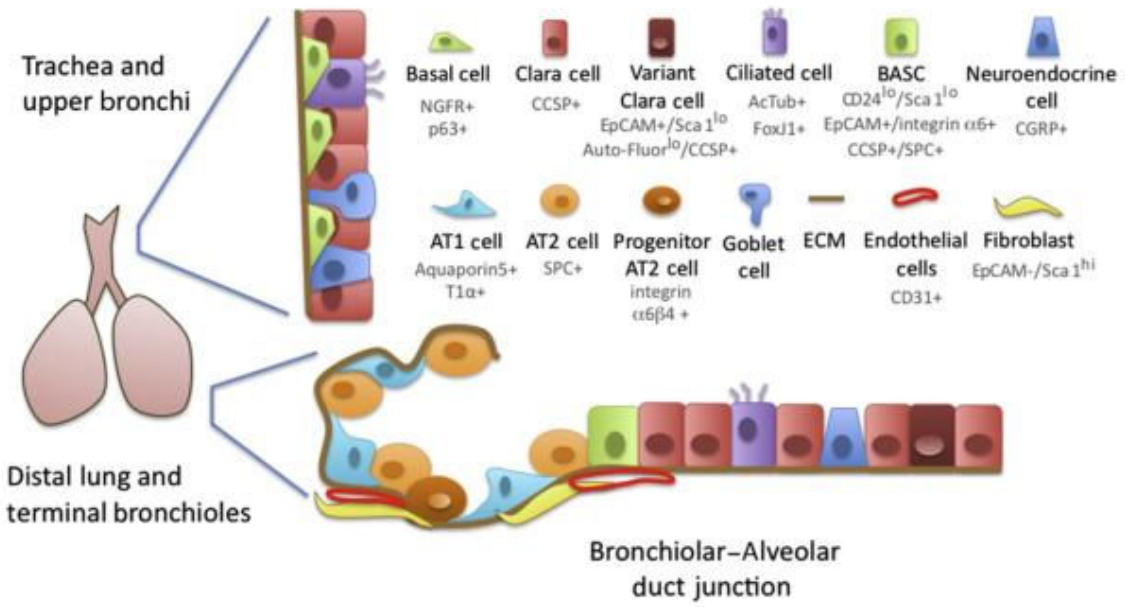

Figure 2: Overview for various types of cells found in the lung and their location inside the proximal and distal airways. Position in the epithelium and shape are indicated. Potential surface markers for identification of cells in an experimental setting are provided as subtext. Adapted from [97]

Recent advances in the definition of regionally distinct cell subpopulations have enabled the discrete examination of different stem cell pools [179]. This has led to the identification of several cell populations with stem cell capacity, including basal cells (BC) and Clara cells (secretory club cells) in the airways and AECII and lineage negative cells (LNEPs) in the alveoli [1].

Lineage tracing studies of AECII showed that they are able to function as stem cells, capable of continuous self-renewal, proliferation and differentiation into AECI [11, 30]. During regular homeostasis, most AECII are quiescent and display only minimal proliferative activity. If alveolar injury occurs, they respond by proliferation and differentiation into AECI in an attempt to recover alveolar structure and function [11, 208]. If faced with distinct AECII injury and depletion, remaining AECII may undergo rapid clonal expansion and daughter cell dispersal [11]. *In vivo,* multifocal clonal AECII expansion has been shown to be stimulated by oncogenic KRAS [30]. Additionally, AECII proliferation and clonal expansion may be induced *in vitro* by purified EGFR ligands, including TGF-alpha, heparin-binding EGF and NRG1, suggesting an EGFR-KRAS dependent pathway [30]. As a critical pathway for self-renewal and specification of stem cells, Wnt-signaling is present in multiple organs, including the lung. Here, it is not only necessary for successful lung development and alveologenesis, but also plays a

vital role in the injury response by stimulating a AECII subset ($AECII^{Axin2}$) capable of self-renewal and rapid clonal expansion [42, 205].

Another important pathway implicated in the regeneration of the airway epithelium is Notch-signaling. Besides being integral in the regulation of airway branching and lung development [117], Notch-signaling is believed to play a role in a multitude of cell functions in the adult lung, functioning as a balancing agent between cell proliferation and apoptosis, consequently deciding cell fate following injury [152, 191]. It has been implicated as a deciding factor in basal and club cell fate, myofibroblast differentiation and EMT. It is also known to regulate the proliferation and maturation of AECII [55, 182].

Despite these advances in the understanding of the multifarious pathways involved in repair in the alveolar compartment, extensive additional research is required to further elucidate these complex interactions.

1.2. Idiopathic pulmonary fibrosis (IPF) in the context of interstitial lung diseases (ILD)

Interstitial lung disease is an umbrella term for a diverse group of diseases affecting the interstitium of the lung, including the alveolo-capillary membranes [12]. They are characterized by inflammatory and fibrotic changes in the interstitium, which can lead to continuous loss of function of the lung [181]. There are both acute and chronic forms which may occur either idiopathic or secondary to chronic or acute exposure to a variety of injurious factors. Known triggers of disease can be inhalative noxes (cigarette smoke, organic and anorganic gases, or dusts) or non-inhalative noxae such as drugs or ionizing radiation. Further known causes include hypersensitivity pneumonitis, metabolic storage diseases and autoimmune connective tissue diseases including vasculitis, collagenosis and sarcoidosis [12], as well as circulatory causes such as chronic congestive heart failure. Despite this, idiopathic interstitial pneumonias (IIPs) account for the majority of cases and have no exact known cause, although a variety of mechanisms have been proposed. [170]. In this subgroup, IPF is the most prevalent and relevant disease, accounting for 55-65% of the IIP cases . [192][68] IPF is an irreversible and progressive lung disease of the elderly, with a median age at diagnosis of 66 years and an estimated survival of 3-5 years after diagnosis [181]. Disease progression routinely leads to pervasive dry cough,

respiratory failure and hypoxia [41]. There is no curative treatment for IPF with the exception of lung transplantation, a procedure only a minority of around 5% of patients are eligible for [94].

1.2.1. Classification of interstitial lung diseases

Chronic fibrotic lung diseases are a group of rare, irreversible conditions affecting the alveolar, interstitial and vascular compartment of the lung with a highly diverse etiologic background. They are uniformly characterized by a terminal process of fibroproliferative destruction of the alveolar compartment, leading to a progressive loss of compliance and impairment of gas exchange, ultimately resulting in loss of everyday capabilities and decreased quality of life in these patients [28].

The diverse etiology is reflected in the classification of interstitial lung diseases. They are usually categorized into five main groups [181]:

- Exposure related ILD of known origin
- Idiopathic interstitial pneumonia (IIPs)
- Connective tissue disease related ILD
- Granulomatose ILDs (Sarcoidosis, Exogenous Allergic Alveolitis, etc.)
- Other ILDs

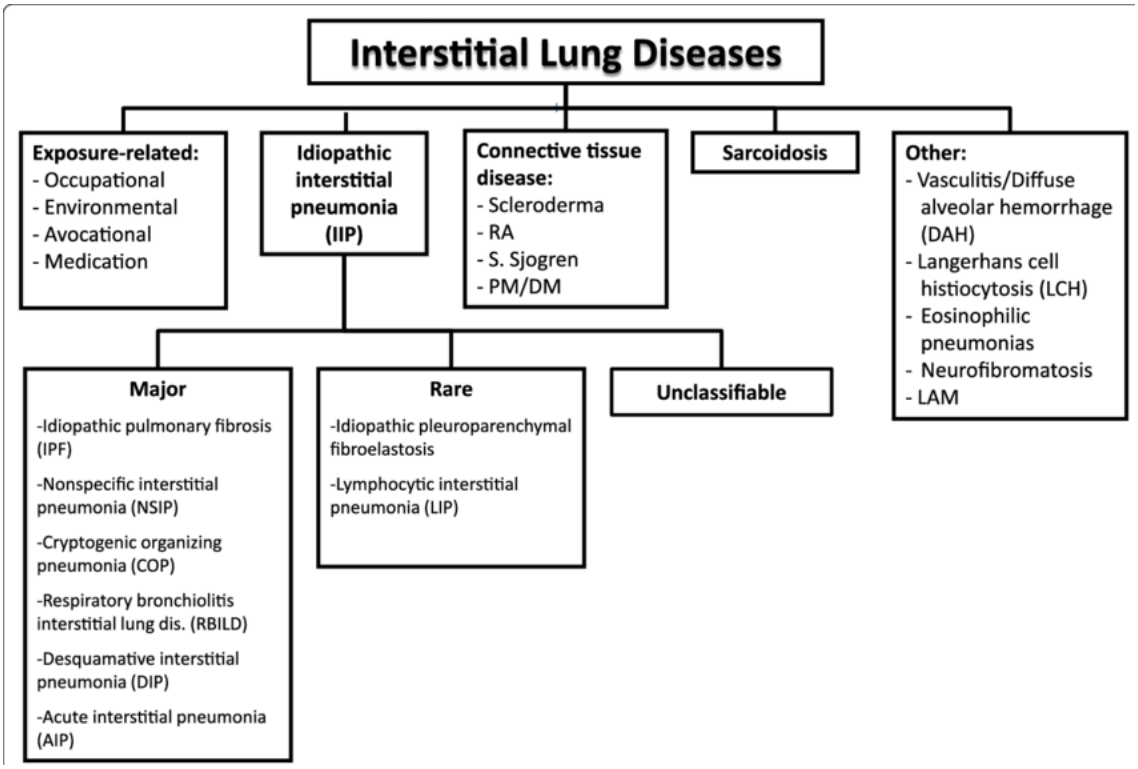

Figure 3. Classification of Interstitial Lung Diseases. RA = Rheumatoid Arthritis; PM/DM = polymyositis/dermatomyositis; LAM = lymphangioleiomyomatosis. Adapted from [38]

Besides IPF, sarcoidosis, collagenosis related forms of ILD and chronic hypersensitivity pneumonitis (EAA) constitute the most frequent disease entities [96]. The group of IIPs is defined by their characteristic clinical, radiological and pathological findings, as well as the not yet fully understood pathogenesis. Though the classification of ILD is rapidly changing with new, emerging research into the pathogenesis being released in rapid succession, there are currently thought to be six major and two rare forms of IIPs. (Fig. 3)

IIP Group and Clinical-Radiologic-Pathologic Diagnosis	CT Pattern	Typical CT Distribution	Typical CT Findings	CT Differential Diagnosis
Chronic fibrosing IIPs				
IPF	Usual interstitial pneumonia (UIP)	Peripheral, subpleural, basal	Reticular opacities, honeycombing, traction bronchiectasis or bronchiolectasis, architectural distortion, focal ground-glass attenuation	Collagen vascular disease, hypersensitivity pneumonitis, asbestosis, sarcoidosis
Idiopathic NSIP	NSIP	Peripheral, basal, symmetric	Ground-glass attenuation, irregular lines, traction bronchiectasis, consolidation	UIP, desquamative interstitial pneumonia, cryptogenic organizing pneumonia, hypersensitivity pneumonitis
Smoking-related IIPs				
Desquamative interstitial pneumonia	Desquamative interstitial pneumonia	Lower zone, peripheral predominance in most cases	Ground-glass attenuation, reticular lines, cysts	RB-ILD, NSIP, hypersensitivity pneumonitis
RB-ILD	Respiratory bronchiolitis	Often upper lung predominant, centrilobular	Bronchial wall thickening, centrilobular nodules, patchy ground-glass opacity	Desquamative interstitial pneumonia, NSIP, hypersensitivity pneumonitis
Acute or subacute IIPs				
Cryptogenic organizing pneumonia	Organizing pneumonia	Subpleural or peribronchial	Patchy consolidation or nodules, perilobular pattern, reverse halo sign	Infection, aspiration, eosinophilic pneumonia, NSIP, vasculitis, sarcoidosis, mucinous adenocarcinoma, lymphoma
Acute interstitial pneumonia	Diffuse alveolar damage	Diffuse or patchy	Consolidation and ground-glass opacity, often with lobular sparing; traction bronchiectasis later	Hydrostatic edema, pneumonia, pulmonary hemorrhage, acute eosinophilic pneumonia
Rare IIPs				
Lymphoid interstitial pneumonia	Lymphoid interstitial pneumonia	More commonly, lower lung predominant	Centrilobular nodules, ground-glass attenuation, septal and bronchovascular thickening, thin-walled cysts	NSIP, sarcoidosis, Langerhans cell histiocytosis and other cystic lung diseases
Idiopathic pleuroparenchymal fibroelastosis	Idiopathic pleuroparenchymal fibroelastosis	Peripheral, upper lung predominant	Pleural thickening and subpleural fibrotic changes	Sarcoidosis, pneumoconiosis, familial pulmonary fibrosis, connective tissue disease, hypersensitivity pneumonitis

Figure 4: ILD groups and their respective radiological and pathologic diagnostic criteria [172]

They can be additionally classified by their clinical course, and by their prognostic relevance. Besides fully reversible and stable forms of disease, the chronic and

irreversibly fibrosing forms of ILD, IPF and NSIP, are of distinct prognostic relevance [159, 193].

To classify any patient suspected of ILD, a thorough and extensive diagnostic algorithm is employed. Such an algorithm is exemplarily outlined for IPF below and may vary by subgroup of suspected ILD. (Fig. 5).

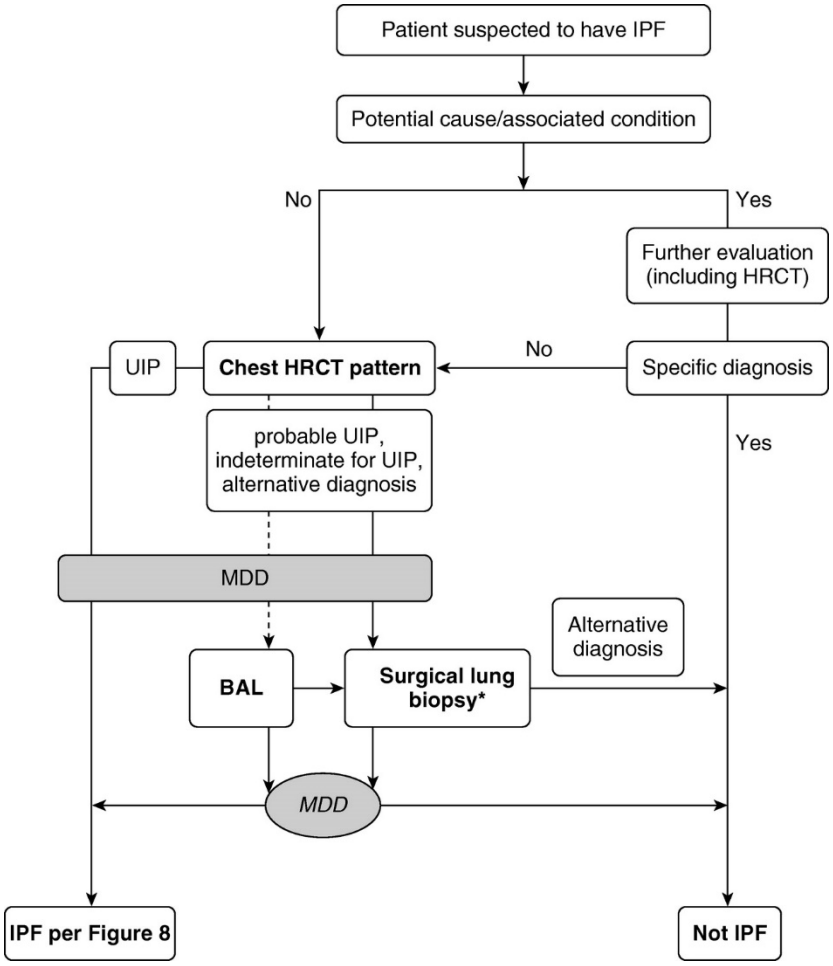

Figure 5: Diagnostic algorithm for patients with suspected IPF, as per the ATS/ERS/JRS/ALAT clinical practice guideline [147]

1.2.2. Epidemiologic and socioeconomic importance of IPF

Recent meta-analysis of IPF epidemiologic data in the European Respiratory journal yielded highly variable incidence statistics ranging from 0.2/100.000 to 93.7/100.000 per year with high regional variation, suggesting possible impact of environmental exposure or occupation. Pooled data analysis yielded an incidence of 3-9 per 100.000 per year [68]. The most reliable data is available for populations in North America and Europe [68, 69]. Despite uncertainties introduced by changing diagnostic criteria over time, data from both

the UK and the US shows a steady increase in prevalence and also suggests rising incidence in the population [145, 170]. Analysis of a primary-care-database based in the UK showed a calculated 78% rise of incidence between 2000-2012 alongside a twofold increase in prevalence, now estimated at 38.8/100.000 per year [170]. The condition is more common in male compared to female patients and more prevalent with advancing age [98]. IPF is recognized as a heterogenous disease with highly variable outcomes [99]. Despite this, mortality in IPF is high with a median survival of 3-5 years after diagnosis, comparable to malignant tumor entities [181]. In the European Union (EU) the median mortality is reported as 3.75 / 100.000 for males and 1.50 / 100.000 per year for females, respectively. Mortality rates seem to increase across the majority of the EU with the exception of some countries, such as Romania, Croatia, Austria and Denmark [110]. Whilst the introduction of novel treatment agents like pirfenidone and nintedanib has improved outcomes and survival in IPF, there is no medication capable of reversing the progression, or increasing quality of life in patients with IPF yet [53, 69]. Furthermore, IPF leads to an increased hospital admission rate, most often due to decrease of respiratory function in the context of an acute exacerbation, which increases with disease progression [38]. A study on hospitalization data of patients in the United States of America from 2001-2010 found a twofold higher all-cause hospitalization rate in the IPF cohort (0.5 per patient year) compared to the control group. Additionally, time spent in hospital, and treatment costs were also doubled in IPF patients compared to controls [98]. Based on this data an incremental cost of about one billion US-Dollars was estimated [144]. With the advance of expensive novel treatment agents and potentially increased survival duration, these costs are expected to rise significantly [118].

1.2.3. Current concepts regarding the pathomechanisms of IPF

A comprehensive understanding of the pathogenesis in IPF remains elusive, though important milestones in the underlying mechanisms have been reached by research efforts in the last few years. This led to a paradigm shift in IPF research. Where formerly a chronic inflammatory process was thought to be the root cause of fibrotic lung disease, it is now considered to be an epithelium driven disease, arising in the aftermath of recurrent damage to epithelial alveolar cells [163]. Here, the injury, especially to alveolar epithelial type II cells (AECII), provokes a tissue repair response and scar formation [54]. However, in the dysfunctional epithelium of IPF patients, this process continues incessantly, thus leading to an imbalance between pro- and antifibrotic agents, ultimately resulting in

exaggerated myofibroblast number and function, and chronic fibrotic alteration of the lung. [163]

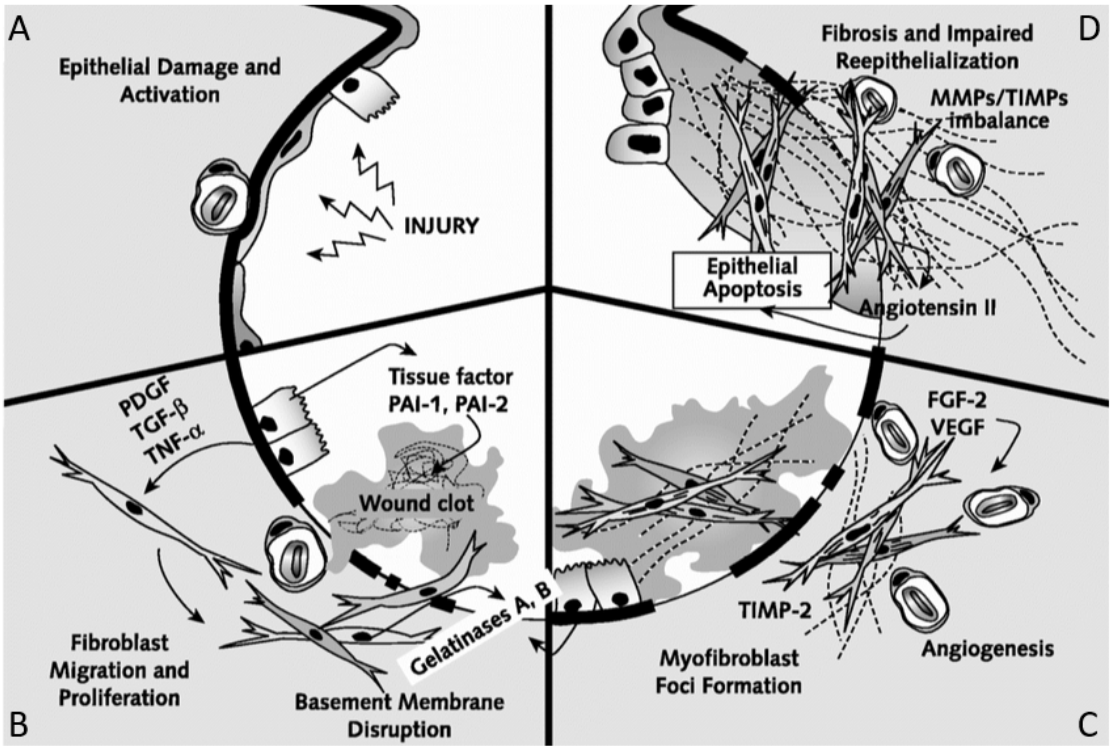

Figure 6: Proposed scheme of the abnormal wound healing model for idiopathic pulmonary fibrosis. The epithelial injury depicted in the top left panel (A) and the subsequent activation of AECII leads to an antifibrinolytic environment and clot formation in the alveolar space. Growth factor release by the epithelial cells leads to the migration and proliferation of fibroblasts as well as transdifferentiation to myofibroblasts. (Panel B) Later, damage to the basal membrane caused by the release of gelatinases by myofibroblasts and epithelial cells, enables an increased immigration of fibroblasts into the tissue (Panel C). Finally, ECM is permanently deposited and epithelial apoptosis occurs (Panel D). Adapted from [162]

1.2.3.1. Risk factors for interstitial lung disease

There are a number of proposed risk factors for interstitial lung disease, including environmental, genetic, infectious and autoimmunity based factors.

Environmental exposures have been shown to be involved in the pathogenesis of IPF in several epidemiological studies [178]. Most prominently, cigarette smoke (CS) is associated with increased risk of IPF (odds ratios for ever smoker: 1.6 (95% CI: 1.1 to 2.4); sustained former smoker (OR = 1.9; 95% CI: 1.3 to 2.9); smoker with 21 to 40 pack-years (OR = 2.3; 95% CI: 1.3 to 3.8) [13]) and poorer survival after diagnosis compared to non-smokers [169]. Other significant correlations for IPF include exposure to livestock, agriculture and farming, wood dust, metal and stone dust, and sands [178]. A role for viral pathogens has been implicated in the initiation of IPF and acute

exacerbations leading to disease progression. Several retrospective studies on the human herpes virus family (HHV) have shown elevated rate of previous infections with at least one type of HHV [175]. Chronic gastric fluid aspiration is discussed as an initial insult triggering faulty tissue remodeling in IPF. Aspiration of gastric fluid was demonstrated to alter the parenchyma of the lung by activating fibrotic cascades [36].

There is substantial evidence suggesting a genetic basis for idiopathic lung fibrosis. In recent years, a variety of genetic predispositions to pulmonary fibrosis have been identified through studies of familial interstitial pneumonia as well as genome wide association studies [39, 124].

Several mutations linked to the development of IPF affect the surfactant system. In familial pulmonary fibrosis, variants of surfactant proteins C (SPC) and A (SPA) have been implicated as key factors [185]. It is believed that these mutations cause incorrect folding of proteins and lead to endoplasmatic reticulum (ER) stress and activation of the unfolded protein response (UPR) [196].

Another strong independent risk factor implicated in the development of both idiopathic as well as familial interstitial pneumonias is a single nucleotide polymorphism in the MUC5B promoter. A paper published in the New England Journal of Medicine found the rs35705950 polymorphism to be present at a frequency of 38% among patients with IPF, 34% among patients with familial interstitial pneumonia and only 9% among the control group [161]. Additionally there was a 14.1 times higher expression of MUC5B in the lung of subjects who had IPF compared to the controls [161, 207]. Despite this, the exact role of this polymorphism in the pathogenesis of fibrotic lung disease has not been fully understood. The overexpression of MUC5B, driven by the promoter polymorphism, is thought to impair mucociliary clearance, increase chronic mucus hypersecretion and thus potentiating chronic inflammation and injury [204] (Fig 7). In a juxtaposition to its predictive implications, the MUC5B promoter polymorphism appears to be of prognostic value as well. Patients expressing the variant were observed to benefit from a twofold improvement of survival rate in IPF cohorts compared to non-carriers [137]. This effect may be indicative of enhanced microbial defense provided by increased mucin secretion [204].

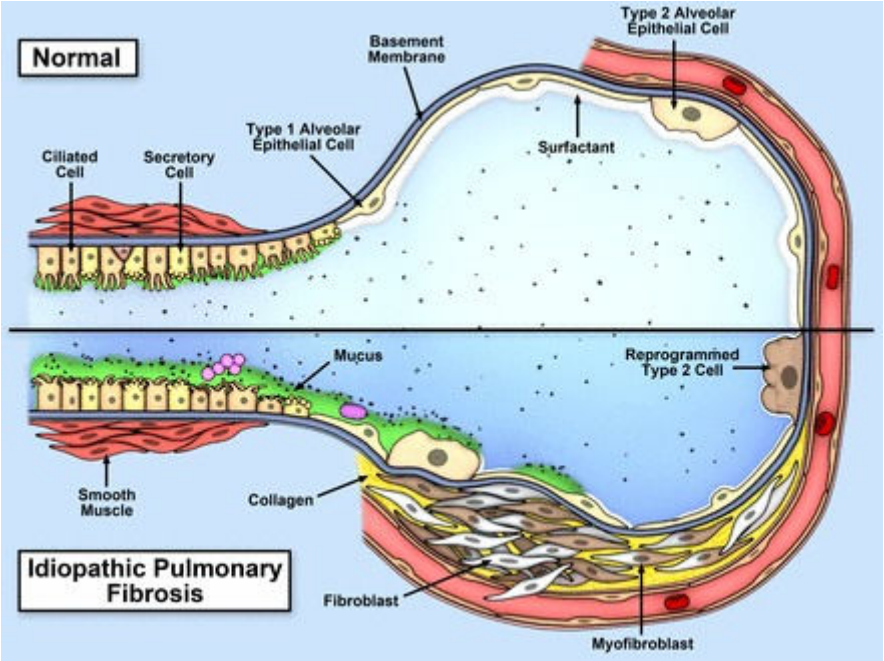

Figure 7: Comparison of recurrent inflammation and repair subsequent to injury at the bronchoalveolar level between healthy lung and in IPF. Evans et al. hypothesize that IPF is a mucocilliary disease caused by enhanced injury due to reduced ciliary function and increased particle retention initiated and exacerbated by MUC5B overexpression. Adapted from [35]

An inverse effect on IPF development has been found for three different single nucleotide polymorphisms in the toll interacting protein gene [125]. Here, a protective effect against the development of IPF has been encountered for the minor allele of rs5743890, whilst it is at the same time associated with increased mortality in IPF patients with established disease [137].

Found at both ends of each chromosome, telomeres are specialized loop structures of repetitive DNA units and associated binding proteins that protect the chromosomal DNA from degradation, thus playing an integral part in preserving the information content of our genome [164]. These telomeres undergo progressive shortening during each normal cell division and DNA replication, up until a lower limit is reached and the cell is forced into senescence and / or apoptosis [166]. Therefore, telomere length may be thought of as a biological clock, indicating the remaining lifespan of a cell or even an organism. In germline and stem cells there is an enzyme capable of preventing telomere shortening during DNA replication called telomerase. It is almost entirely absent in normal somatic cells [164]. An increase in shortening of telomeres has been associated with premature ageing and degenerative diseases such as bone marrow failure, cryptogenic liver cirrhosis and idiopathic lung fibrosis [3]. Induced telomere dysfunction in mice, effected through

telomerase deficiency or disruption of the shelterin complex formation in AECII, has been shown to induce pulmonary fibrosis, indicating the importance of telomere dysfunction on the development of IPF. Links to interstitial lung diseases have been established for six different telomere related genes [141].

In a study on patients with verified mutations in telomere related genes linked to pulmonary fibrosis, there appears to be a weak genotype-phenotype correlation. Identical genotypes are leading to a variety of diagnoses including IPF, unclassifiable lung fibrosis, chronic hypersensitivity pneumonitis, pleuroparenchymal fibroelastosis, interstitial pneumonia with autoimmune features, idiopathic interstitial pneumonia and connective tissue disease related fibrosis. Despite this, all cases of telomere dysfunction related pulmonary fibrosis showed a consistently progressive disease [119].

1.2.3.2. Detailed pathomechanism of IPF

The pathobiology of IPF has increasingly been targeted by research efforts in recent years. This has led to a vastly improved understanding of several pathomechanisms involved, but no definitive cause could be established. Instead, several promising concepts in the development of IPF have emerged, all of which are worthy of additional research [149].

Fibrosis is thought to evolve over long time intervals. At the time of diagnosis, lung structure is already widely modified, and different stages of contributing factors such as AECII hyperplasia, epithelial damage, fibroblast proliferation, formation of fibroblast foci and dense fibrosis can be observed. The dysfunctionality of an ageing and/or genetically predisposed epithelium, and the initiation of an aberrant wound healing process are postulated to be key in understanding IPF pathogenesis [163]. In healthy subjects, injury and loss of AECI is routinely followed by differentiation and proliferation of AECIIs effecting the restoration of the alveolar space integrity through different mechanisms, including epithelial regeneration, new vessel formation, activation of the coagulation cascade, activation and migration of fibroblasts, and the induction of collagen synthesis. This process is mediated by many different chemokines, most notably platelet derived growth factor (PDGF), fibroblast growth factor (FGF), transforming growth factor - ß1 (TGF-ß1) and vascular endothelial growth factor [16]. If this process fails to restore homeostasis, an inflammatory phase of wound healing with heightened levels of tumor necrosis factor alpha (TNF-A) and interleukin 1 (IL-1) may occur, thus leading to a biochemical environment propagating chronic maladaptive regeneration and thereby

tissue remodeling and fibrosis [16]. Several of the aforementioned predispositions, such as mutations in surfactant genes, the MUC5B promoter region and telomere dysfunctionality result in such a dysfunctional epithelium, and consequently lead to susceptibility to an aberrant repair process and diminished capability to respond to injury [54, 149, 196]. With the majority of the necessary epithelial repair following repetitive lung injury being performed by AECII, a lot of research has focused on the maladaptive restorative efforts of these cells. The repair effort leads to intracellular protein overexpression and subsequently to endoplasmatic reticulum stress (ERS), a usually cytoprotective mechanism intended to restore cell homeostasis by helping the cell to improve the folding and processing of misfolded proteins [206]. However, if the conditions invoking the ERS-response are prolonged or overwhelming, a switch towards apoptotic signaling will occur [90]. Signaling through ATF6 and IRE1 leads to downstream activation of CHOP and ATF4, two molecules integral in ultimately effecting apoptosis [91, 174]. Another consequence is the activation of an additional inherently cytoprotective pathway, the unfolded protein response (UPR). By inhibiting protein translation and targeting of defective proteins for degradation, the UPR also tries to reestablish cell homeostasis [196]. At the same time, under unrelenting outside stressors, UPR may stimulate the production of profibrotic mediators such as TGF-ß1, PDGF and C-X-C-motif chemokine 12 (CXCL12) [196] and lead to cellular apoptosis and expansion of the fibroblast pool [75, 140].

Although AECII injury is an established mechanism in the propagation of IPF, the transition from AECII injury to manifest lung fibrosis remains yet to fully be elucidated. There are a multitude of possible pathways linking AECII injury to IPF [163].

Epithelial-mesenchymal transition (EMT) is a process that has been shown to occur in vivo in mice, involving the transdifferentiation of epithelial cells and their migration into the provisional matrix [83]. The significance of this mechanism in IPF however remains a topic of debate, with estimates ranging from almost none of the involved fibroblasts originating from EMT up to 50% of them stemming from EMT [151, 176]. The deregulation and subsequent proliferation and increased collagen production of surrounding mesenchymal cells following AECII apoptosis, is another theory proposed in the progression of lung fibrosis. Here, levels of Prostaglandin E2 (PGE2), a key factor in regulating fibroblast proliferation and differentiation [131], have been shown to be

severely reduced, indicating an absence of control over fibroblastic proliferation and differentiation. Another component in the apparent expansion of the local fibroblast pool and fibroblast activation is the release of several chemokines attracting circulating mesenchymal cells and profibrotic compounds, including VEGF, TGF-ß1 and stromal cell-derived factor 1. [16]

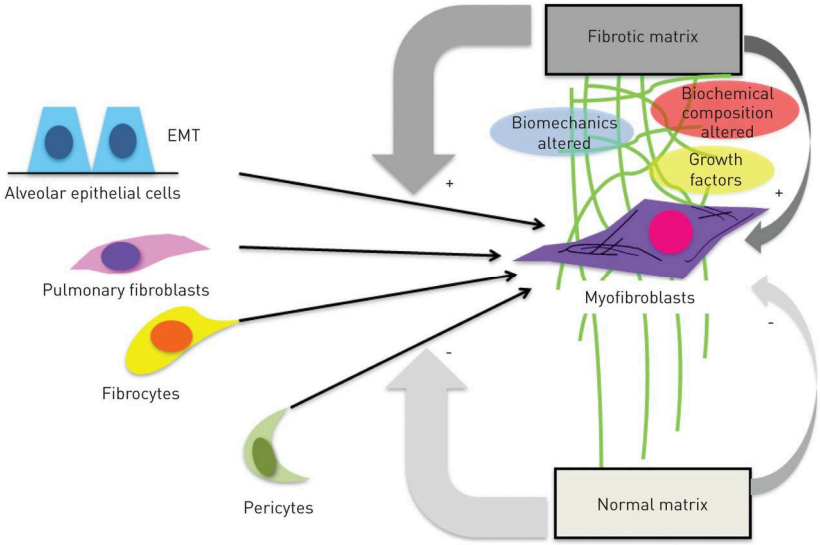

Figure 8: Schematic overview for proposed sources of cells taking part in the formation of fibroblast foci and the shift to fibrotic matrix. Different cells may serve as fibroblast progenitors, including fibrocytes, pericytes and also alveolar epithelial cells through EMT. Changes in the biochemical composition of extracellular matrix are believed to have an impact on these processes and consequently drive the permanent accumulation of fibrogenic cells. Adapted from [104].

During the normal wound healing process in a healthy individual, fibroblasts are mesenchymal cells committed to repair and reestablishment of functional structure in the lung and its extracellular matrix (ECM). However, in the damaged lung of IPF patients, being consistently exposed to an environment rich with a variety of profibrotic signals and mediators due to continuous epithelial damage and repair, they may demonstrate excessive ECM production and / or transdifferentiation to myofibroblasts [104].

Myofibroblasts, the aforementioned differentiated fibroblasts that have contractile properties akin to smooth muscle cells, have been suggested to represent the ultimate effector in pulmonary fibrosis [209]. These cells inflict the final result of IPF: Destruction of the lung parenchyma, extensive deposition of connective tissue and abnormal tissue remodeling [180].

The excessive ECM deposition ultimately leads to an increase in lung stiffness and reduced lung compliance in IPF. Besides negatively impacting lung function in the patient, the increase in ECM stiffness has recently been implicated as being a propagative factor of IPF itself [63, 66]. It has been shown that the mechanical properties of the scarred lung tissue resulting from myofibroblast aggregation, at the same time promote additional myofibroblast differentiation and contraction, mediated via an increased release of TGF-ß1 stored in the ECM [63, 165].

1.2.4. Current and upcoming therapies

As of today there is no cure for IPF and only limited treatment options are available [146]. With IPF being a disease entity which routinely leads to severe reduction in quality of life and is accompanied by a variety of comorbidities – including pulmonary hypertension, lung cancer, chronic obstructive pulmonary disease (COPD), obstructive sleep apnea and ischemic heart disease - providing adequate care to these patients is difficult. Therefore a multifaceted approach to treatment is necessary [143]

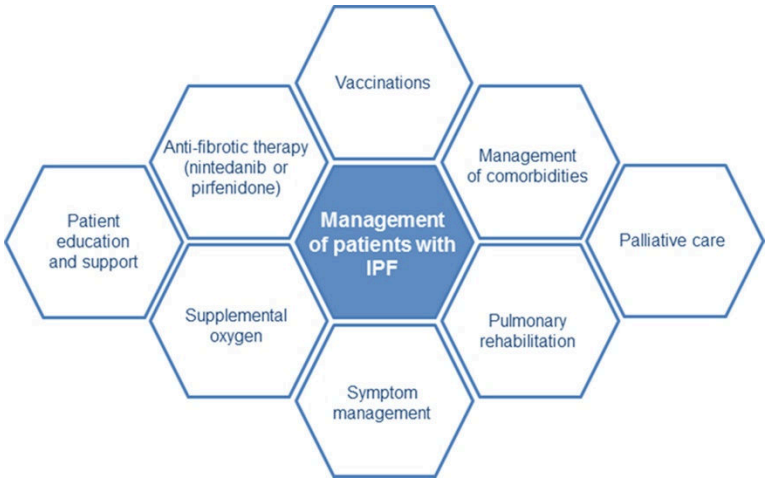

Figure 9: The multimodal and interdisciplinary aspects of IPF treatment, taken from [143]

Looking at medical treatments seeking to combat IPF directly, there has been a significant shift in therapeutic approach recently. After immunosuppressive treatments including prednisolone, azathioprine and N-Acetylcysteine were shown to be ineffective and even detrimental to patient outcomes [111], novel antifibrotic agents such as pirfenidone and nintedanib have been developed, which have been shown to reduce FVC decline and mortality by up to 50% [4, 103, 146]. As a result, these drugs are now approved for the treatment of IPF in the US and the EU [12, 28, 96].

Despite these advances in drug therapy, lung transplantation remains the only treatment capable of not only slowing disease progress, but partially restoring function and improving quality of life in recipients [94, 156].

Nintedanib is a tyrosine kinase-inhibitor targeting VEGF, PDGF and FGF, thus possessing an antifibrotic and antiproliferative effect [61, 148]. Pooled data from randomized controlled trials (TOMORROW and INPULSIS 1/2) showed an increase in the time to first acute exacerbation and decrease of FVC decline compared to placebo, thus indicating a beneficial effect on disease progression. [148] Adverse events which led to treatment discontinuation were more frequent in the nintedanib group (20,6%) compared to placebo (15,0%) [148]. The most frequent adverse event reported was diarrhea, occurring in up to 61,5% of patients [148].

Pirfenidone is an antifibrotic agent available for oral application. It takes effect by downregulating the activity of both TGF-ß1 and TNF- α, which was shown in several in vitro trials [64, 129, 130], thus leading to an inhibition of fibroblast proliferation and collagen synthesis. Additionally, in animal models of lung fibrosis, pirfenidone has been shown to reduce histological and cellular markers of fibrosis [64, 71]. The effectiveness of pirfenidone has been shown in several Phase III trials (CAPACITY and ASCEND) [85, 122]. Pooled analysis of the data showed a 43,8% reduction of the proportion of patients experiencing a >10% of predicted FVC decline or death after one year of treatment, and an increase of the proportion of patients with no decline by 59,3% [123]. Additionally there were observable benefits for both progression-free survival (38%) and a reduction in the decline in the 6 minute walking distance [123]. However it should be noted that there is high interindividual variance in treatment response, with as many as 20% of patients not responding to pirfenidone treatment at all [101]. The most common adverse events were gastrointestinal (nausea (36%), vomiting (14%) and dyspepsia (19%)), and dermatologic (rashes (32%), and photosensitivity (12%)) [123].

Recent analysis of an unselected cohort undergoing treatment for IPF, derived from the eurIPFreg, yielded evidence for a considerable and significant increase in average survival under antifibrotic treatment from 68 to 123 months [53]. There have been trials looking into potential benefits of a combination of Pirfenidone and Nintedanib (INJOURNEY) suggesting an enhanced treatment efficacy at the cost of an increased rate

of adverse events, but this treatment regimen is not yet indicated outside of clinical trials [186].

Recent advances in the understanding of the pathomechanisms underlying IPF, as outlined above, have led to a multitude of potential new targets in the treatment of fibrotic lung disease. Based on current models of disease propagation, they target a wide range of growth factors, cytokines and intracellular pathways (Figure 11). Many of these agents are currently undergoing phase I or phase II trials [12].

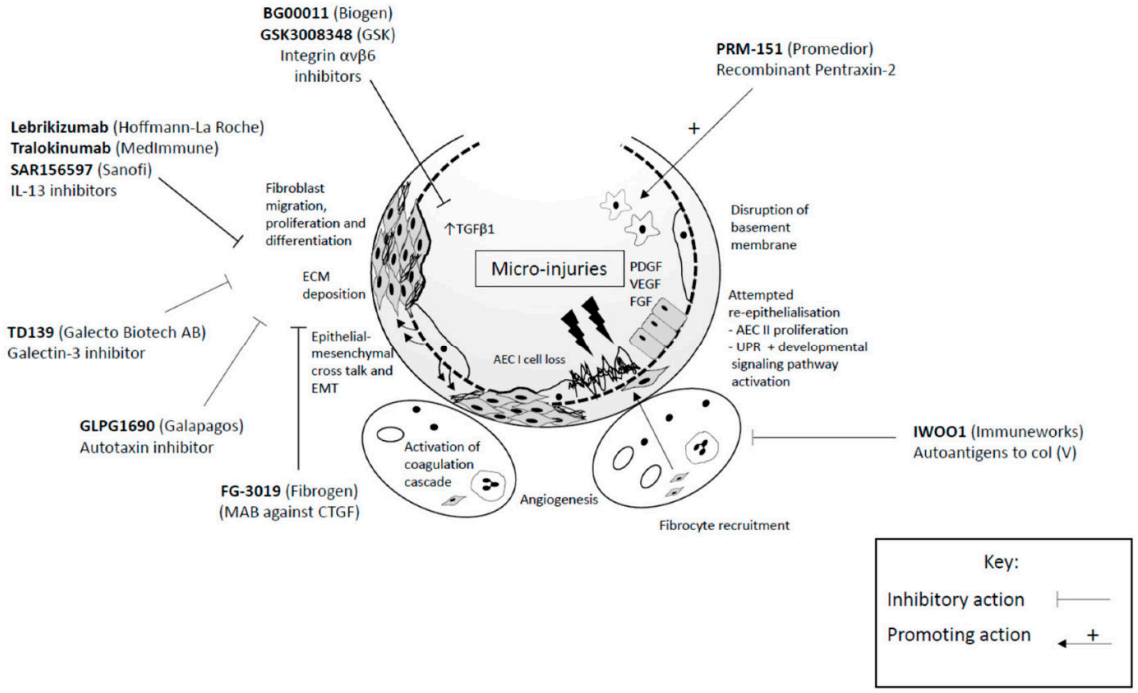

Figure 10: Prospective therapeutic agents and their molecular targets in IPF. Abbreviations: MAB: monoclonal antibody; CTGF: connective tissue growth factor; Col (V): type V collagen; IL-13: interleukin-13. The biotech company currently developing the respective drug is found in brackets behind the respective treatment agents name. Adapted from [12]

Despite these recent advances, lung transplantation remains the only curative treatment option, with the best outcomes in survival and quality of life [94, 156]. IPF-Patients receiving a transplant have a median post-transplant survival time of 4.5 years, with 47%-53% of patients surviving more than 5 years [86]. However, less than 5% of ILD patients receive a lung transplant [53], and the amount of possible transplantations is highly limited by the scarce supply of donor organs [50, 134]. With IPF being one of the most prevalent indications for lung transplantation [94] and high mortality rates during time on the organ wait lists [23, 107], the demand for transplantable organs is continuously high.

One possibility to meet this demand is found in the rapidly growing field of regenerative medicine [112]. The *in vitro* generation of lungs meant for transplantation can be achieved by repopulation of decellularized tissue scaffolds which may be generated from a donor organ that would not have been suited for transplantation otherwise [62]. These decellularized organ scaffolds can - in principle - be recellularized using the recipients own stem cells, therefore circumventing many issues related to graft/host incompatibility [62]. Although there have been promising results in experiments conducted on rats allowing for short term gas exchange of transplanted lungs generated *in vitro* [138], the implementation of the procedure into clinical practice remains a difficult task yet to be accomplished.

1.3. Current models for the study of fibrotic lung disease

1.3.1. Animal models

To help unravel the highly complex pathogenesis of fibrotic lung disease, multiple animal models trying to mimic IPF have been developed. Despite the inability of current models to accurately recapitulate the full histopathological and radiographic pattern of usual interstitial pneumonia (UIP), the hallmark feature of IPF used for diagnosis, they have been indispensable in the research of IPF pathogenesis [116].

The intratracheal instillation of bleomycin (BLM), a chemotherapeutic agent, in adult mice, is widely regarded as the most relevant IPF model available [77]. BLM is thought to introduce single and double-strand DNA breaks in cells and induce oxidative stress, thus leading to apoptosis. This leads to widespread epithelial cell death, excessive inflammation and subsequently to fibrotic remodeling of the lung via fibroblast activation and ECM deposition [29, 177]. Fibrotic changes in the lung can be observed two to four weeks after intratracheal instillation. These include structural features such as intra-alveolar fibrosis, septal thickening and dilation of bronchioles as well as changes in cellular composition, with epithelial cell death and increases in alveolar macrophages [72]. However, the Bleomycin model of lung fibrosis is limited in its capability to replicate the irreversible progression of IPF in patients, with mice showing self-limiting, spontaneously regressive fibrosis [115].

An alternative method to induce fibrosis in mice is the intratracheal instillation of amiodarone (AD). Amiodarone, a benzofuran derivative, is a drug commonly used in the

therapy of atrial fibrillation and during cardiopulmonary resuscitation [76]. Although the pathomechanisms of lung injury via AD are not yet fully elucidated, a variety of different pathways and effects are implicated. These include direct cytotoxicity, inflammatory reactions, liberation of oxidants and accumulation of intracellular phospholipids [105, 106, 158]. Exposed to repeated intratracheal application of amiodarone, mice begin to exhibit reduced compliance alongside histopathological signs of fibrosis, including septal thickening, ECM deposition, patchy interstitial fibrosis and lymphoplasmacellular infiltration [105]. However, despite repeated AD application, the extent of fibrosis and epithelial cell death diminished over time, in contrast to the clinical appearance of IPF [105].

Epithelial cell dysfunction has been implicated as the driving force in the development of IPF [54, 100, 163]. Mutations in surfactant related genes have been found in familial and sporadic forms of IPF and have been shown to lead to this epithelial dysfunctionality, and more specifically to ER stress in AECII [126, 185]. Based on these insights, a novel model of fibrotic lung disease introduces a cysteine-to-glycine substitution in the Sftpc gene. Whilst introduction of this mutation during fetal development leads to disrupted lung morphogenesis und subsequently fatal postnatal respiratory failure, the introduction in adult mice leads to the development of ER stress in AECII with eventual onset of spontaneous pulmonary fibrosis and restrictive lung impairment [80]. The model therefore provides an important link between AECII ER stress and pulmonary fibrosis.

There are a variety of other animal models of fibrotic lung diseases, including injury by environmental fibrotic agents such as asbestos or silica, as well as genetic models of forced senescence or cytokine overexpression [5, 177].

Despite this, most compounds found to be effective in the treatment of fibrosis in the belomycin model, have failed to produce comparable results in human IPF, thus indicating an ongoing need for even more precise and therefore relevant for human disease models and methods to study fibrotic lung disease [77].

1.3.2. In vitro models

1.3.2.1. Precision cut lung slices

A potential way to "close the gap" between animal models and human disease is to study precision cut lung slices (PCLS). Precision cut lung slices are generated by filling the lung intended for study with agarose in order to stiffen the tissue and the subsequent sectioning of said tissue into thin slices (200µm – 500µm), a procedure feasible for both animal and human lungs [40, 93]. PCLS are 3D cultures and therefore incorporate many aspects of the organs original structural and cellular organization [157]. Paired with the intrinsically easy accessibility for imaging, PCLS have proven useful in the evaluation of a variety of processes, including infectious disease response, toxicology, allergies, and measurement of vascular responses and bronchoconstriction [7, 10, 95, 150, 202]. In addition to offering an easily observable *ex vivo* model open to experimental manipulation, PCLS also represent a potentially high throughput and high yield way of using oftentimes limited supplies of human tissue [7, 40, 157]. They can be stored using cryopreservation, supporting efficient use of donor tissue and long term experiments [7]. With the recent advances in imaging techniques allowing for precise three-dimensional imaging and time-lapse imaging, PCLS offer a versatile powerful tool to study *ex vivo* cell behaviors and interactions [157].

1.3.2.2. Decellularization of lung tissue and generation of ECM-Scaffolds

The excessive accumulation of matrix components, extracellular matrix remodeling and fibrosis resulting in loss of function are hallmark features of fibroproliferative diseases. The ECM has therefore become a target for research, aiming to generate insights into the role of ECM in pathophysiology [12, 120]. The generation of acellular scaffolds by means of whole organ decellularization has emerged as a powerful tool in studying ECM function and effects [8, 46]. Decellularized ECM scaffolds have been successfully employed in the generation of various tissues, including blood vessels, cornea, liver, heart and lung [43, 58, 114, 135, 139].

Decellularization of tissue can be achieved by physical, chemical or enzymatic procedures, or a combination of them [46]. Physical methods utilized in decellularization efforts include freezing/thawing, sonication and agitation, intended to achieve cell lysis and detachment [73]. Chemical methods include a wide variety of detergents, as well as alkaline and acid treatments and hypo-/hypertonic treatments. Detergents are the most

commonly used chemicals and are typically grouped into ionic, non-ionic and zwitterionic detergents. In most protocols, the lung is exposed to detergents *via* whole organ submersion and/or instillation in the airways or bloodstream in a bioreactor setup [46, 142].

Non-ionic detergents largely leave protein-protein interactions intact, whilst disrupting lipid-lipid and protein-lipid interactions. The most widely studied non-ionic detergents include Triton X-100 and Tween20, which have been used in the decellularization of various tissues with mixed results, sometimes failing to provide complete cell removal [21, 46]. Despite their relatively limited impact on the structure of decellularized tissue, partial depletion of glycosaminoglycans (GAG), laminin and fibronectin may occur [52].

Sodium dodecyl sulfate (SDS) and sodium deoxycholate (SDC) are the most frequently used ionic detergents. Due to their ability to disrupt protein-protein interactions, they are very effective in removing any cellular remnants, but at the same time may inflict extensive disruption of the tissue structure [160, 198].

Zwitterionic detergents combine the characteristics of ionic and non-ionic detergents. Common zwitterionic agents such as 3-[(3-cholamidopropyl) dimethylammonio]-1-propane sulfonate (CHAPS) perform well in preservation of ECM structure, but may have limitations in cell removal [26, 82].

Cell removal may be verified by a number of methods. These can range from standard histological staining (HE), staining of possible DNA remnants with DAPI or propidium iodine (PI) to PCR verification [26, 79]. The influence of possible cellular remnants in decellularized biological scaffolds on recellularization efforts remains yet to be fully elucidated [81]

Decellularization protocols aim to achieve a balance between the complete removal of cells and the preservation of ECM structure and composition. However, a deterioration in matrix integrity to a varying degree is inevitable [37]. The “optimal” decellularization protocol has therefore been and continues to be a topic of discussion [20, 127]. Since the success of reseeding decellularized scaffolds has been shown to be reliant on the retainment of structural integrity and native ECM proteins, an accurate proteomic readout is a vital tool necessary for the appraisal of potential new decellularization protocols [27, 60]. However, producing reproducible quantitative information about the extensively

crosslinked and therefore highly insoluble matrix elements has proven difficult. The very properties providing the ECM with its structural strength make it very hard to solubilize the proteins of interest, thereby hampering classical bottom-up proteomics approaches like immunoblotting [56]. Even the introduction of strong chaotropes or sonication may not fully remedy these shortcomings [62]. Recent research has suggested that these obstacles can be overcome with elaborate targeted proteomics using a multistep protein digestion protocol (Fig. 11) followed by liquid chromatography tandem mass spectrometry analysis [21, 62].

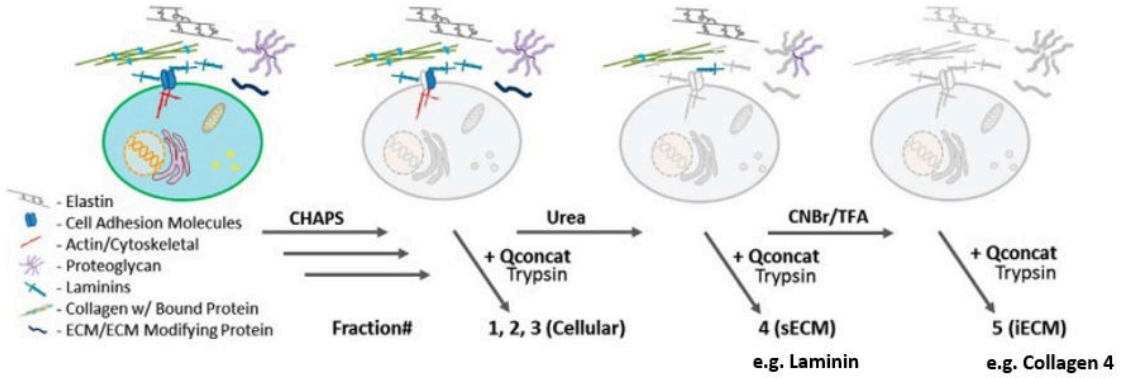

Figure 11: Schematic overview for a proposed multi-step protein extraction method to analyze both native and decellularized lungs. The first step incorporates mechanical tissue homogenization and the use of a CHAPS buffer to facilitate the extraction of cellular proteins. SolubleECM (sECM) is extracted in the second step, which utilizes a urea buffer and vortexing. Finally, insolubleECM (iECM) is made available to analysis by chemical digestion. Modified after [62]

1.4. Regenerative Medicine and stem cell therapy

In the United States alone, more than 25 million people are estimated to be afflicted by some form of chronic lung disease, of which about 135,000 yearly are expected to die from complications of the respective diseases [89]. For many of these patients with end-stage lung disease, the only treatment promising prolonged survival and increased quality of life is lung transplantation, thus creating a high demand for donor organs which cannot be met, despite vast improvements to organ allocation and distribution [2, 134, 184]. Additionally, lung transplantation is a complex procedure, burdened with unavoidable complications like allograft rejection and increased risk of infection caused by the need for lifelong immunosuppression, which leads to low long-term survival rates of about 60% in 5 years following the procedure [156, 184]. Regenerative medicine, and more specifically bioengineered lungs, may offer a promising future in the attempts to remedy these problems and possibly lead to a paradigm shift in lung transplantation [188].

Decellularized allogeneic or xenogeneic lungs repopulated with stem cell populations derived from the patient may provide a reliable source of transplantable organs and avoid classical allogeneic transplantation drawbacks [45]. (Fig. 12)

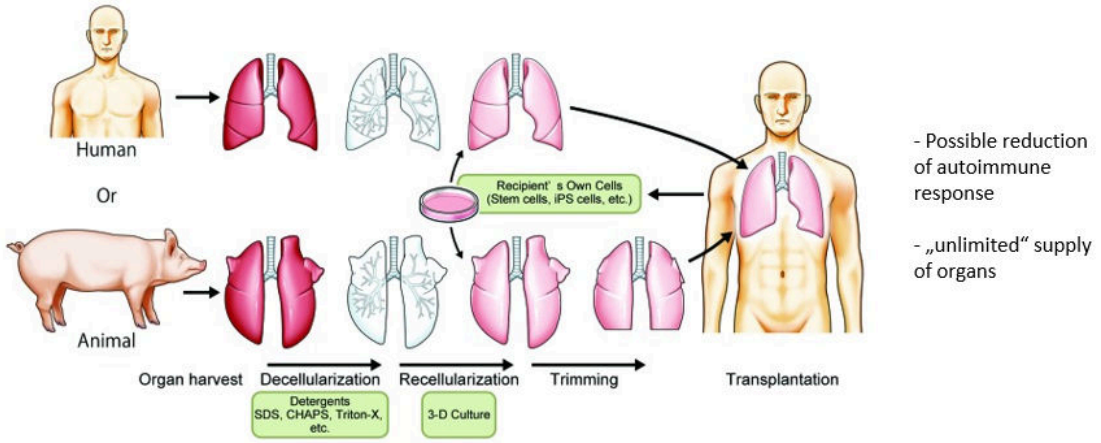

Figure 12. Schematic representation of a possible future procedure where patients in need of a transplant may be provided with a "tailor-made" whole lung for transplantation by decellularization and recellularization of whole lungs. Harvested human or animal lungs are decellularized by detergents such as SDS, SDC, CHAPS, or Triton-X. Subsequently a decellularized lung may be recellularized with stem/progenitor cells or iPSCs sourced from the recipient. Modified after [183]

Due to its highly complex three dimensional structure, tissue engineering efforts in the lung have focused on using decellularized ECM scaffolds [6, 136]

The recellularization of decellularized lung scaffolds is a complex endeavor posing several challenges. There is a need to ensure stem cell engraftment in order to achieve epithelialization of the alveolar space to facilitate gas exchange and endothelialization of blood vessels to ensure circulation [183]. Recellularization attempts have therefore been undertaken with a variety of protocols featuring different cell populations, ranging from isolated embryonic stem cells (ESCs), mesenchymal stem cells (MSCs), induced pluripotent stem cells (iPSCs), endothelial or epithelial cell populations, to mixtures of different cell groups with varying success [33, 45, 48, 183, 188]. There have been promising results in rats, albeit with time-limited participation in gas exchange by bioengineered lungs for up to 180 minutes and subsequent failure from haemorrhage, thrombosis and decrease in gas exchange capability [136]. These failures may be related to insufficient epithelialization or endothelialization, possibly caused by spatial seeding failure, insufficient cell populations or fragility of underlying ECM [33, 183]. Further research is needed to fully elucidate the underlying mechanisms.

2. Scientific Question

With the emergence of tissue engineering as a highly promising research avenue, models to study the regenerative capacities of the lung need to be constantly improved. Previous studies in tissue engineering focused on full organ decellularization and recellularization in animal models. Translating these models for human therapies poses a large challenge. At the same time, human donor organs remain a highly scarce commodity. Therefore, the efficient use of available tissue is paramount to enabling future research success. PCLS may offer a chance to provide a tissue efficient, high throughput model that allows for constant monitoring during culture. Our goal was to design a method to efficiently decellularize PCLS and subsequently achieve repopulation by seeding them with unfractionated lung cells.

Based on the current level of knowledge we defined the following research questions:

2.1. What is the most efficient method for PCLS cell removal that has the least impact on lung structure and extracellular matrix components?

2.2. Is it possible to repopulate decellularized PCLS ECM-scaffolds with unfractionated lung cells?

2.2.1. Is prolonged culture of unfractionated lung cells on PCLS ECM-scaffolds possible?

2.2.2. What is the cellular composition of the repopulated ECM scaffolds?

2.2.3. Are mouse PCLS scaffolds a viable assay for studying the regenerative capacity of alveolar epithelial cells?

3. Materials and Methods

3.1. Mouse lung tissue

For the experiments conducted in this thesis, lungs harvested from adult C57B/6N mice held in standard conditions with 12h of daylight, 25°C temperature and fed with standard mouse chow were used. Mice were purchased from Charles River Wiga, Sulzfeld, Germany.

All animal studies were performed in accordance with the Helsinki convention for the use and care of animals and were approved by the local authorities at Regierungspräsidium Giessen under "GI20/10-Nr. A53/2012 Zellisolation und Organkultur – Lungenfibrose".

3.2. Materials

3.2.1. Scientific instruments

Instrument	**Manufacturer**
Cell culture bench MSC Advantage	Heraeus, Hanau, Germany
Centrifuges Rotina 380, Rotina 46R	Hettich, Tuttlingen, Germany
BD FACSCanto II	BD Bioscience, Franklin Lakes, USA
Heracell Vios 160i CO2 incubator	Thermo-Fischer-Scientific, Waltham, USA
Leica VT1000S Vibratome	Leica Biosystems, Nussloch, Germany
Leica RM 2235 Microtome	Leica Biosystems, Nussloch, Germany
Pipettes	Eppendorf, Hamburg, Germany
Pipetting aid	Eppendorf, Hamburg, Germany
Precision scale AB54	Mettler Toledo, Gießen, Germany
Slidescanner NanoZoomer 2.0 RS	Hamamatsu, Japan
Vortex-Genie 2	Scientific Industries, New York, USA
Waterbath	Leica Biosystems, Nussloch, Germany
Zeiss Axiovert 25	Zeiss, Oberkochen, Germany
Zeiss Observer Fluorescence Apotome	Zeiss, Oberkochen, Germany

Table 1: Laboratory equipment used

3.2.2. Chemicals and consumables

Name	Manufacturer
Amphotericine B	Sigma-Aldrich, München, Germany
Aqua ad Injectabilia	Braun Melsungen, Melsungen, Germany
BSA (Bovine-serum-albumin)	Carl Roth, Karlsruhe, Germany
Cell Strainer 100µm, 70µm	BD Bioscience, Franklin Lakes, USA
CHAPS (3-[(3-Cholamidopropyl)-dimethylammonio]-1-propanesulfonate hydrate)	Sigma-Aldrich, München, Germany
Citric-acid-monohydrate	Carl Roth, Karlsruhe, Germany
DAKO Fluorescence mounting medium	Agilent, Santa Clara, USA
DNAse (Powder)	Sigma-Aldrich, München, Germany
Dispase (Powder)	Corning, Corning, USA
4′,6-diamidino-2-phenylindole (DAPI)	Sigma-Aldrich, München, Germany
Dulbecco's Phosphate Buffered Saline (PBS)	Sigma-Aldrich, München, Germany
Dulbecco's modified eagle medium + 10% FBS ((-) Glutamine) (DMEM)	Gibco, Carlsbad, USA
EDTA (Ethylendiamintetraacetate)	Merck, Darmstadt, Germany
Ethanol 100 Vol% Ethanol 99 Vol% Ethanol 96 Vol% Ethanol 70 Vol%	Carl Roth, Karlsruhe, Germany
Falcon Tubes 10ml, 50ml	Thermo-Fischer-Scientific, Waltham, USA
Fetal Bovine Serum (FBS)	Sigma-Aldrich, München, Germany
Low melt Agarose (3 Vol%)	Carl Roth, Karlsruhe, Germany
Hank's balanced salt solution (HBSS)	PAN Biotech, Aidenbach, Germany
Matrigel Matrix (Phenolred-free)	Corning, Corning, USA
Natriumcitrate-dihydrate	Carl Roth, Karlsruhe, Germany

Name	Manufacturer
Paraformaldehyde	Carl Roth, Karlsruhe, Germany
Penicillin-Streptomycin	Sigma-Aldrich, München, Germany
2-(4-(2-Hydroxyethyl)-1-piperazinyl)-ethansulfonsäure (HEPES)	Carl Roth, Karlsruhe, Germany
Propidium iodide (PI)	Thermo-Fischer-Scientific, Waltham, USA
Normal donkey serum (NDS)	Jackson Immunoresearch, West Grove, USA
RPMI Medium 1640 (1x)	Gibco, Carlsbad, California
Sodium Deoxycholate (SDC)	Carl Roth, Karlsruhe, Germany
Sodium Dodecyl Sulfate (SDS)	Carl Roth, Karlsruhe, Germany
Sudan Black	Sigma-Aldrich, München, Germany
Tween 20	Sigma-Aldrich, München, Germany
Triton-X 100 (Tr-X)	Sigma-Aldrich, München, Germany
Culture plates: 12 and 24 wells	Greiner Bio, Kremsmünster, Austria
Xylene (Dimethylbenzen)	Carl Roth, Karlsruhe, Germany

Table 2: List of chemicals and consumables

3.2.3. Solutions for decellularization, cell culture and staining

Name	Formula
CHAPS-solution	8 mM solution in PBS + 1M NaCl + 25mM EDTA
DNAse solution	30µg/ml + MgSO4in PBS
Dispase-solution	PBS (+Ca^{2+} and Mg^{2+}) + 10 Vol% Dispase + 10µg/ml DNAse
FACS buffer	HBSS + 2% FBS + 10µg/ml DNase + 0.1mM HEPES
Antigen retrieval-Solution A	Citric-acid-monohydrate-solution 100mM in water
Antigen retrieval-Solution B	Natriumcitrate-dihydrate-solution 100mM in water
Matrigel-Mix	Volume-Proportionate 1:1 mixture with DMEM
SDC-solution	2 Vol% / 4 Vol% in PBS
SDS-solution	1,8 mM solution in PBS
Staining buffer	PBS + 5 Vol% BSA + 2 Vol% NDS + 0,1 Vol% Triton-X
Sudan Black	3 m% in 70% Ethanol
Tween20-solution	3 m% solution in PBS

Table 3: List of solutions prepared for individual experiments

3.2.4. Antibodies

3.2.4.1. Primary antibodies for immunofluorescence images

Antibody	Manufacturer code	Concentration used
Anti-Laminin (rabbit polyclonal)	Abcam (ab11575)	1:500
Anti-Collagen 4 (rabbit polyclonal)	Abcam (ab6586)	1:500
Anti-Fibronectin (mouse polyclonal)	BDBiosciences (BD610077)	1:500
Anti-ABCA3 (mouse polyclonal)	Seven Hills (WMAB-17-H5-24)	1:200
Anti-Podoplanin (goat polyclonal)	R&D Systems (AF3244)	1:500
Anti-TTF1 (rabbit monoclonal)	Abcam (ab76013)	1:200
Anti-pan-Cadherin (mouse monoclonal)	Abcam (ab6528)	1:100
Anti-Alpha smooth muscle actin (rabbit polyclonal)	Abcam (ab5694)	1:500
Anti-Vimentin (rabbit polyclonal)	Abcam (ab92547)	1:500
Anti-Ki67 (rabbit polyclonal)	Abcam (ab15580)	1:500
Anti-pSPB (rabbit polyclonal)	Abcam (ab3430)	1:500
Anti-pSPC (rabbit polyclonal)	Millipore (AB3786)	1:200
Anti-PCNA (mouse monoclonal)	Santa-Cruz (sc-56)	1:500
Anti-SPC (goat polyclonal)	Santa-Cruz (sc-7706)	1:500

Table 4: List of primary antibodies used for immunofluorescence imaging

3.2.4.2. FACS antibodies and dyes

Name	Color	Concentration	Manufacturer Code
Anti-mouse CD326 / EPCAM	APC/Cy7	1:400	Biolegend (118218)
Anti-mouse CD45	PE/Cy7	1:400	Biolegend (103114)
Anti-mouse CD31	PE/Cy7	1:400	Biolegend (102418)
LysoTracker Green DND-26	488	1:100	Invitrogen (L7526)

Table 5: List of primary antibodies and dyes used for flow cytometry

3.2.4.3. Secondary antibodies

Antibody	Manufacturer code	Concentration used
Polyclonal Anti-Rabbit-IgG 488	A21206	1:500
Polyclonal Anti-Rabbit-IgG 555	A31572	1:500
Polyclonal Anti-Rabbit-IgG 647	A31573	1:500
Polyclonal Anti-Goat-IgG 488	A32814	1:500
Polyclonal Anti-Goat-IgG 555	A21432	1:500
Polyclonal Anti-Goat-IgG 647	A21447	1:500
Polyclonal Anti-Mouse-IgG 488	A21202	1:500
Polyclonal Anti-Mouse-IgG 555	A31570	1:500
Polyclonal Anti-Mouse-IgG 647	A32787	1:500

Table 6: List of secondary antibodies, their manufacturer code and used concentrations

3.2.5. Kits

LIVE/DEAD® Viability/Cytotoxicity Kit (Thermo-Fischer Scientific)

- Calcein AM (Component A) 4mM in Anhydrous DMSO, diluted to 2µM
- Ethidium-homodimer-1 (Component B) 2mM in DMSO/H2O, diluted to 4µM

3.3. Methods

3.3.1. General considerations in method development

The goal of this work was to develop protocols suitable for both de- and recellularization of precision cut lung slices. For this reason, an iterative approach was followed. Therefore, the decision to start out with several initial protocols based on previous literature was made. Based on preliminary analysis, various improvements were then included in a step wise manner and again analyzed for potential progress.

In such an iterative approach, a protocol may be retired at any given step based on interim results.

3.3.2. Precision cut lung slice generation

Adult C57 B6/J mice were euthanized after sedation by intraabdominal injection with a mixture of xylazin, heparin and ketamin (2:1:2, 200 µl total) and subsequent exsanguination via the abdominal aorta. The mice were then fixed onto a cork board with needles. The thoracic compartment was opened by transversal incision, the heart and lung were harvested and the trachea cannulated and secured with a knot. Simultaneously, a 3% solution of low melt agarose in 1xPBS was prepared and mixed 1:1 with sterile DMEM to achieve the target concentration of 1.5%. About 1-2ml of Agarose solution was instilled via the trachea until the lobes were fully inflated. Then, the lobes were submerged in cold medium and kept on ice for 15 minutes to facilitate solidification of the agarose.

Sectioning of individual lobes was performed using the HM650V Vibrating Blade Microtome (Thermo-Scientific) using standard razor blades. Entire lung lobes were attached to the object carrier at the bottom with super-glue (Hampton Research SUPER GLUE 2GR). Sectioning into slices of 200µm to 500µm thickness was performed after hardening of the glue and prepared PCLS were transferred into of 12 well plates with DMEM and maintained on ice. After sectioning, PCLS were stored in well plates or Falcon vials with DMEM 10% FBS at 4C until use.

3.3.3. Decellularization

3.3.3.1. Initial Protocols (P1-P4)

In the initial experiments (P1-P4) the PCLS were exposed to detergent and washing steps in 50ml Falcon® vials. Detergent solutions according to Tab. 3 were prepared immediately prior to the experiments. PCLS were transferred to the Falcon vials individually with forceps. Fifteen PCLS were exposed to each detergent under mechanical agitation for 60 min, followed by five minutes of washing in distilled water, and two cycles of 15 minutes washing in PBS. Solution changes were performed by separation through a 100µm strainer. These steps were repeated an additional three times following detergent changes. Following the detergent treatment, remaining DNA from cell dissolution was removed by 30 min of DNase I solution. Two additional washes ensured the removal of residual detergent and cellular debris. All procedures were performed at room temperature with the exception of the DNase treatment, which was performed at 37°C.

After protocol completion, PCLS were stored in Falcon vials in PBS supplemented with Penicillin/Streptomycin solution at 4°C until further use.

3.3.3.2. Refined Protocols (P5-P6)

For these experiments, PCLS were exposed to detergent in 12 well plates with 2-3 PCLS per well. PCLS were transferred into the well plates individually with forceps. Detergent solutions according to Tab. 3 were prepared immediately prior to the experiments. To remove residual agarose prior to undergoing decellularization, a heating step (40°C for 30 minutes) was introduced. PCLS were treated according to the protocols as follows:

After initial washes with distilled water (P5) / PBS (P6), PCLS were exposed to each detergent for 24 hours at 4°C. After a subsequent wash with distilled water (P5) or PBS (P6), another 24 hours detergent exposure was performed. On the third day, the PCLS were washed with distilled water (P5) or PBS (P6) and 1M NaCl + P/S (P5) or PBS + Ca^{2+} + P/S (P6) to ensure the removal of residual detergent and cellular debris. They finally underwent treatment with DNase-Solution for 60 minutes, followed by a final thorough wash in distilled water (P5) or PBS (P6) before storage or use in subsequent experiments. Washes and detergent changes were performed by carefully pipetting out detergent at the very edge of the well to avoid tissue damage and subsequent resuspension

in the next solution. Well plates were kept on a radial shaker during detergent exposures to avoid tissue agglutination. With the exception of the DNase treatment, which was performed at 37°C, all the protocols were performed at room temperature.

Further improvements to the decellularization protocols will be implemented if necessary based on the preliminary results.

3.3.4. Lung cell isolation

Adult C57 / B6/J mice were euthanized and their heart and lung block harvested as described in 3.3.2. Then, the lung was inflated with 1-2 ml dispase-solution (Tab. 3) and simultaneously submerged in dispase-solution and incubated for 45 minutes at 37°C in a 50ml Falcon® vial. After incubation the trachea was removed and the remaining lung tissue was minced with a razorblade and scissors into 1mm or smaller pieces. Additional dissociation was achieved by repeatedly pipetting tissue pieces up and down in 10mls of DMEM 10%FBS with 30ug/ml DNase. Then the resulting cell suspension was filtered through a 100µm cell strainer, centrifuged at 450g and the supernatant discarded. Cells were then resuspended in 10ml of culture medium. Cell number and viability were assessed by Trypan Blue (1:1 mixture with cells) and counting in a Neubauer counting chamber. After filtering through a 40um cell strainer, cells were kept in FACS-buffer or DMEM culture medium, depending on subsequent use in either FACS or recellularization.

3.3.5. Flow cytometry

Flow cytometry is a method in which different cell types are identified by the expression of cell surface specific markers. These markers are detected by incubation with antigen-specific antibodies that are directly coupled with fluorescent dyes. Cells are then separated in individual droplets in the fluidics part of the instrument. These droplets pass in front of different LASERs which excite the fluorophores and the emitted signal is captured by PMT (photo-multiplier tubes) detectors which transform the photon numbers into an equivalent number of electrons. The data is then displayed in plots where each individual dot represents a single cell and its position on the plot is determined by the fluorescence intensity in the two fluorescent channels being depicted

Cells isolated from mouse lungs as described above (3.3.4) were counted and resuspended at 10^6 cells / 100µl and incubated with the appropriate directly conjugated antibodies or

Lysotracker Green (100nM) (Tab. 5) in FACS buffer for 30 minutes at 37°C. Following incubation, samples were washed one time with 1ml FACS buffer and resuspended in 200µl FACS buffer with DAPI. Data was acquired on a BD Canto II (BD Biosciences) using BD FACSDiva software (BD Biosciences). Data was further analysed using FlowJo software (FlowJo, LLC). cells.

3.3.6. Recellularization

Recellularization was achieved by introducing and culturing unfractionated lung cells on a matrix scaffold, which provides biophysical cues for cell development.

For the recellularization of extracellular matrix scaffolds prepared as described in 3.3.3, different culture conditions were set up to facilitate cell growth in individual matrix scaffolds. Every sample was cultured in its own compartment on 24-well plates in 2ml of medium. During the first development Stage, individual wells were prepared in three different conditions as shown in Figure 3a, b, c and seeded with 500µl of cell suspension containing either C1=1.000.000 cells or C2=3.000.000 cells.

3.3.6.1. Three initial protocols designed for recellularization purposes

PCLS-matrigel (Pm)-Protocol:

First, 100µl of a 1:1 mixture of Matrigel with DMEM was spread evenly on the bottom on the well and then allowed to polymerize at 37°C. The PCLS were then carefully placed on top of the Matrigel layer to avoid folding. C1 = 1.000.000 or C2 = 3.000.000 unfractionated lung cells in 500µl of medium were added to the PCLS. Afterwards 2ml of DMEM (Tab. 2) were added carefully to the sides of the well. The matrix scaffold was then cultured at 37°C, and medium was exchanged every 24 hours.

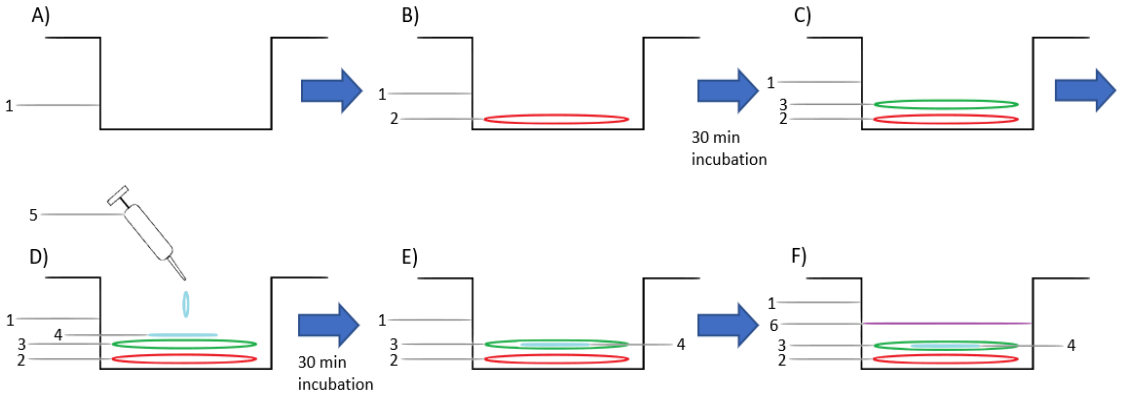

Figure 13a: Graphic representation of Pm-protocol. Step by step implementation from A) through F). A) empty well plate, B) preparation of Matrigel layer, C) Introduction of decellularized PCLS, D) Seeding of cell suspension, E) Cell incubation for adherence to PCLS F) Adding of cell culture medium and commencement of culture. 1: 24-well plate, one sample per well 2: 50µl Matrigel spread 3: Decellularized PCLS 4: Cell suspension 5: Pipette 6: Cell culture medium

PCLS-only (Pc)-Protocol:

The PCLS were carefully placed on the bottom of the well to avoid folding. C1 = 1.000.000 or C2 = 3.000.000 unfractionated lung cells in 500µl of medium were added to the PCLS evenly. Immediately afterwards 2ml of DMEM (Tab. 2) were added carefully to the sides of the well. The matrix scaffold was then cultured at 37°C, medium was exchanged every 24 hours.

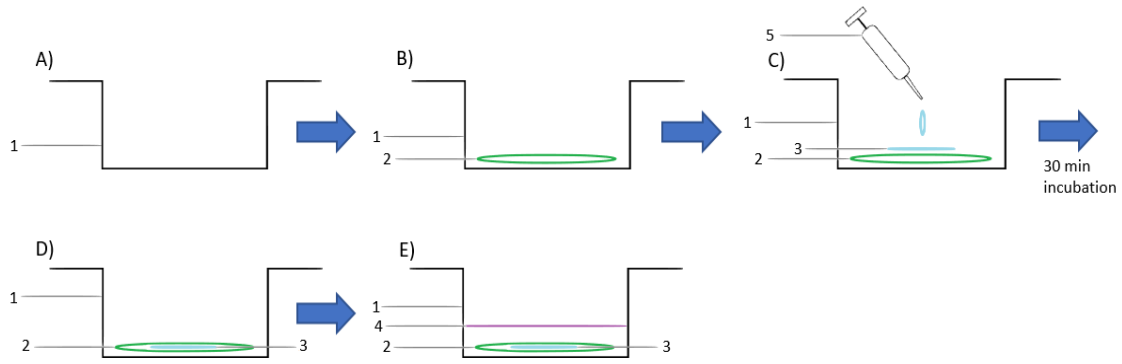

Figure 13b: Graphic representation of Pc-protocol. Step by step implementation from A) through E). A) empty well plate, B) Introduction of decellularized PCLS,C) Seeding of cell suspension, D) Cell incubation for adherence to PCLS E) Adding of cell culture medium and commencement of culture. 1: 24-well plate, one sample per well 2: Decellularized PCLS 3: Cell suspension 4: Cell culture medium 5: Pipette

Matrigel-PCLS-matrigel (mPm)-Protocol:

First, 100µl of a 1:1 mixture of Matrigel with DMEM was spread evenly on the bottom on the well and then allowed to polymerize at 37°C. The PCLS were carefully placed on top of the Matrigel layer to avoid folding. C1 = 1.000.000 or C2 = 3.000.000

unfractionated lung cells in 500µl of medium were added to the PCLS evenly. Immediately afterwards, 100µl of a 1:1 mixture of Matrigel with DMEM was carefully spread on top of the PCLS and allowed to polymerize for 30 minutes. Then 2ml of DMEM (Tab. 2) were added carefully to the sides of the well. The matrix scaffold was then cultured at 37°C, medium was exchanged every 24 hours.

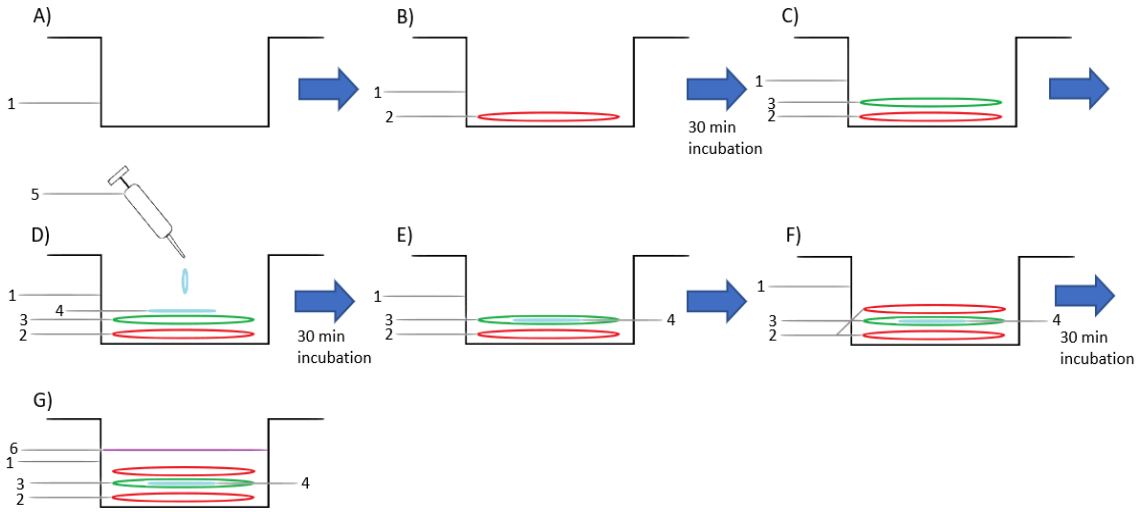

Figure 13c: Graphic representation of mPm-protocol. Step by step implementation from A) through G). A) empty well plate, B) preparation of Matrigel layer, C) Introduction of decellularized PCLS, D) Seeding of cell suspension, E) Cell incubation for adherence to PCLS F) preparation of secondary Matrigel layer, G) Adding of cell culture medium and commencement of culture. 1: 24-well plate, one sample per well 2: 50µl Matrigel spread 3: Decellularized PCLS 4: Cell suspension 5: Pipette 6: Cell culture medium

3.3.7. Histology

3.3.7.1. Sectioning

In order to enable the histological analysis of tissue, the formaldehyde-fixed PCLS were dehydrated in a closed vacuum-tissue fixation device, in previously PBS-bathed embedding cassettes, overnight. The lung tissue was then paraffin embedded and sectioned into 3µm thick slices with a microtome.

3.3.7.2. Deparaffinization and rehydration

Prior to staining, samples were deparaffinized and rehydrated. Deparaffinization was achieved by first heating the samples to 60°C for 60 minutes and then submerging them in xylene for 10 minutes after cooling down Afterwards the samples were rehydrated using alcohol in descending concentrations (Tab. 7). Following the ethanol steps, sections were washed briefly in distilled water, and kept in PBS for the following steps.

Purpose	Reagent	Duration (min)
Deparaffinization	Xylene	10
Rehydration	Alcohol 100 Vol%	5
Rehydration	Alcohol 96 Vol%	5
Rehydration	Alcohol 80 Vol%	5
Rehydration	Alcohol 70 Vol%	5
Rehydration	Alcohol 50 Vol%	5

Table. 7: Sample treatment sequence for deparaffinization and rehydration

3.3.7.3. Immunhistochemical staining

To assess the condition of treated precision cut lung slices and the cell population within them, indirect immunofluorescence staining for a variety of cell markers was employed.

Immunofluorescence staining relies on labeling of target antigens with fluorescent dyes. In indirect immunofluorescence, this labeling is achieved by first incubating samples with an unconjugated primary antibody targeted to the desired antigen and then introducing the fluorophore with a secondary antibody targeting the primary antibody. The samples can then be imaged with a fluorescence microscope capable of exciting the fluorescent agent. Both paraffin embedded sections and wholemount PCLS were stained as follows.

3.3.7.3.1. Immunohistochemical staining of paraffin embedded sections

Samples were first deparaffinized and rehydrated according to 3.3.7.2. Then the following protocol was employed.

1. Antigen-retrieval: Submerging of samples in 450ml dH2O + 9ml of Solution A + 41ml of Solution B, then microwaving at 900 watts for 2 x 10 minutes. Subsequent cooling and wash with PBS.
2. Blocking of unspecified protein binding sites: Blocking solution is applied to samples and incubated for 30 minutes at room temperature. Subsequent rinse with PBS.
3. Incubation with primary antibodies in specified concentration (Tab.3) at 4°C overnight. Afterwards, sections were washed 3 x 5 minutes with PBS
4. Incubation with secondary antibodies in specified concentration (Tab.4) at room temperature for 60 minutes. Subsequent washes with PBS similar to the washes after the primary antibody.

5. Incubation with DAPI DNA stain for 30 seconds followed by immediate PBS wash.
6. Incubation with Sudan-Black-solution (3m% in 70Vol% Ethanol) for one minute then 3 x 5min PBS washes
7. Adding of DAKO fluorescence mounting medium and application of cover slip
8. Storage in closed container until imaging

3.3.7.3.2. Immunohistochemical staining of wholemount PCLS

To assess structural integrity and three-dimensional structure, PCLS were imaged wholemount.

PCLS (200µm) were taken after decellularization and washed with PBS to remove detergent residue. Then, samples were stained for direct imaging by employing the following steps:

Blocking of unspecified protein binding sites: Blocking solution is applied to samples and incubated for 30 minutes at room temperature. Subsequent rinse with PBS.

Incubation with primary antibodies in specified concentration (Tab.3) at room temperature for 60 minutes followed by 3 x 15 min PBS washes.

Incubation with secondary antibodies in specified concentration (Tab.4) at room temperature for 60 minutes. Subsequent wash with 3 x 15 min PBS.

Incubation with DAPI DNA dye for 30 seconds followed by immediate PBS wash.

Samples are carefully placed onto microscope slides to avoid folding, covered with a glass coverslip and immediately imaged.

3.3.8. Immunofluorescent Imaging

Fluorescence microscopy is based on the illumination of fluorophores - fluorescent chemical compounds capable of emitting light upon excitation - with light of specific wavelengths, leading to the emittance of light of longer wavelengths. The light used for the excitation of the fluorophore is then separated by a spectral emission filter, leaving the weaker emitted fluorescence to be analyzed. Different fluorophores may be excited

by light of specific wavelengths. Images of several types of fluorophore may be combined into multi-color images. [34]

Immunostained wholemount and paraffin samples were imaged on a Zeiss Observer Fluorescence microscope. Images were obtained at different magnifications, ranging from 100x to 400x. All settings, including color intensity and exposure times were kept identical between samples from the same experiment to ensure comparability. Images were optimized, saved and exported using Zeiss Axiovision Software. Multi-channel images were exported as both composite images and in split channels to allow for later analysis (3.3.8).

Full sample imaging

Before scanning, sample areas were delineated with a marker to aid in scanning area selection. Up to 6 samples were loaded on the slide cassette. Exposure times were optimized on predefined areas to ensure adequate color saturation and to avoid potential bleaching. After the adequate exposure times were set, automatic multi-channel scanning commenced. All the samples within the same experiment were imaged under identical conditions.

3.3.9. Image analysis

In the course of this study, two types of image analysis were performed. Fluorescence quantification analyses was performed to evaluate protein content in decellularized PCLS and cell count analysis was performed to evaluate cell culture success.

Image analysis was performed using the Fiji 1.52i Version of ImageJ.

3.3.9.1. Comparison of relative mean fluorescence intensity in decellularized samples

For the analysis of decellularized scaffolds, images obtained from wholemount PCLS were used. To assess protein content, the fluorescent signal was quantified using ImageJ software as follows.

First, a region of interest (ROI) was set to exclude sample edges, sample disruptions or folding and artifacts. Using the ROI-manager feature, the analyzed area of 723*326 Pixels was kept identical between all samples to ensure comparability. Color intensity for each

pixel is mapped in a 256-step analysis reaching from black (0) to maximum intensity (255). The chosen ROI included 235698 data points for each sample. Then, the intensity data were exported in the form of a histogram with color intensity on the x-axis and frequency on the y-axis. Histograms were averaged from n=5 samples for each condition and then compared against controls (non-decell and no primary). Histogram data were exported into excel for further analysis.

Qualitative structural comparison was performed on both detail images and full sample scans.

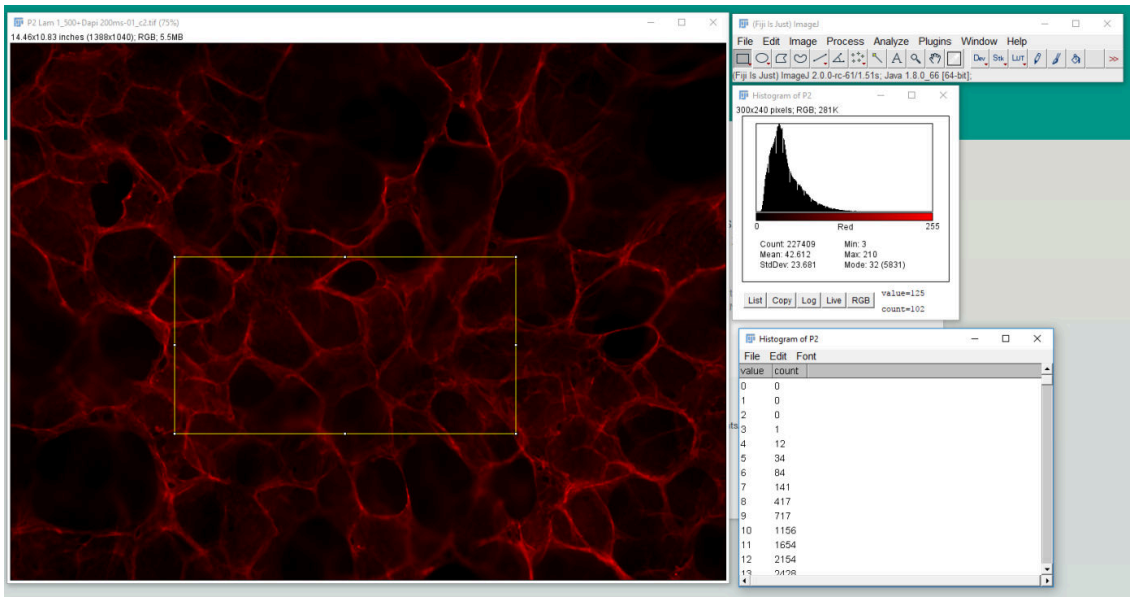

Figure 14: Example of fluorescence intensity readout. The ROI is marked with a yellow border. Sample histogram and correlated intensity measurement numbers can be seen on the right.

3.3.9.2. Quantification of recellularization by automated counting using ImageJ-software

For the analysis of recellularized PCLS, paraffin embedded sections as per 3.3.7.1 were imaged and analyzed. Qualitative analysis of cell types, cell location and scaffold structure were performed on 100x, 200x and 400x magnification. Quantitative analysis of total and proliferative cell numbers was performed on n=24-29 disjunct 20x images from n=5 samples per culture condition and timespan. For the purpose of cell counting, single channel images of DAPI (blue channel) and Ki67 (647nm channel) were processed and utilized as follows.

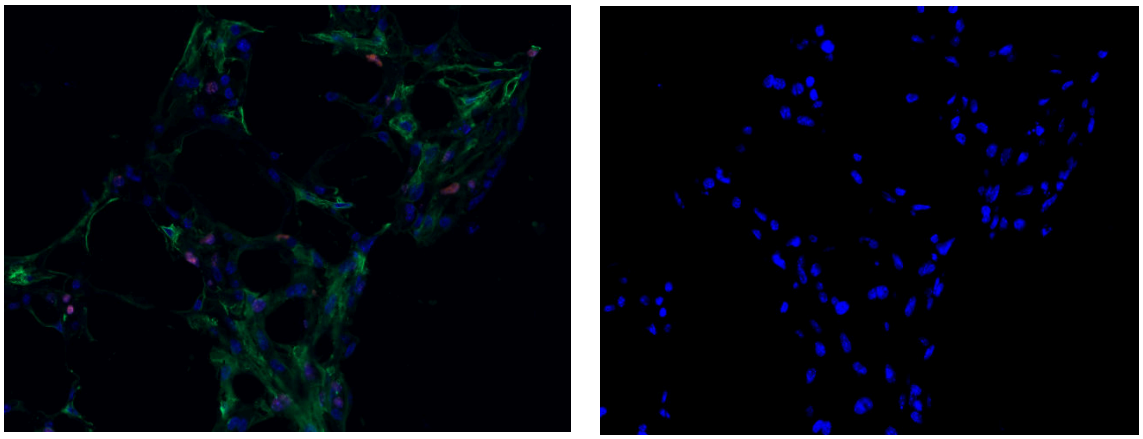

Figure. 15: Example of composite 20x image on the left with all color channels and single channel image used for cell counting on the right

Cell counting was automated using the following macro implemented via the macro recorder feature of ImageJ. In the first step, the single channel image is processed into a binary image. Background signal is eliminated by thresholding. The threshold (x) was set individually, depending on brightness of the source image. Additionally, intranuclear "holes" introduced by thresholding are filled using the "Fill holes" plugin of ImageJ and potentially overlapping cells are separated using the "Watershed" plugin based on local minima and maxima.

"run("8-bit");
run("Threshold...");
setThreshold(x, 255);
setOption("BlackBackground", false);"
run("Convert to Mask");
run("Fill Holes");
run("Watershed");

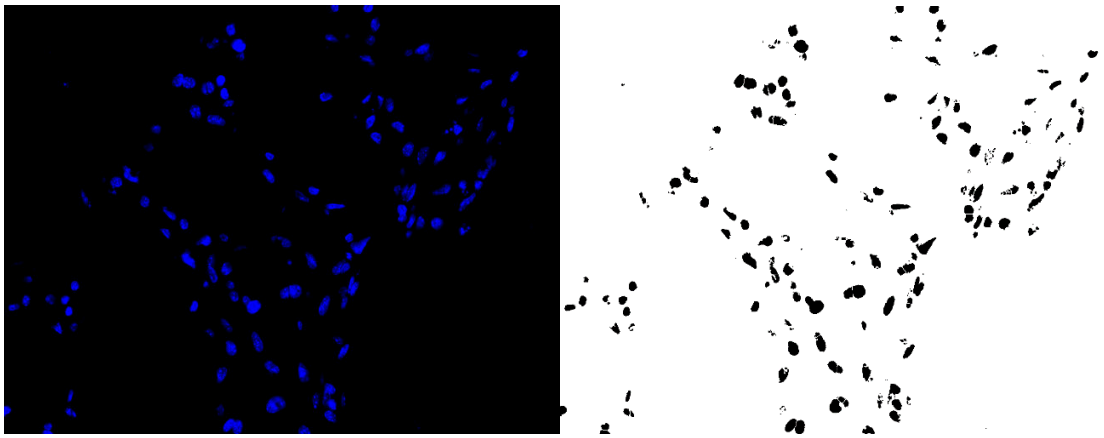

Figure. 16: Single channel image of DAPI fluorescence on the left. Example of converted binary image after thresholding and processing on the right.

Finally, cells are counted using the “Analyze particles” function. Here, minimum size in pixels and a form factor (circularity: 0 means completely random form, 1.00 means only perfect circles are included) are introduced to avoid counting of impurities or other “dirt” in the image. The thereby counted cells are outlined and numbered.

run("Analyze Particles...", "size=100-Infinity pixel circularity=0.3-1.00 show=Outlines display summarize");

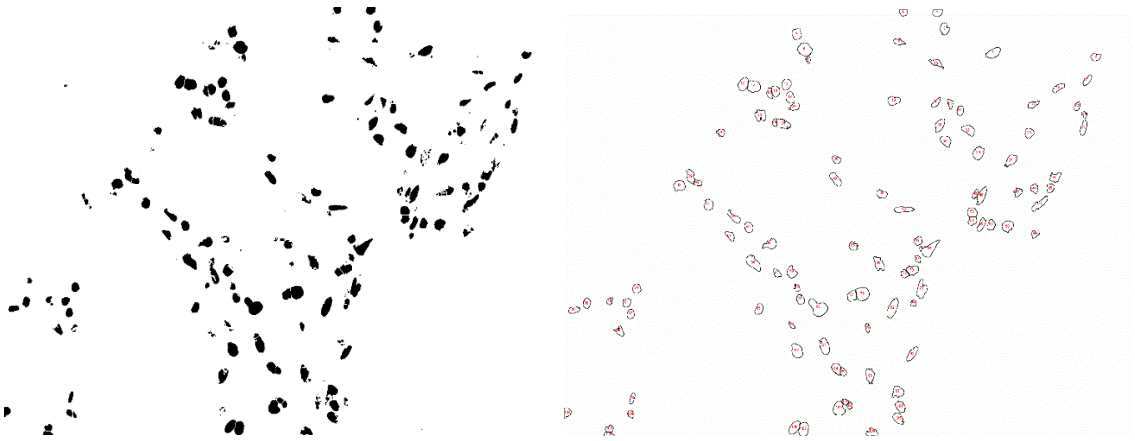

Figure 17: Converted binary image after thresholding and processing on the left. Example of counting result from processed image on the right.

The results were verified by inspection and comparison with manually counted data, and the data then exported to excel.

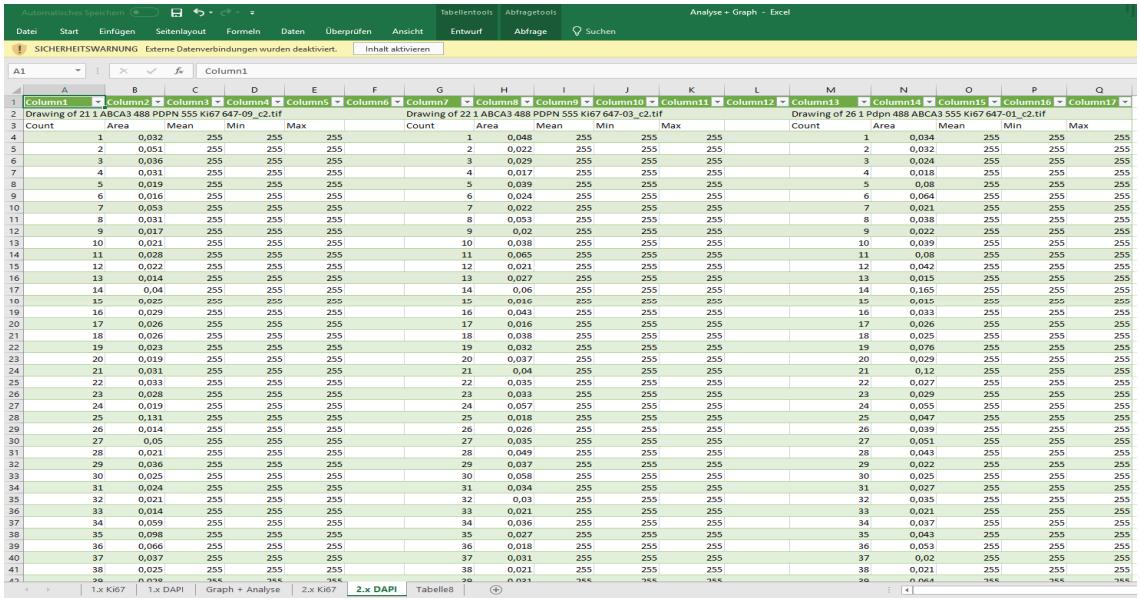

	Column1	Column2	Column3	Column4	Column5	Column6	Column7	Column8	Column9	Column10	Column11	Column12	Column13	Column14	Column15	Column16	Column17
2	Drawing of 21 1 ABCA3 488 PDPN 555 Ki67 647-09_c2.tif						Drawing of 22 1 ABCA3 488 PDPN 555 Ki67 647-03_c2.tif						Drawing of 26 1 Pdpn 488 ABCA3 555 Ki67 647-01_c2.tif				
3	Count	Area	Mean	Min	Max		Count	Area	Mean	Min	Max		Count	Area	Mean	Min	Max
4	1	0,032	255	255	255		1	0,048	255	255	255		1	0,034	255	255	255
5	2	0,051	255	255	255		2	0,022	255	255	255		2	0,032	255	255	255
6	3	0,036	255	255	255		3	0,029	255	255	255		3	0,024	255	255	255
7	4	0,031	255	255	255		4	0,017	255	255	255		4	0,018	255	255	255
8	5	0,019	255	255	255		5	0,039	255	255	255		5	0,08	255	255	255
9	6	0,016	255	255	255		6	0,024	255	255	255		6	0,064	255	255	255
10	7	0,053	255	255	255		7	0,022	255	255	255		7	0,021	255	255	255
11	8	0,031	255	255	255		8	0,053	255	255	255		8	0,038	255	255	255
12	9	0,017	255	255	255		9	0,02	255	255	255		9	0,022	255	255	255
13	10	0,021	255	255	255		10	0,038	255	255	255		10	0,039	255	255	255
14	11	0,028	255	255	255		11	0,065	255	255	255		11	0,08	255	255	255
15	12	0,022	255	255	255		12	0,021	255	255	255		12	0,042	255	255	255
16	13	0,014	255	255	255		13	0,027	255	255	255		13	0,015	255	255	255
17	14	0,04	255	255	255		14	0,06	255	255	255		14	0,165	255	255	255
18	15	0,025	255	255	255		15	0,016	255	255	255		15	0,015	255	255	255
19	16	0,029	255	255	255		16	0,043	255	255	255		16	0,033	255	255	255
20	17	0,026	255	255	255		17	0,016	255	255	255		17	0,026	255	255	255
21	18	0,026	255	255	255		18	0,038	255	255	255		18	0,025	255	255	255
22	19	0,023	255	255	255		19	0,032	255	255	255		19	0,076	255	255	255
23	20	0,019	255	255	255		20	0,037	255	255	255		20	0,029	255	255	255
24	21	0,031	255	255	255		21	0,04	255	255	255		21	0,12	255	255	255
25	22	0,033	255	255	255		22	0,035	255	255	255		22	0,027	255	255	255
26	23	0,028	255	255	255		23	0,033	255	255	255		23	0,029	255	255	255
27	24	0,019	255	255	255		24	0,057	255	255	255		24	0,055	255	255	255
28	25	0,131	255	255	255		25	0,018	255	255	255		25	0,047	255	255	255
29	26	0,014	255	255	255		26	0,026	255	255	255		26	0,039	255	255	255
30	27	0,05	255	255	255		27	0,035	255	255	255		27	0,051	255	255	255
31	28	0,021	255	255	255		28	0,049	255	255	255		28	0,043	255	255	255
32	29	0,036	255	255	255		29	0,037	255	255	255		29	0,022	255	255	255
33	30	0,025	255	255	255		30	0,058	255	255	255		30	0,025	255	255	255
34	31	0,024	255	255	255		31	0,034	255	255	255		31	0,027	255	255	255
35	32	0,021	255	255	255		32	0,03	255	255	255		32	0,035	255	255	255
36	33	0,014	255	255	255		33	0,021	255	255	255		33	0,021	255	255	255
37	34	0,059	255	255	255		34	0,036	255	255	255		34	0,037	255	255	255
38	35	0,098	255	255	255		35	0,027	255	255	255		35	0,043	255	255	255
39	36	0,066	255	255	255		36	0,018	255	255	255		36	0,053	255	255	255
40	37	0,037	255	255	255		37	0,031	255	255	255		37	0,02	255	255	255
41	38	0,025	255	255	255		38	0,021	255	255	255		38	0,021	255	255	255

Figure. 18: Example of the analysis output including number and area of each individual cell in Excel software.

3.3.10. Statistical analysis

All statistical analysis was done with the Excel software. The data were expressed as mean ± standard error of measurement. Normal distribution of datasets was confirmed by Kolmogorov-Smirnof test. The *t*-tests were performed to evaluate whether two groups were significantly different from each other. For analysis of multiple datasets with differing variance, Kruskal-Wallis tests were performed. The *p* values less than .05 (two-tailed) were considered statistically significant. For post-hoc analysis with multiple sets a Bonferroni-Correction was performed. Statistical values were displayed as follows: *p<0.05, **p<0.01, ***p<0.001, n.s. not significant.

4. Results

4.1. Development of the decellularization protocol

With the goal of developing a reliable method to decellularize precision cut lung slices, several different detergents, exposure durations and agitation techniques were compared (Fig. 1). The final goal was to determine the optimal protocol that would allow for proper cell removal while maximizing ECM structural and bio-chemical retainment. To that end, several endpoints which included cell removal efficacy, matrix protein retainment and structural integrity of decellularized samples were used. The combination of detergents, duration and succession of treatments were compiled based on previously published data on whole organ decellularization.

4.1.1. Identification of optimal detergents for decellularization.

Based on literature research, four detergent based protocols incorporating SDS, Tween20 + SDC, Triton-X + SDC and CHAPS, were adjusted for the use on precision cut lung slices (see Fig. 19). In a first step, PCLS from C57B6 mice were exposed to detergent in 50ml conical vials as follows; The first protocol (P1) was based on the work of O'Neill et Al. [133] and made use of SDS (1.8mM). The second protocol (P2) used Tween 20 and SDC and was based on the same work. The third protocol (P3) used 0.1% Triton X-100 and 2% SDC and was based on the work of Wallis et Al., [190] and the fourth protocol (P4) was based on the work of Calle et Al. [20] and made use of a 8mM CHAPS solution (3.3.3.1).

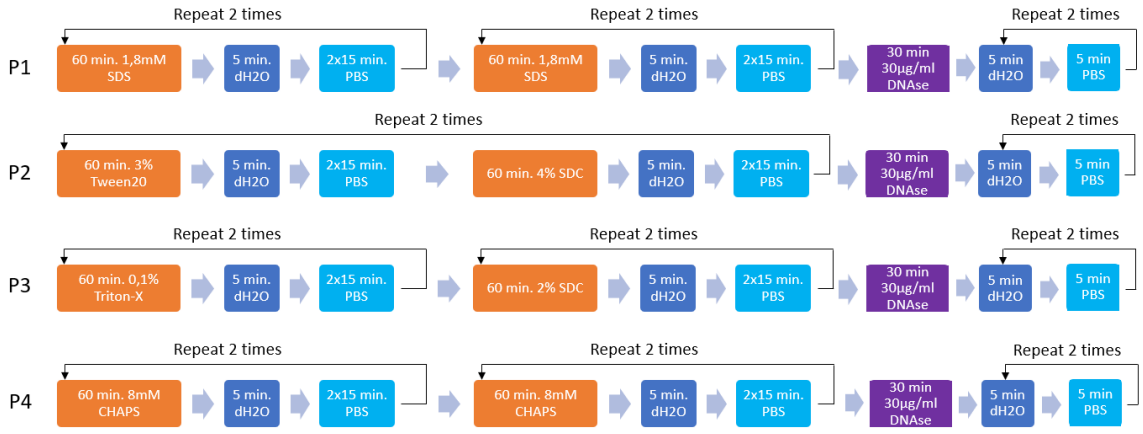

Figure 19: Initial decellularization protocols based on literature research. Protocols are labeled P1-P4 and employ four different cell removing agents: P1 – SDS, P2 – Tween/SDC, P3 – TritonX/SDC, P4 – CHAPS

4.1.1.1. Decellularization endpoint: Cell removal

To assess the efficacy of cell removal, the presence of remaining nuclei of incompletely removed cells was evaluated. To that end, the samples (n=5 PCLS) were fixed and stained with a DNA incorporating dye (propidium iodine - PI) as described in 3.3.4. While P1 and P2 achieved largely complete cell removal in the alveolar compartment, incomplete de-cellularization was noticed in the conducting airways. P3 showed incomplete cell removal in both the alveolar space and conducting airways. The highest number of cells were retained in the samples treated according to protocol P4.

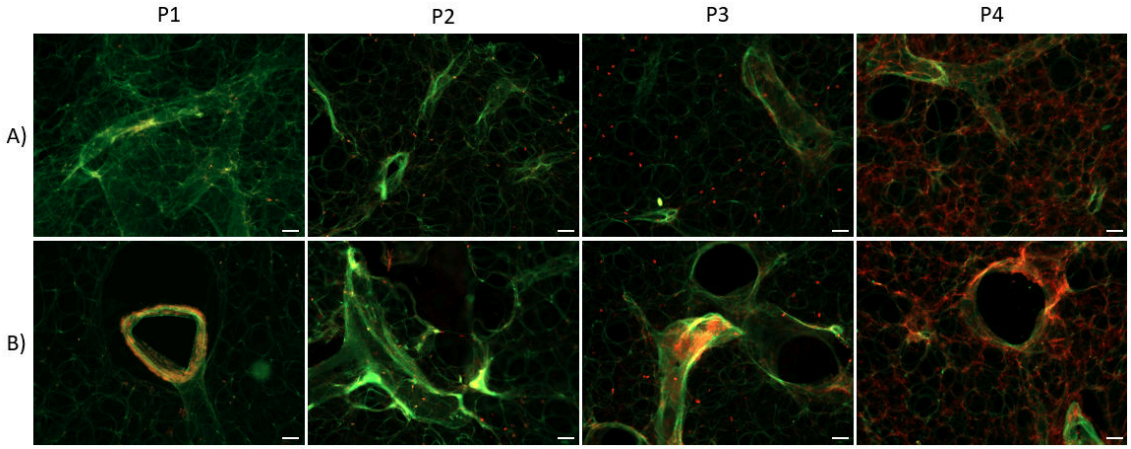

Figure 20: Cell removal achieved by the P1-P4 protocols (n=5 PCLS per condition). (A) Alveolar space, (B) conducting airways, showing remaining nuclei (PI – red signal) following each decellularization protocol (P1-P4). Green signal represents tissue autofluorescence. P1: SDS protocol, P2: SDC protocol, P3: TrX protocol P4: CHAPS protocol. Scale bars - 200µM

4.1.1.2. Decellularization endpoint: Structural integrity and protein retainment

One of the very important goals of the decellularization process is to succeed in removing cells while maintaining intact tissue morphology and biochemical composition of the extracellular matrix (ECM). In order to assess the quality of decellularized samples, whole-mount immunofluorescence analysis for core ECM proteins Collagen IV, Laminin and Fibronectin as per 3.3.8 was performed.

To more adequately evaluate the structural integrity after treatment, whole-mount PCLS were stained and imaged directly after decellularization. Compared to non-decellularized controls, the most structural disruption at the alveolar level could be observed in samples treated according to P1 (Fig. 20, 21) whereas protocols P2-P4 showed less structural disruption on the microscopic level. A uniform reduction in Laminin and Fibronectin was – in principle - observed in all samples, but appeared to be especially pronounced in

samples treated according to the P1 protocol. Additionally, protocols P1 and P2 resulted in extensive morphological changes with increased airspaces suggestive of alveolar destruction.

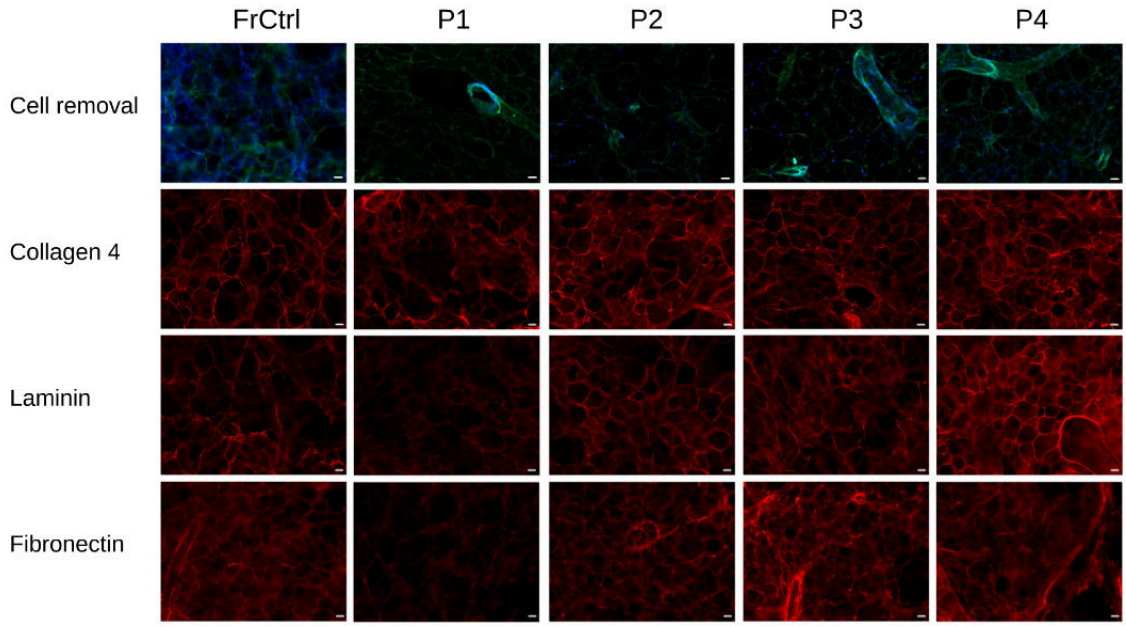

Figure 21: Extracellular matrix protein retainment achieved by protocols P1-P4 (n=5 PCLS per condition). Representative images of wholemount 200µm thick PCLS staining. Top row: Images showing cell removal efficacy in protocols P1-P4 versus non-decellularized sample (FrCtrl) by staining for remaining nuclei (DAPI - blue signal), green signal represents tissue autofluorescence. Rows 2-4 show retainment of ECM-proteins in protocols P1-P4 versus non-decellularized (FrCtrl): Collagen 4, Laminin and Fibronectin represented by red signal. Scale bars - 100µM

To confirm the representativeness of the above microscopic images, whole sample immunofluorescence imaging scans were conducted on the PCLS specimens after decellularization. On a macroscopic level, structural damage to the tissue caused by handling during the decellularization protocol became apparent in all samples. Additional analysis of whole scan images proved difficult due to tissue damage and subsequent folding, eliciting the impression of increased brightness in certain areas. (Fig. 22)

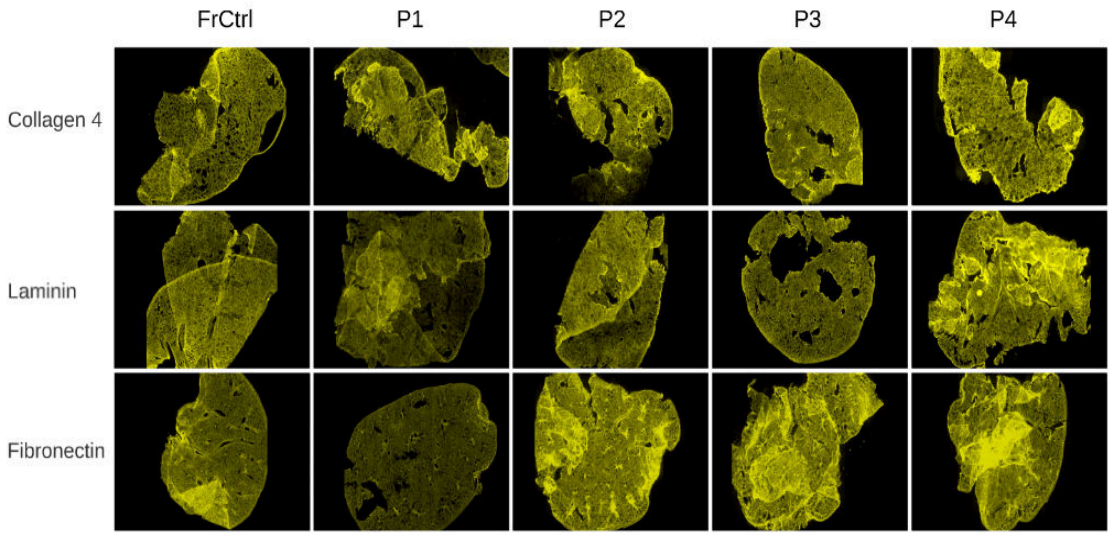

Figure 22: Full sample immunofluorescence imaging scans showing ECM protein retainment and morphology achieved by protocols P1-P4 (Fig. 1) versus untreated control (FrCtrl). Representative images of wholemount 200µm thick PCLS staining. ECM-proteins (Collagen 4, Laminin, Fibronectin) represented in yellow signal.

To further assess the level of protein retention in a quantitative manner, the fluorescence intensity for the three extracellular proteins shown above (Fig. 21) was quantified and compared. Therefore, the distribution of fluorescence intensities as a histogram was determined and mean fluorescence intensity in samples that underwent the decellularization protocols were compared to non-decellularized control samples. Protocols were compared for the three central ECM proteins Collagen 4, Laminin and Fibronectin.

For Collagen IV, there was no significant change in mean fluorescence intensity for any protocol compared to controls (Fig. 23a).

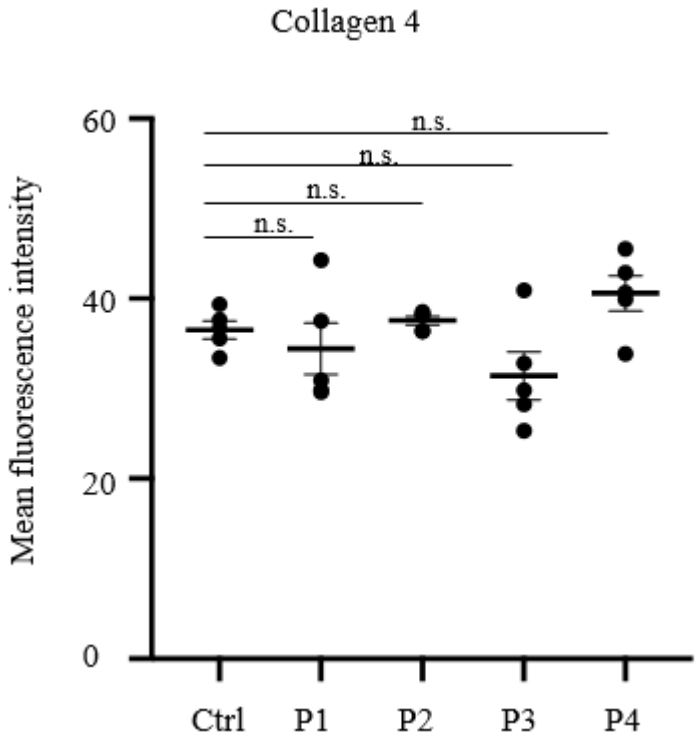

Figure 23a: Fluorescence intensity comparison between untreated samples (Ctrl) to protocols P1-P4 for the ECM-protein Collagen 4 (Col4). No significant difference in signal was observed. n=5 samples per protocol. Statistical analysis by Kruskal-Wallis Test for independent samples with differing variance and post-hoc analysis by t-test with Bonferroni correction for multiple tests.
n.s. = not significant, *p<0.05, **p<0.01, ***p<0.001

The analysis of Laminin showed a shift towards weaker signal in the mean fluorescence intensity for protocols P1-P3 compared to the control, indicating protein loss. The observed loss was most pronounced in P1, and less severe for P2 and P3. This effect was highly significant compared to controls in P1 with p<0,001. (Fig. 23b)

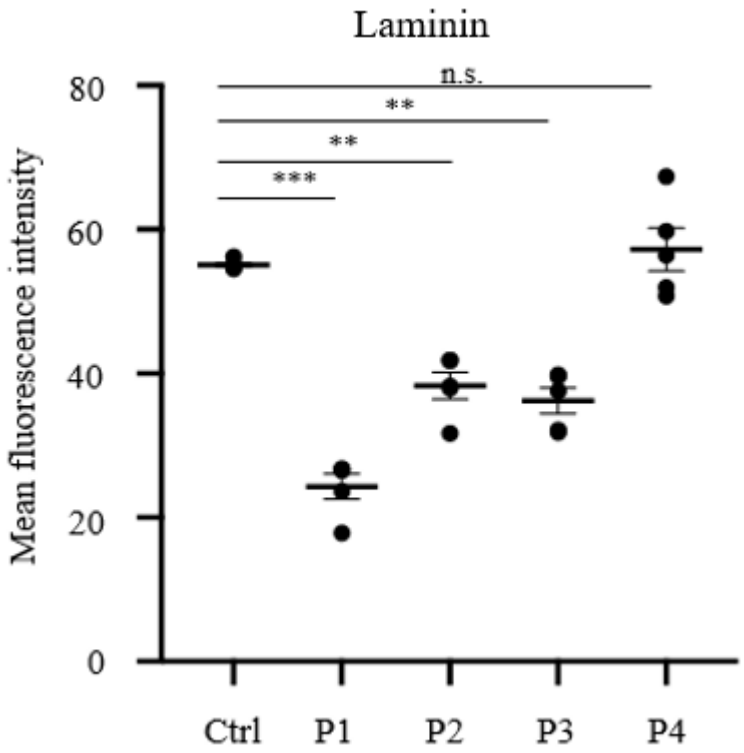

Figure 23b: Fluorescence intensity comparison between untreated samples (Ctrl) to protocols P1-P4 for the ECM-protein Laminin (Lam). Significant difference in signal was observed. n=5 samples per protocol. Statistical analysis by Kruskal-Wallis Test for independent samples with differing variance and post-hoc analysis by t-test with Bonferroni correction for multiple tests.
n.s. = not significant, *p<0.05, **p<0.01, ***p<0.001

Fibronectin analysis also revealed a shift to weaker signal in the fluorescence intensity analysis with highly significant (p<0,01) loss in P1 (Fig. 23c). A fluorescence intensity decrease could be observed in P2-P4 as well but only reached statistical significance in P2.

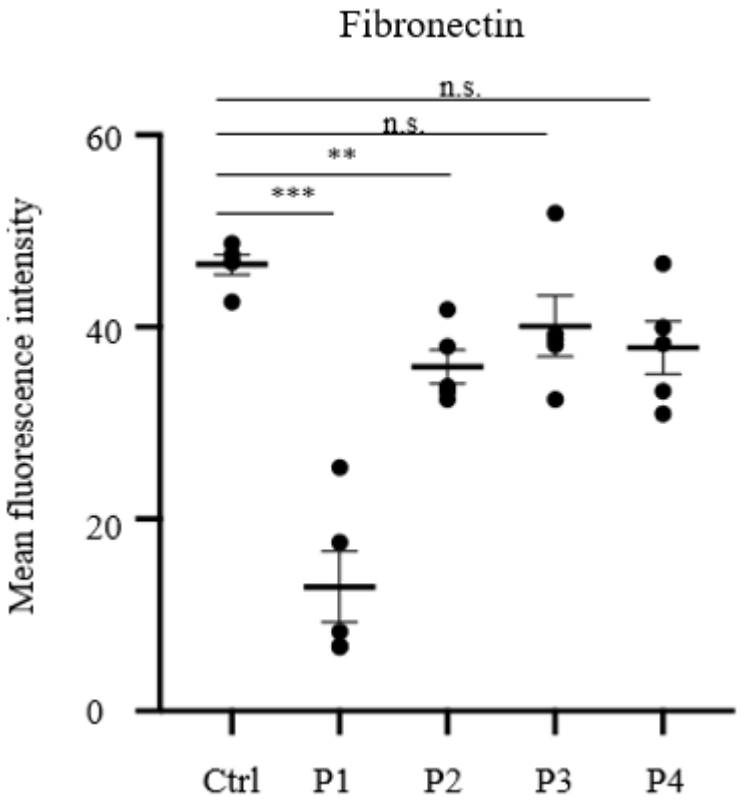

Figure 23c: Fluorescence intensity comparison between untreated samples (Ctrl) to protocols P1-P4 for the ECM-protein Fibronectin (Fbr). Significant difference in signal was observed. n=5 samples per protocol. Statistical analysis by Kruskal-Wallis Test for independent samples with differing variance and post-hoc analysis by t-test with Bonferroni correction for multiple tests.
n.s. = not significant, *p<0.05, **p<0.01, ***p<0.001

The preliminary findings indicated both increased structural damage as well as reduced protein retainment in P1 and P2 compared to P3 and P4 protocols for the three representative ECM-proteins chosen.

Based on these observations, Protocols P1 and P2 were excluded in further experiments.

Based on the apparent shortcomings in cell removal and preservation of macroscopic structure a new set of protocols based on the detergents employed in P3 and P4 were developed (P5-P6).

The agglutination of samples, possible agarose residuals and low detergent exposure times were identified as the most likely reasons for incomplete decellularization. Therefore, in the improved protocols in P5-P6, a heating step to remove the Agarose was introduced prior to the actual decellularization protocol, the exposure times were increased to 2x24 hours and the detergent exposure was conducted on well plates instead

of 50ml conical vials. A maximum of 3 samples were decellularized per inlet under constant mechanical agitation to further avoid agglutination.

4.1.2. Optimization of decellularization conditions

To remedy the shortcomings in cell removal and tissue preservation, protocols P3 and P4 were improved by introducing longer exposure times to detergents at reduced temperature, as well as gentle mechanical agitation to facilitate cell removal in conducting airways. Thus, we exposed the PCLS to detergent overnight at 4°C under constant agitation on a shaker. Additionally, to avoid the extensive manipulation necessary when working in 50ml conical tubes, further experiments were conducted in 6 well plates.

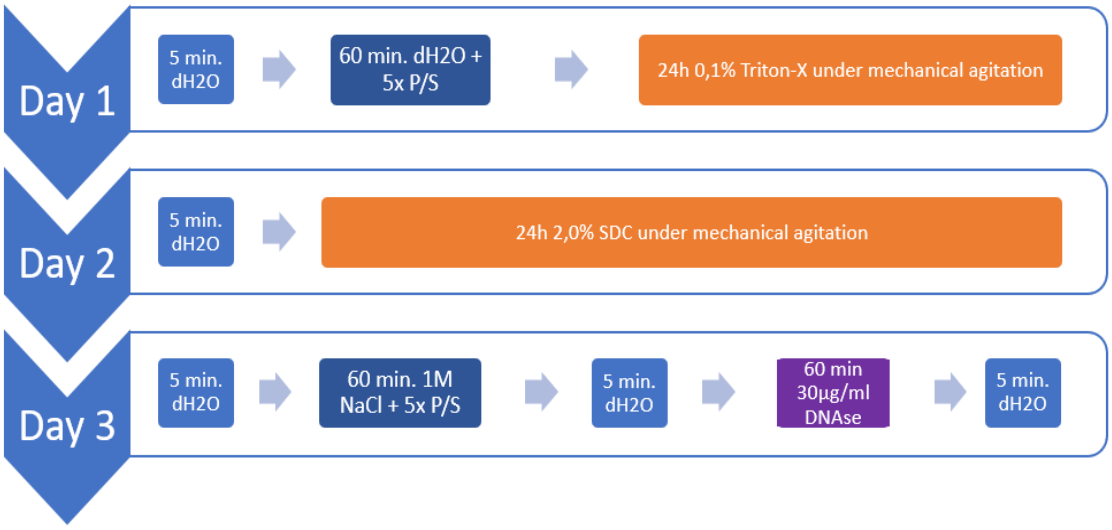

Figure 24a: Refined SDC/TrX based decellularization protocol (P5) based on P1-P4 results.

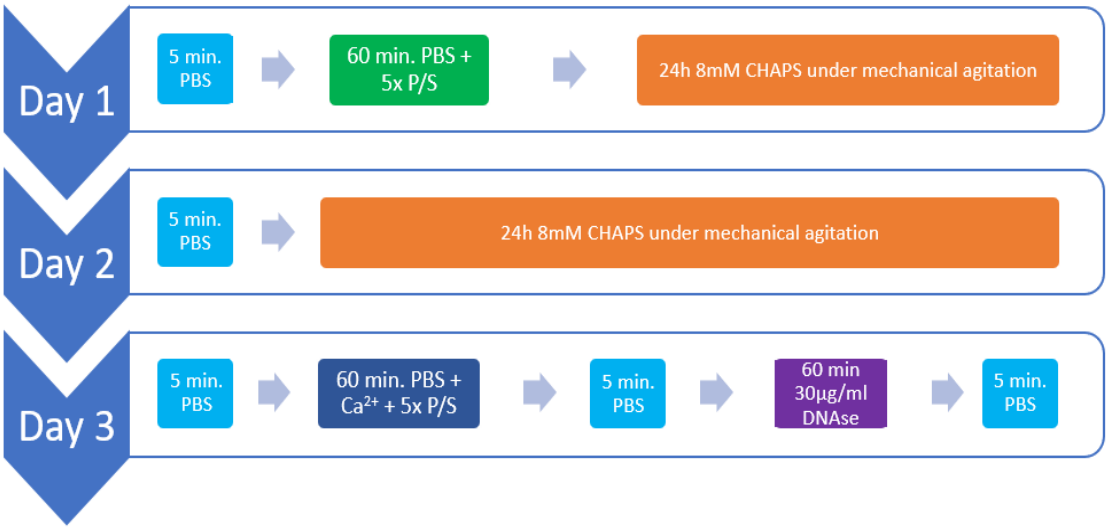

Figure 24b: Refined CHAPS decellularization protocol (P6) based on P1-P4 results.

To assess the cell removal efficacy and preservation of morphology and extracellular proteins, the same end-points as in 4.1.1.1. were used.

4.1.2.1. Decellularization end-point: Cell removal

The changes introduced in the new iteration of the decellularization protocols (P5-P6) improved the outcome towards the primary endpoint of cell removal: It became apparent that only P6 achieved comprehensive decellularization of both the alveolar space and the conducting airways, as evidenced by lack of detectable cell remnants. Contrarily, P5 showed a qualitative difference with nuclei remaining throughout the tissue, primarily in the walls of conducting airways. (Fig. 25)

4.1.2.2. Decellularization end-point: Structural integrity and protein retainment

To evaluate the changes in histological structure, the samples were immuno-stained for the same structural proteins as in previous section (Collagen 4, Fibronectin and Laminin, see 4.1.1.2). Despite the increase in detergent exposure time, the samples showed no increased morphological damage to the alveolar structure, in both P5 and P6 protocols.

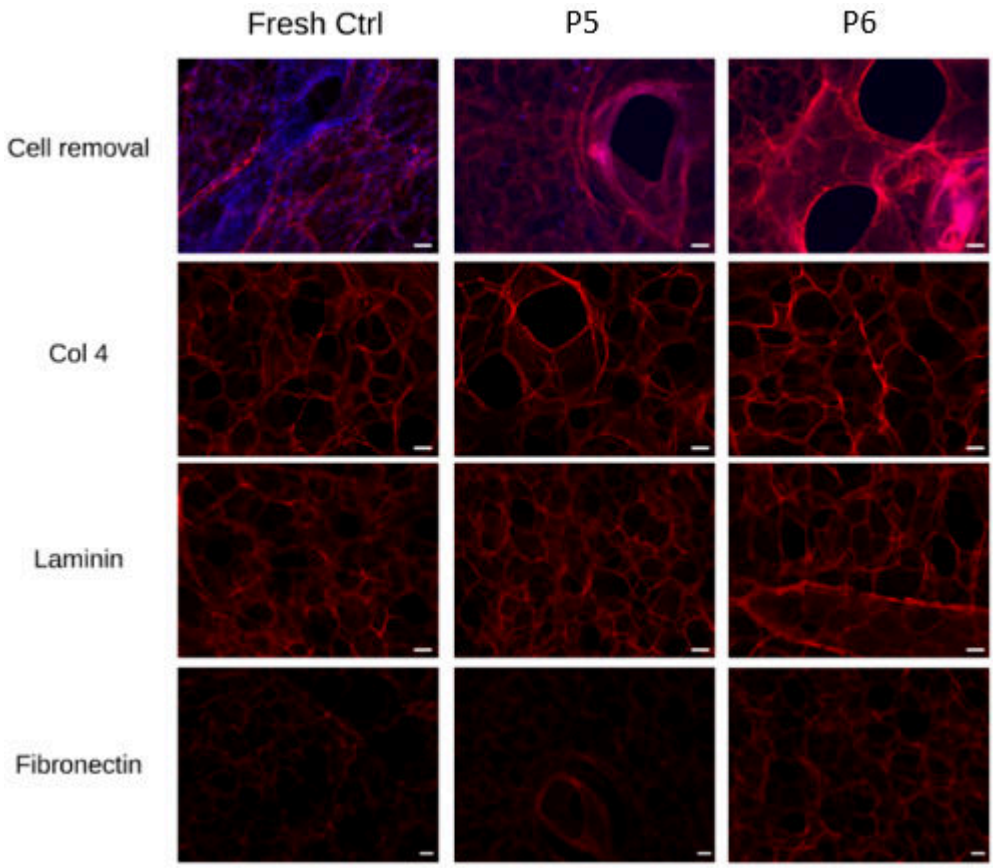

Figure 25: Extracellular matrix protein retainment achieved by P5-P6 protocols (n=5 PCLS per condition). Representative images of wholemount 200µm thick PCLS staining. Top row: Images showing cell removal efficacy in protocols P5 and P6 versus non-decellularized sample (Fresh Ctrl) by staining for remaining nuclei (DAPI - blue signal). Rows 2-4 show retainment of ECM-proteins in protocols P5 and P6 versus non-decellularized (Fresh Ctrl): Collagen 4, Laminin and Fibronectin represented by red signal. Scale bars - 100µM

To verify the representativeness of microscopic images, whole sample scans were conducted again on 200µm thick slices after decellularization according to P5-P6 protocols and immunofluorescence staining with Collagen 4, laminin and fibronectin antibodies. The optimized protocol and handling technique led to decreased structural damage on the macroscopic level compared to P1-P4 protocols. Even distribution of fluorescence signal was observed.

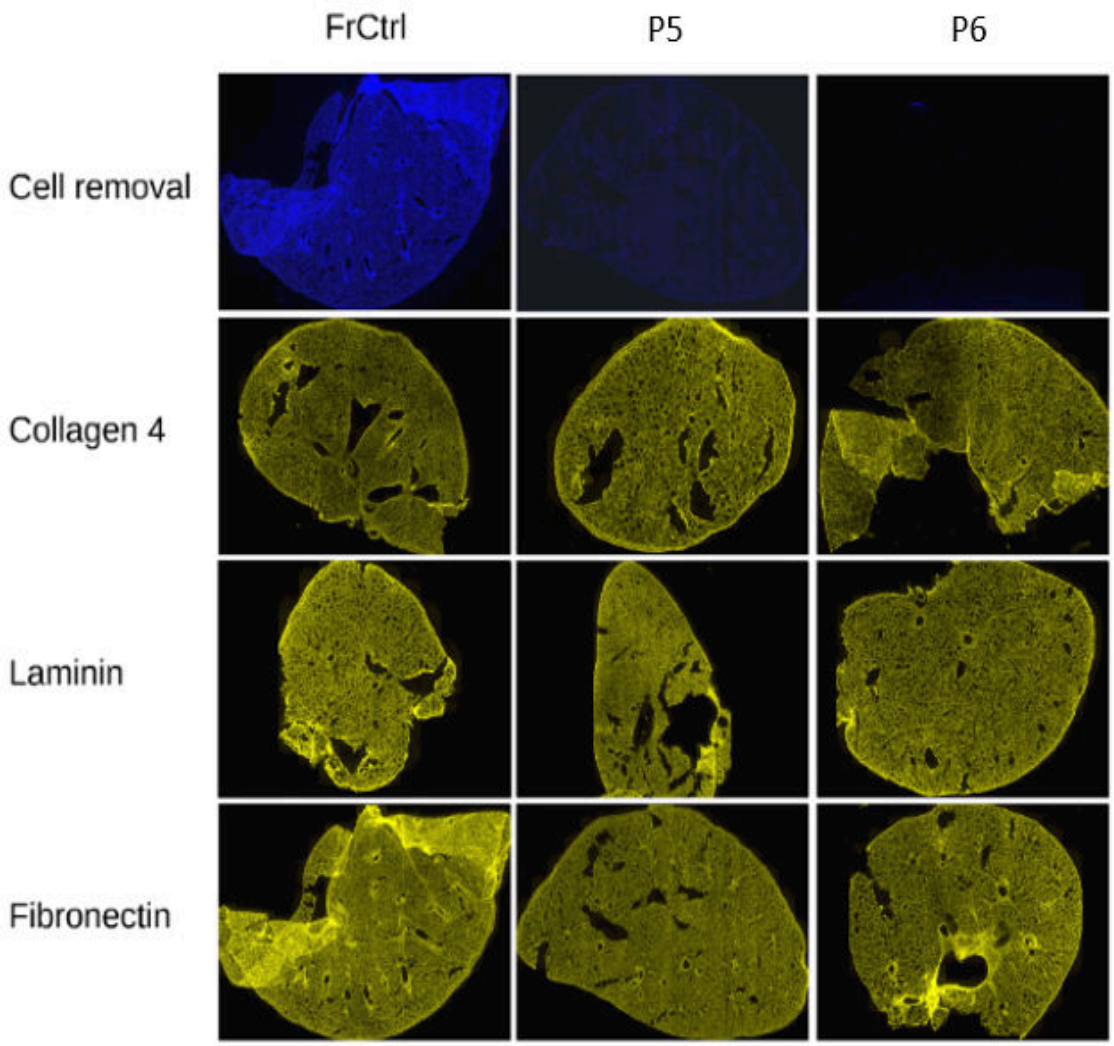

Figure 26: Full sample scans showing ECM protein retainment and morphology achieved by P5-P6 protocols (Fig. 2) versus untreated control (FrCtrl). Representative images of wholemount 200µm thick PCLS staining. ECM-proteins (Collagen 4, Laminin, Fibronectin) represented by yellow signal. Remaining nuclei in blue signal – DAPI.

Analogous to the assessment of P1-P4 protocols, a quantification and comparison similar to Fig. 7a-7c. was conducted for the three extracellular proteins Collagen 4, Fibronectin and Laminin (see 4.1.1.2). Therefore, the distribution of fluorescence intensities and mean fluorescence intensity was determined and shown as a histogram in samples that underwent the P5-P6 decellularization protocols and compared to untreated control samples and the unstained control (Fig. 27 a-c).

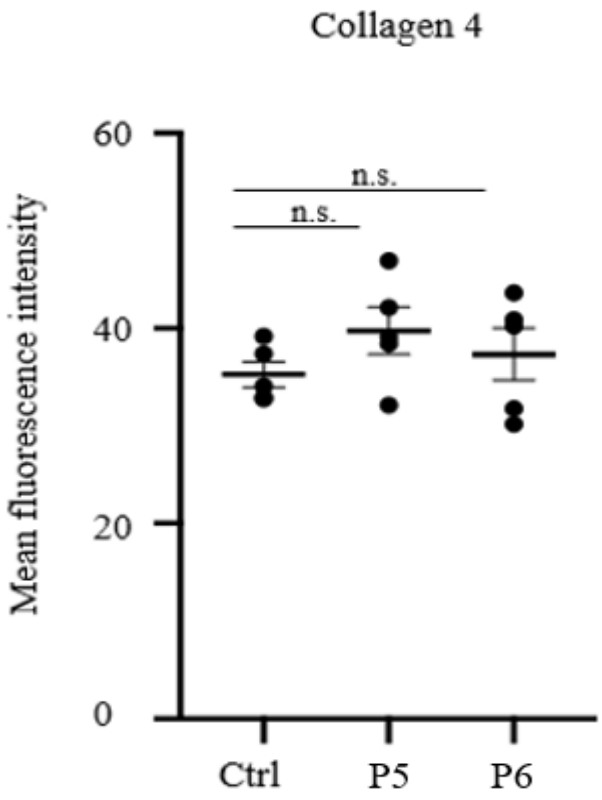

Figure 27a: Fluorescence intensity comparison between untreated samples (Ctrl) to P5-P6 protocols for the ECM-protein Collagen 4 (Col4). No significant difference in signal was observed. n=5 samples per protocol. n.s. = not significant, *p<0.05, **p<0.01, ***p<0.001

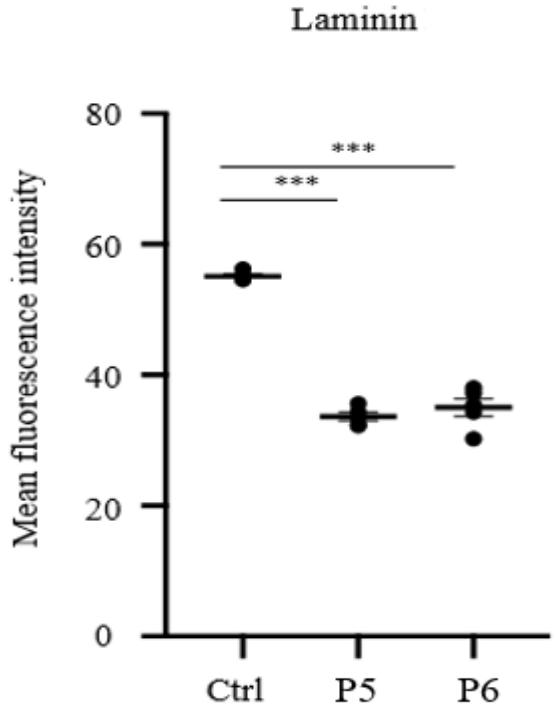

Figure 27b: Fluorescence intensity comparison between untreated samples (Ctrl) P5-P6 protocols for the ECM-protein Laminin (Lam). A significant loss of signal was observed between controls and P5 and P6 protocols both. n=5 samples per protocol. n.s. = not significant, *p<0.05, **p<0.01, ***p<0.001

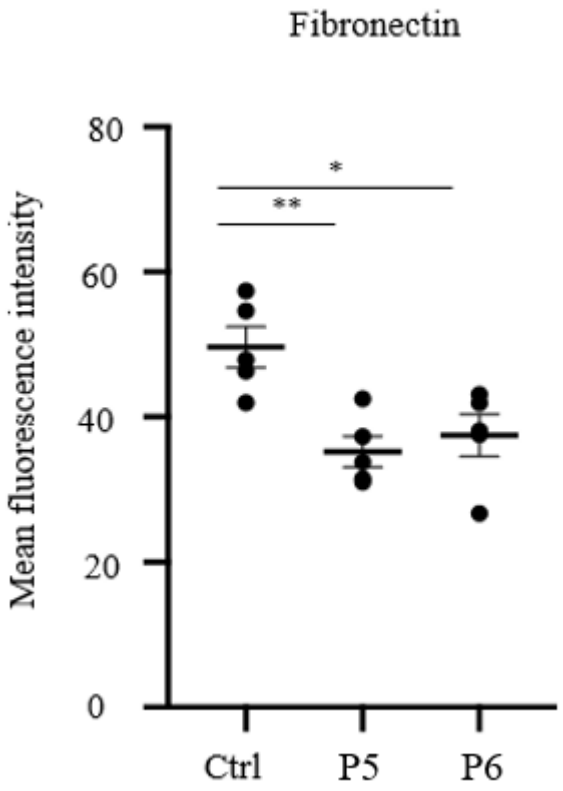

Figure 27c: Fluorescence intensity comparison between untreated samples (Ctrl) to P5-P6 protocols for the ECM-protein Fibronectin (Fbr). A significant loss of signal was observed between controls and P5 and P6 protocols both. n=5 samples per protocol. n.s. = not significant, *p<0.05, **p<0.01, ***p<0.001

The improvements introduced in the P5-P6 protocols – different handling, mechanical agitation and longer detergent exposure – led to better outcomes for all endpoints as compared to P1-P4 protocols. Cell removal was improved, structural damage was minimized and ECM protein retainment results were equally favorable. In the comparison of P5 versus P6, the improved CHAPS based protocol (P6) yielded comprehensive cell removal whilst showing similar results towards the endpoints of retaining structural integrity and ECM protein content. Thus, based on the data obtained from analysis of P1-P4 and P5-P6 treated samples, it was concluded that CHAPS-detergent based cell removal augmented with mechanical agitation is the most efficient method for cell removal in precision cut lung slices and has the least impact on matrix protein content and structural integrity.

Therefore, the P6 decellularization protocol was consistently used thereafter to generate extracellular matrix scaffolds for subsequent recellularization method development.

4.2. Development of the recellularization protocol

The final proof of quality of the decellularized matrices was to demonstrate that they support cellular growth. Therefore, repopulation of the decellularized precision cut lung slices with unfractionated lung cells was attempted first.

4.2.1. Analysis of seeded lung cells

To ensure successful cell isolation and to provide a comprehensive cell mixture for seeding, in which all cell types were represented, the cell type composition of the isolated cells, obtained according to 3.3.4, was analyzed by flow cytometry. To assess cellular viability prior to seeding, advantage was taken of the changes in cellular permeability associated with cell death, which allow DAPI, a DNA incorporating dye to penetrate the membrane of dead cells. Dead cells were consequently identified as DAPI positive. To exclude cell doublets, disproportions between signal height, width and are in forward scatter signal were used. Subsequently, cell-type composition was evaluated based on the expression of cell type specific markers. The following markers were used: CD45 for cells of hematopoietic origin, CD31 for endothelial cells, EpCAM as an epithelial marker, while mesenchymal cells were identified by exclusion of all the other cell types. According to this data, the seeded cell composition was as follows: On average, it contained 79% haematopoetic/endothelial cells, 11,2% mesenchymal cells and 4,64% epithelial cells.

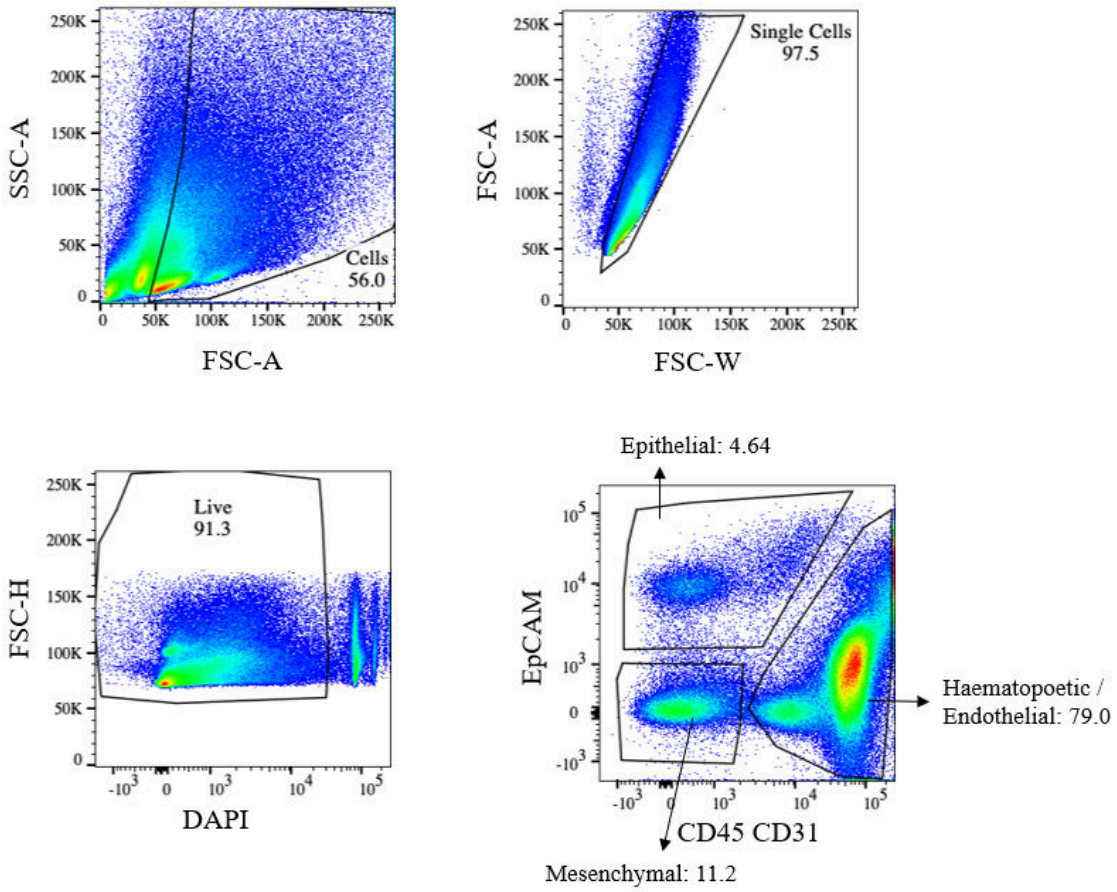

Figure 28: FACS Data of isolated lung cells used for recellularization. Gating steps from top left to bottom right: Exclusion of non-cell material, exclusion of doublets, exclusion of non-viable cells, target populations.

4.2.2. Identification of optimal seeding conditions

To facilitate the attachment and growth of cells inside the extracellular matrix scaffolds, several approaches (Fig. 14) were devised (See Materials and Methods, 3.3.6) and tested. It is well known that Matrigel, a basement matrix extract secreted by the "Engelbreth-Holm-Swarm" murine sarcoma cell line, can facilitate cell adhesion and growth. Therefore, to facilitate the growth of isolated lung cells, Matrigel coating of previously decellularized PCLS was tested. In the Pm-protocol, the decellularized PCLS was placed on top of a Matrigel coated well. For the mPm-protocol, the PCLS were coated with a layer of Matrigel before seeding in addition to being placed on top of a Matrigel layer.

In the initial experiments, well plates were prepared according to 3.3.6 and subsequently seeded with 500µl of cell suspension containing either C1=1.000.000 cells or C2=3.000.000 cells.

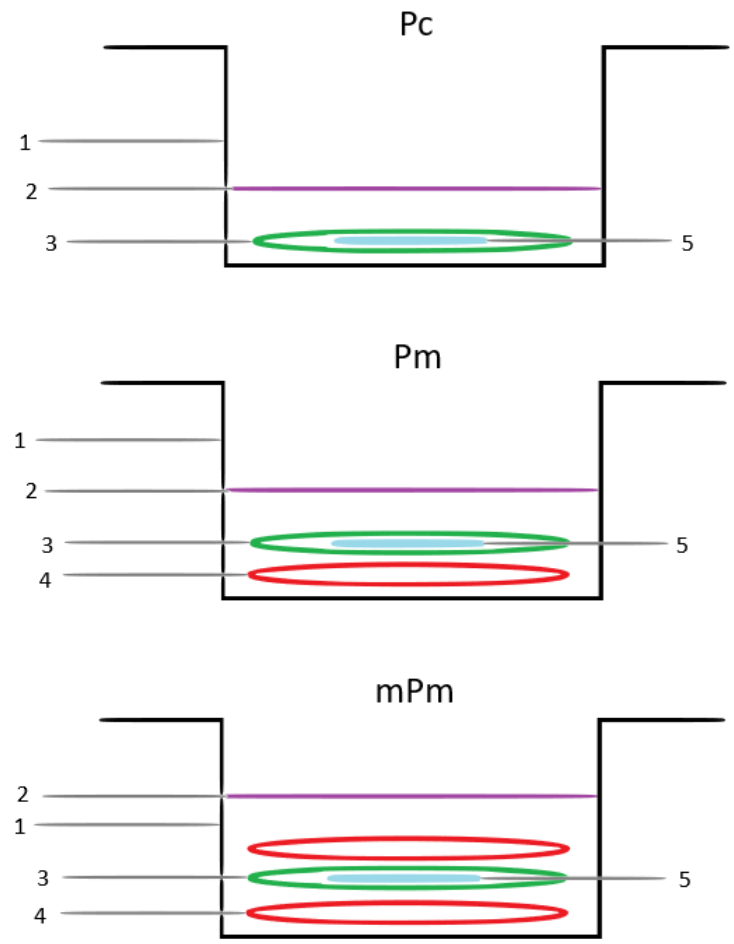

Figure 29: Visualization of completed setup of initial recellularization protocols Pc (no matrigel), Pm (Matrigel bottom) and mPm (matrigel sandwich). Detailed steps in 3.3.6 Cells were seeded together with 2ml of medium after polymerization of matrigel layers in Pm and mPm
1: 24 well plate, one sample per well 2: Cell culture medium 3: Decellularized precision cut lung slice 4: 50µl matrigel spread 5: Cell suspension: C1 = 1.000.000 cells in 500µl C2 = 3.000.000 cells in 500µl

4.2.2.1. Cell adhesion and survival

To monitor cell adhesion and initial culture progression, the ThermoFischer Live/Dead-Kit (3.2.4) was used to detect and discriminate growing and dead cells after 7 and 10 days. Here, a heterogenous distribution of cells both into the matrix scaffold as well as outside of the matrix was observed (Fig. 30). Additionally, the higher concentration (C2) during seeding led to more densely populated samples and was therefore used in subsequent experiments. The Matrigel embedding protocol, mPm, offered no apparent improvements in culture outcome whilst also impeding wholemount imaging and was therefore discontinued in further experiments.

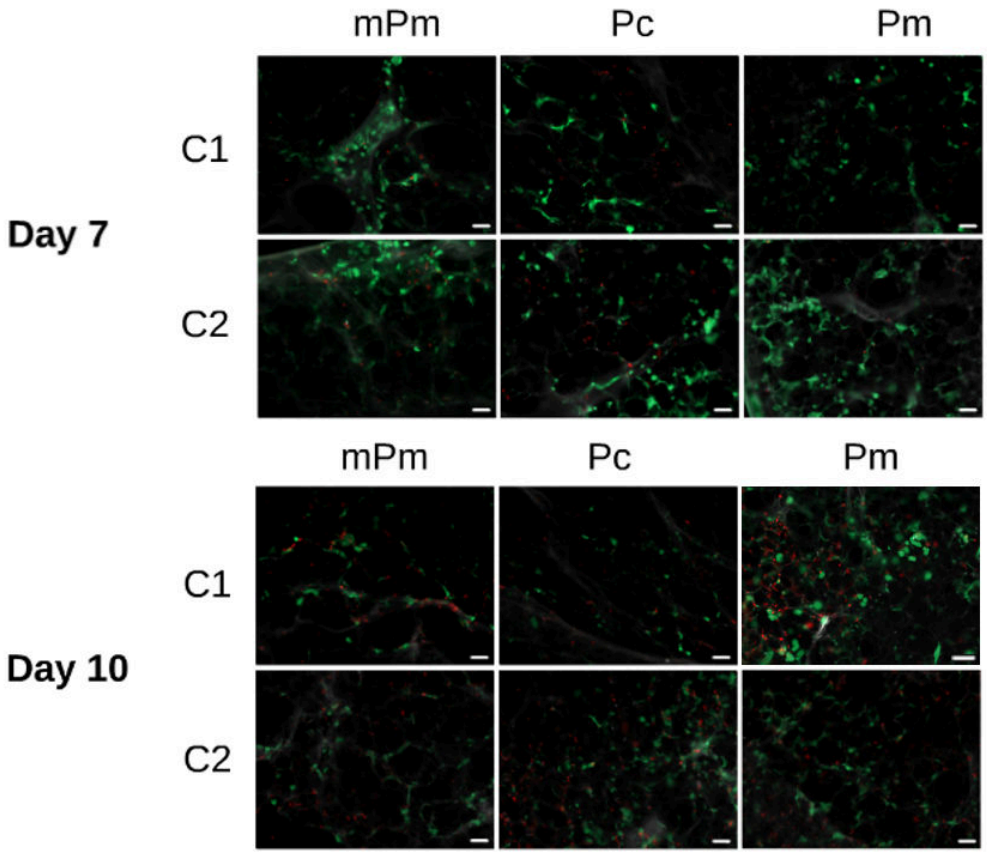

Figure 30: Live-dead staining of the recellularized PCLS in mpm, Pc, Pm protocols (Fig. 13) Live cells stained in green (Calcein AM*),* dead cell nuclei stained in red (Ethidium homodimer-1, ThermoFischer Live/Dead Kit). C1 and C2 represent the number of cells seeded: C1– 1.000.000 cells, C2 – 3.000.000 cells in different seeding conditions mPm, Pc, Pm. Scale bars 200µm

In these preliminary experiments, the majority of cells populated the bottom of the wells.

4.2.2.2. The cellular composition of recellularized matrix scaffolds

After 14 days of culture, following the exclusion of the mPm samples, recellularized PCLS were fixed with 4% paraformaldehyde and analyzed for a diverse range of biomarkers (Tab. 4, 3.2) identifying different cell types. Using these biomarkers several subpopulations including fibroblasts, macrophages, AECI and AECII could be identified.

(Myo-)Fibroblasts were identified by antibodies against alpha-smooth muscle actin (Asma), a microfilament forming protein out of the actin protein family; Vimentin, an intermediate filament protein; Collagen 4 (Col4), a structural protein of the basal lamina.

The overall epithelial cell distribution was determined based on panCadherin staining, which indiscriminately identifies all epithelial cells. AECI were identified by Podoplanin

(Pdpn), a small mucin-like transmembrane protein characteristically expressed by these cells.

To identify cells undergoing proliferation two cell cycle markers were used: Proliferating Cell Nuclear Antigen (PCNA), which is expressed in the nucleus of a cell during the phase of DNA synthesis in the cell cycle, and Antigen Ki67 (Ki67), a protein expressed on the chromosomal surface during mitosis, were used.

Pro-surfactant protein B (pSPB)and Pro-surfactant protein C (pSPC) as well as Thyroid transcription factor 1 (TTF-1), a gene transcription regulating protein, were employed to identify AEC II.

Vimentin, an intermediate filament protein, was used as a marker for macrophages.

The structure of samples was visualized using collagen 4, which is an integral part of the ECM.

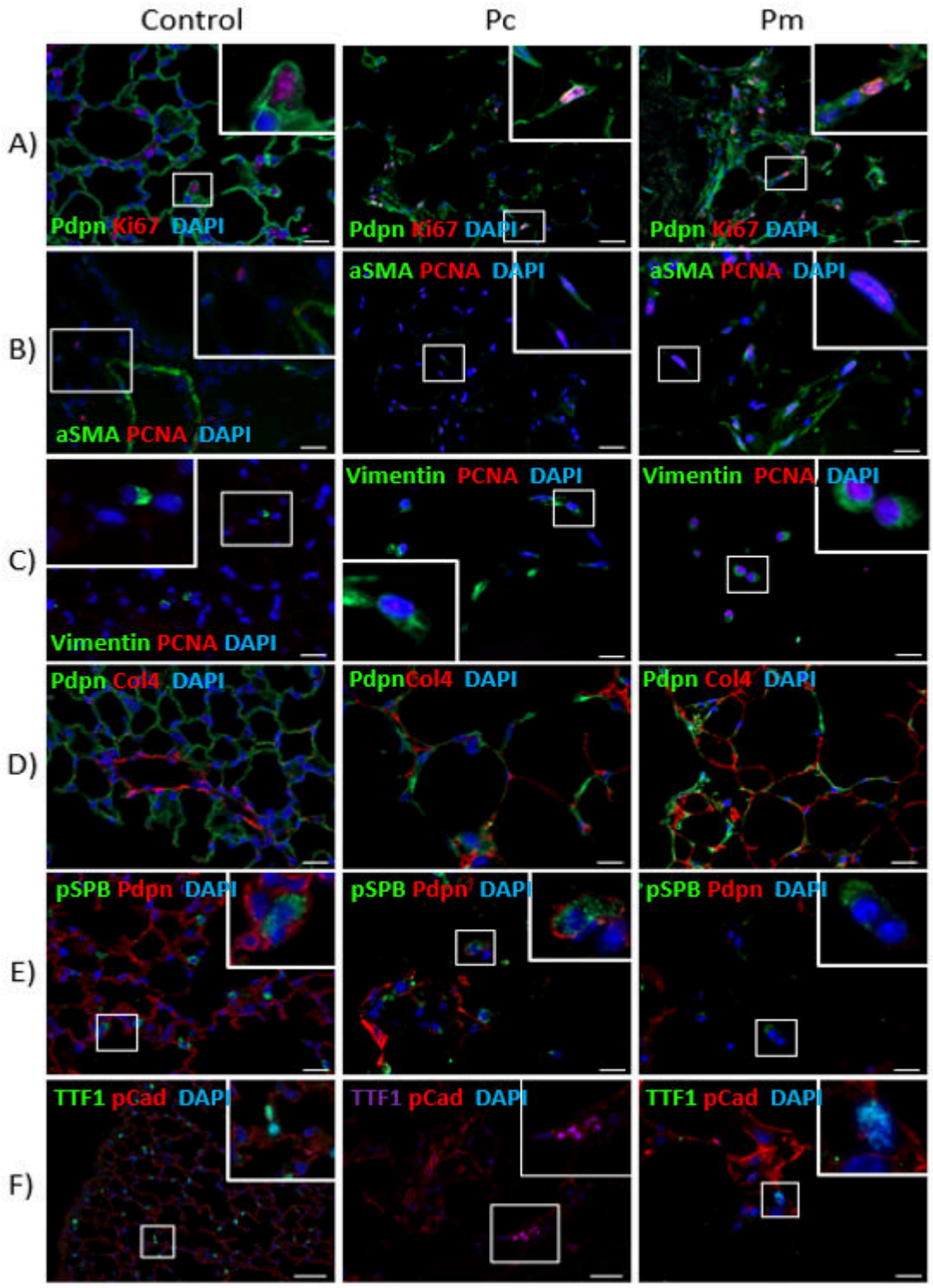

Figure 31: Cellular composition of recellularized extracellular matrix scaffolds (PCi): Columns in order from left to right: Control; no Matrigel, Matrigel. Lines from top to bottom: A) Green: Pdpn Red: Ki67 Blue: DAPI B) Green: Asma Red: PCNA Blue: DAPI C) Green: Vimentin Red: PCNA Blue: DAPI D) Green: Pdpn Red: Col4 Blue: DAPI E) Green: pSPB Red: Pdpn Blue: DAPI F) Green/Purple: TTF1 Red: pCad Blue: DAPI; Scale bars 100µm.

4.2.2.3. Cell count and proliferative activity after 14 days of culture

To identify the most efficient method between the remaining protocols (Pm and Pc) for recellularization, samples were fixed with 4% paraformaldehyde for 20 min after 14 days of culture and analyzed for both total amount of cells settled into the scaffolds and proliferative activity. Paraffin embedded tissue was sectioned, co-stained with DAPI and Ki67, to count cells and to evaluate their proliferative activity via automated counting as outlined in 3.3.9.2.

Samples seeded according to the Pc protocol (no Matrigel, C2 = 3 million cells) showed significantly ($p<0.01$) more total cells (84,67 +- 35,69 cells) compared to the Pm protocol (Matrigel below PCLS, C2 = 3 million cells) (47,83 +- 21,19 cells) inside the scaffold, demonstrating better adherence of cells to the matrix scaffold in the absence of Matrigel. At the same time, a comparable rate of proliferative cells with (30,31% +- 9,70% of cells) for the Pc protocol compared to (34,44% +- 6,95% of cells) for the Pm protocol could be observed.

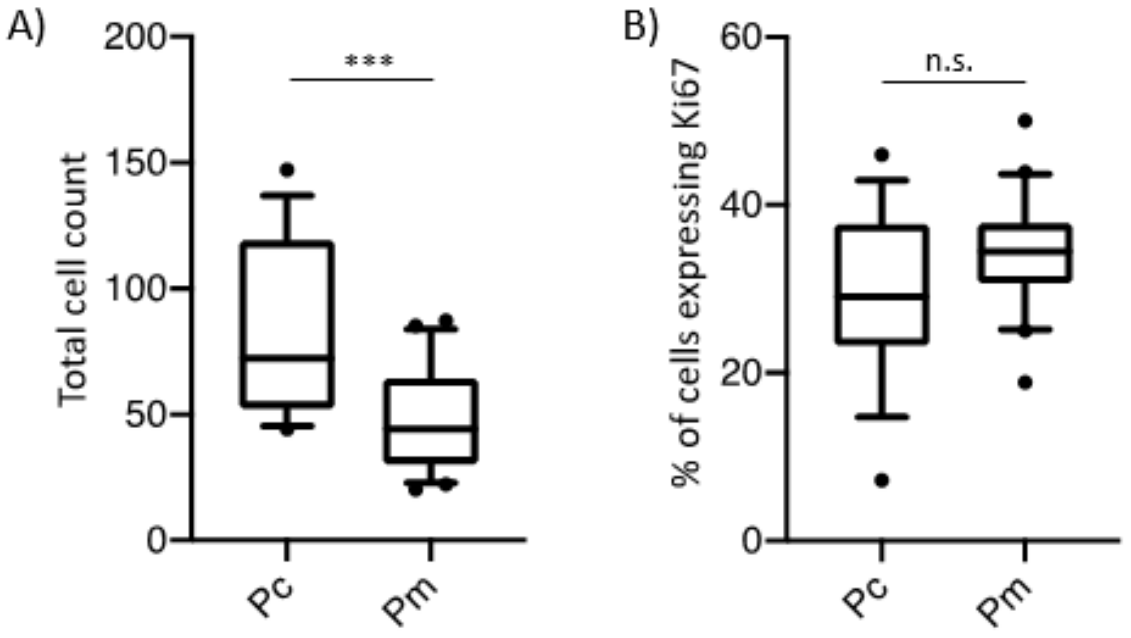

Figure 32: A) Total cell count and B) percentage of cells expressing Ki67 per 20x image from n=15 for Pc and n=23 for Pm images after 14 days of culture. Box plots with 10.-90. percentile inside of the box. Pc = Pc-protocol (cells seeded directly on decellularized PCLS); Pm = Pm-protocol (cells seeded on decellularized PCLS with Matrigel coat). n.s. = not significant, *$p<0.05$, **$p<0.01$, ***$p<0.001$

4.2.2.4. Improvements on the initial protocols

Based on the observations made in the initial experiments, an additional step to facilitate cell settlement and adhesion to the matrix was introduced in subsequent experiments. Furthermore, on the basis of the PC protocol showing superior cell adherence (Fig. 32), subsequent experiments were conducted using an improved form of the PC-protocol (PCi). In this improved PC protocol, cells were therefore incubated for 30 minutes after adding the cell suspension onto the scaffolds. To further optimize cell-PCLS-adherence, the same number of cells were seeded by increasing the cell concentration and reducing the cell suspension volume to 50 µl.

4.2.3. Final recellularization protocol (PCi)

After selecting the Pc protocol and implementing the seeding condition optimizations derived from the first recellularization experiments (PCi protocol), the final goal was to establish the feasibility of prolonged culture of recellularized PCLS, which were previously decellularized with the newly developed method.

4.2.3.1. Cell count and proliferative activity during prolonged culture

To answer the question whether prolonged culture of unfractionated lung cells on decellularized lung scaffolds is possible, samples were cultivated for 21 days after seeding according to the PCi protocol. Samples were fixed after 7, 14 and 21 days and analyzed for cell growth and proliferation by co-staining 3µm paraffin embedded sections with DAPI and Ki67 to detect cells and evaluate their proliferative activity, again by use of the automated counting method as outlined in 3.3.9.2. A steady increase in total number of cells was observed whilst the share of cells positive for Ki67 peaked 7 days after seeding and diminished at day 21, suggesting that tissue capacitance was nearly reached. Thus, the average number of cells per 20x field was 54,45 +/- 24,57 cells at day 7, 83,29 +/- 27,03 cells at day 14 and 109,21 +/- 21,96 cells at day21. The proliferation rate at each time point was as follows: 41,37% +/- 14,66% of all cells were positive for proliferation marker Ki67 at day 7, 33,25% +/- 10,76% at day 14 and 19,27% +/- 4,26% at day 21.

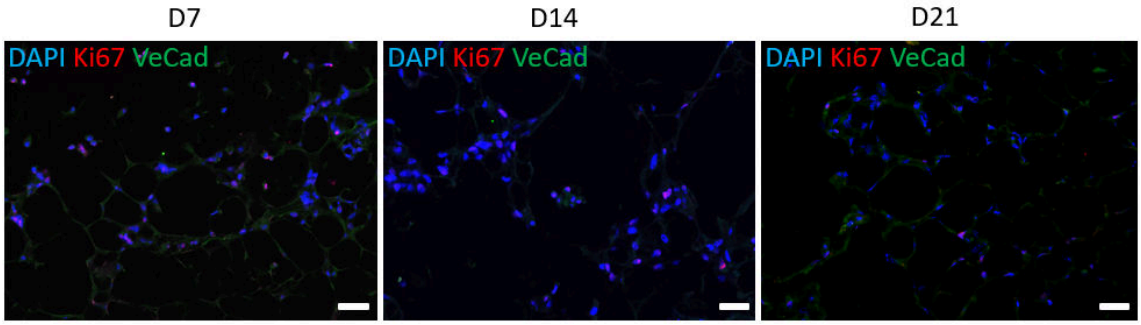

Figure 33: Example images at the 7, 14 and 21 day timepoints depicting cells and marker positivity for cellular proliferation. Green**:** VeCad Red: Ki67 Blue: DAPI. Scale bars 100µm.

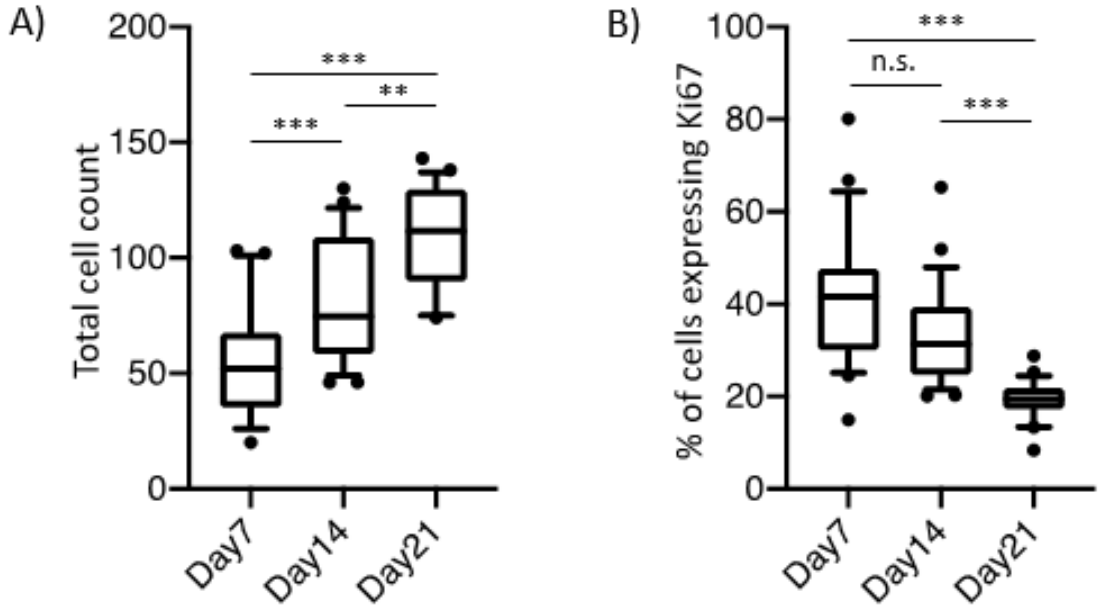

Figure 34: A) Total cell count and B) percentage of cells expressing Ki67 over three weeks of culture with optimized PC protocol (3.3.6) Samples were taken out of culture and processed after 7 (D7, n=29), 14 (D14, n=24) and 21 (D21, n=24) days of culture and analyzed with immunohistochemistry (3.3.7). Box plots with 10.-90. Percentile inside of the box. n.s. = not significant, *p<0.05, **p<0.01, ***p<0.001

4.3. Summary

In conclusion, the PCLS decellularization protocol developed in this work produced ECM scaffolds with minimal structural damage on the macroscopic and microscopic level. Matrix proteins were partially depleted to differing degrees, depending on the type of detergent used.

Moreover, the final decellularization protocol yielded matrices that were permissive of cell adhesion and growth. In addition, to successfully culture mixed lung cells on previously decellularized precision cut lung slices, a recellularization method was developed.

There was no observable benefit of the use of Matrigel during the seeding procedure. Using the final recellularization method, cells were cultivated successfully over a period of 21 days. At three different time points during culture, cell attachment, growth and proliferation could be observed.

Certain crucial cell types such as AECI, AECII, as well as fibroblasts and macrophages were readily identified in our staining, showing that the newly developed decellularization protocol generates PCLS that can be used to further study the regenerative and re-population capacity of different cell populations in the lung. Further experiments will need to establish optimal culture conditions for each cell type of interest, but so far, our data suggests that all cell types can attach and grow in the optimized model.

5. Discussion

5.1. Introduction

The heterogenous group of fibrosing lung diseases stems from a variety of underlying causes, yet they all share the common outcome of progressive fibrotic remodeling and destruction of the alveolar surface and lung parenchyma, leading to a loss of compliance and progressive gas exchange impairment [28, 100, 149, 163]. IPF represents the most prevalent and significant form of interstitial lung disease [69, 84, 96, 145]. Despite recent advances in pharmacological therapies targeting IPF, the prognosis remains dire with a median survival of 3-5 years after diagnosis [101, 123, 148, 197]. Lung transplantation is the only available curative treatment, but is only available to a minority of IPF patients due to scarcity of donor organs and is burdened with the possibility of extensive complications and graft rejection [23, 86, 94, 156]. Recent advances in the field of regenerative medicine and tissue engineering have produced promising results in animal models, yet clinical implementation and translation to humans still appear far away from clinical reality [6, 136]. Recellularization of decellularized rodent lungs has been proposed as a valid model to study lung regeneration and how this process is affected by lung fibrosis.

The aim of this study was to establish a high throughput model to examine the regenerative capacity of the lung and potentially provide a method to more efficiently use the oftentimes limited amount of human tissue [7, 40, 157].

Because of this scarce supply of human lungs, the protocol development in this work was conducted on mouse PCLS, with the hope of extrapolating it to human PCLS at a later point in time. The results of this work - in principle - show the feasibility of using decellularized PCLS as a model for studying the regenerative capacity of different cell populations in health and disease.

5.2. Decellularization of PCLS

Decellularization of tissue scaffolds has been performed using a wide variety of methods and detergents. Detergents are the most common approach of decellularizing tissues, especially in structurally delicate organs with thin tissue like the lung [26, 46]. The initial development of the PCLS decellularization protocol was based on previously published

protocols for whole organ decellularization. Finetuning of this process was made keeping in mind the fine balance between the need of cell and DNA removal, which is generally achieved by detergents, and the need to maintain matrix integrity both structurally and in terms of protein composition.

5.2.1. Development and implementation of PCLS decellularization protocols

With regard to the efficacy of different decellularization protocols to remove cells, this varies with detergents used, method of detergent application, duration of exposure and combination with supportive measures [26, 47, 82]. In the initially developed protocols (P1-P4), there were marked differences regarding the removal of cells between the different detergents. While the ionic detergent SDS achieved almost complete cell removal in the alveolar space with the exception of conducting airways, the other protocols employing the nonionic detergents SDC and Tr-X and the zwitterionic detergent CHAPS, showed varying levels of unremoved cells in both the alveolar space and conducting airways. (Fig 20, 4.1.1.1).

Remaining DNA in the tissue, both from non-removed cell bodies as well as cell-free DNA, may impede recellularization efforts by eliciting an inflammatory response in seeded cells. [81, 82]. Although staining for nuclei and DNA content with PI and DAPI are established methods [173, 194], additional semi-quantitative analysis of DNA content exist to provide further information on the effectiveness of the different detergents. However, these methods based on tissue homogenization and consecutive DNA extraction have two major disadvantages: (1) nucleic acid extraction from agarose filled tissue is notoriously difficult, most likely due to the target proteins binding the agarose during the extraction protocol and (2) tissue homogenization leads to the loss of spatial information which is crucially important in heterogenous tissues like the lung. As shown in figures 20+21, the cells lining the conducting airways are more difficult to remove than the ones from the alveolar space. Thus, a different representation of conducting airways and airway space could lead to erroneous conclusions regarding the remaining DNA in different samples.

For all four of the employed detergents, complete removal of cells in lung tissue has been previously described [26, 82, 142, 173, 190]. However, these studies featured perfusion-based models of detergent exposure in full organ decellularization setups with longer detergent exposures of up to 48 hours [26, 82, 142, 173, 190]. The initial results of the

first round of decellularization protocols indicated insufficient time of detergent exposure in the newly developed method when compared to literature [9, 153].

In summary, agglutination of samples, residual content of agarose and low exposure times were identified as the most likely reasons for the partial failure in decellularization. Therefore, in the consecutive improved protocols, a heating step to remove the low melt agarose was introduced prior to the actual decellularization protocol. The detergent exposure times were increased to 2x24 hours and the detergent exposure was conducted on well plates instead of falcon vials to avoid tissue agglutination. Taken together, these methods of decellularization used for whole organs were successfully adjusted to precision lung cut slices through step-wise changes and re-evaluation of the results.

With regard to the maintenance of ECM components, mainly structural proteins, it is clear that these provide stimuli and guidance to the cells populating the scaffold and that the ECM plays a central role in both health and disease conditions [120, 165]. Consequently, preservation of matrix structure and protein content are key metrics in lung decellularization efforts. Three representative proteins were chosen based on the previous literature. Collagen 4 is vital in the structural stability of the lung and therefore indicative of the overall structural integrity [57]. Laminins are proteins of the ECM with a high molecular weight. They are an important part of the basal lamina, due to their biological activity in influencing cell adhesion, migration and differentiation. Similar functions are attributed to fibronectin, a protein dimer, which is secreted into the extracellular matrix primarily by fibroblasts [120].

The different detergents employed in P1-P4 yielded significantly different results, both in structural preservation as well as ECM protein loss. On a structural level, both on the macroscopic and microscopic scale, changes and damage to the ECM structure varied with the employed detergent. In samples treated according to protocol P1, there was widespread disruption of alveolar structure on the microscopic level (Fig. 21, 22). Additionally, wholemount scans showed multiple tears in the tissue, most likely due to the manipulation necessary when working with conical vials and strainers during solution changes. These disruptions coincided with significantly reduced content of both fibronectin and laminin in samples treated according to P1 (Fig. 23 b, c). Protocols P3 and P4 showed the least damage to the tissue both on a microscopic and a macroscopic

level. Additionally, relative levels of protein observed were favorable towards the nonionic and zwitterionic detergents, when compared to ionic detergents.

The effects of detergents on decellularized scaffolds have been described in a variety of tissues, including skin, cartilage, bone, intestinal [22, 41, 107]and corneal grafts [22, 46, 194].

Despite heterogenous results regarding the preservation of ECM integrity and protein content, zwitterionic detergents have recently been featured in many successful models of lung decellularization [8, 47, 142].

Ideally, protein content would be evaluated based on western blotting for ECM matrix proteins. However, accurately analyzing the protein content of decellularized tissues in a comprehensive manner has proven difficult, mostly due to the sturdy, structure providing nature of the ECM proteins leading to pellet formation and inaccessibility of target proteins to standard analytic techniques such as western blotting [21, 62]. The techniques necessary to fully disintegrate and analyze ECM-scaffolds include sonication, urea treatment and cyanobromide extraction [21, 120]. Even when complete protein extraction is achieved, one is faced with the reality of an inhomogeneous tissue, making normalization of data very difficult. For example, a PCLS that is richer in airway tissue would have a different protein content than one in which mostly peripheral tissue is used. These differences would be even more obvious in human fibrotic tissue, which is notorious for the spatially heterogenous distribution of fibrotic and non-fibrotic tissue. One way around this issue is to analyze the relative protein content and distribution in decellularized ECM scaffolds by immunofluorescence staining and imaging [27, 49, 190], with the caveat of being able to provide only relative quantitative measures of protein content.

Thus, the relative quantification provided by immunofluorescence analysis was used to evaluate which detergent based decellularization protocol led to the least protein loss.

These data allowed for the conclusion that the CHAPS and SDC based protocols had the least disruptive effect on microscopic and macroscopic tissue integrity, as well as promising relative protein content compared to controls.

5.2.2. Protocol refinements derived from the initial decellularization experiments

The step-wise implementation of the aforementioned optimizations led to improvements towards the primary endpoint, which was successful cell removal while retaining macroscopic and microscopic structure. Whilst the nonionic SDC based protocol yielded structurally sound PCLS with acceptable rates of protein depletion, DNA and cell remnants could be observed in the airway compartment (Fig. 21).

In contrast, the CHAPS based decellularization protocol yielded ECM scaffolds with minimal structural impairment and acceptable protein depletion, whilst at the same time showing no residual DNA or cell remnants by DAPI and PI staining.

These findings align with those in recent literature, indicating that the generation of ECM scaffolds with low content of residual DNA is possible by detergent based protocols with additional DNAse incubation [9, 133]. Furthermore, the resistance of Collagen 4 to depletion is apparent in a wide array of detergent based decellularization methods, across different species including mice, porcine and human samples [8, 82, 190]. The depletion of fibronectin and laminin compared to controls observed in our experiments is mild when compared to recent literature [21, 37]. This might be caused by the difference in detergent application via perfusion vs submersion or it could be the result of the employed measurement methods.

A more extensive characterization of protein retention in decellularized PCLS, which was beyond the scope of this work, might provide additional insights into the strengths and weaknesses of different detergents and protocols. [21, 62].

In summary, as an answer to the scientific question posed in 2.1., the experiments conducted in this work allow for the conclusion that a detergent based protocol adapted to use in PCLS can be used to efficiently produce viable ECM scaffolds, whilst having the least severe impact on ECM protein retainment and integrity.

5.3. Recellularization of PCLS

The main goal of this work, as formulated in the scientific question under 2.2, was to demonstrate that the decellularization protocol established in the first part of the work results in PCLS that can be repopulated by various lung cells, using newly devised methods of lung cell culture on decellularized PCLS.

5.3.1. Seeding of mixed isolated lung cells on previously decellularized ECM scaffolds

The goal was to establish a culture method of total isolated lung cells on decellularized ECM scaffolds. Unfractionated lung cells were chosen in order to maximize the chances of cell attachment and growth. To that end, three different seeding conditions (Fig. 13a-c, 3.3.6) were developed and implemented and subsequently seeded with either 1 million or 3 million total lung cells.

Matrigel, a basement matrix extract secreted by the "Engelbreth-Holm-Swarm" murine sarcoma cell line, is known to facilitate cell adhesion and growth [87]. Therefore, it was tested if coating with Matrigel would improve the growth of isolated lung cells and Matrigel was included in two of the experiments (Fig. 13a, c, 3.3.6)

To monitor the cells during culture, a viability/cytotoxicity dye combination that allows for assessment of the dynamics of cell growth and death during the experiment was used.

In the samples seeded with fewer cells, there appeared to be extensive cell-free areas after 7 and 10 days of culture. Samples seeded with more cells initially showed better overall cell coverage. However, areas with little to no cell adhesion were also found.

Further experiments with quantitative evaluation of cells per area between Pc and Pm - protocols after 14 days of culture showed that there was no relevant benefit attributable to the Matrigel coating. In contrast, the total number of cells was significantly higher in samples seeded without Matrigel.

Bio-engineering of a diverse range of tissues and organs has been a topic of extensive research in recent years. The recellularization of acellular lung scaffolds of species including rat, mouse, porcine and human has been attempted in a variety of ways [6, 45, 48, 136, 189].

In contrast to the approach utilizing PCLS as shown in this work, different types of "bioreactor" setups are most commonly featured in recellularization efforts described in literature. Whilst offering the closest approximation of physiological conditions for cell growth and differentiation, they are complex to setup and operate and require full organs or lobes for operation. [33, 45] A wide range of cell lines has been employed in the repopulation of acellular lung scaffolds. These include iPSCs-derived epithelial cells,

bone marrow-derived mesenchymal stromal cells (MSCs), alveolar epithelial cells type II, endothelial cells, mouse embryonic stem cells (ES cells) as well as mixed lung cells [24][44] [60].

A commonality between different studies has been the indication that organ specific ECM provides stimuli regarding cell growth, multiplication and differentiation. Analogous to the results of this work, this has been shown to lead to regional differences in repopulated tissue scaffolds. This effect can be observed across different tissues. [33, 45, 60].

Matrigel has been used as a replacement for ECM in various studies, but not as a supplementary resource alongside decellularized ECM [67, 87]. It was also previously known that lung cells grow well on Matrigel, therefore the expectation was that various ways of coating would have two effects: preventing the cells from diffusing away from the PCLS and provide some initial growth support for the freshly isolated cells. However, the experimental approach of adding Matrigel seemed to provide no additional benefits to the recellularization process while it led to significant increase in complexity and cost.

In general, it had been shown previously that decellularized lung scaffolds can be cultured for up to 21 days [189].

While overall successful, repopulation in the initial experiments was patchy and the observed regional differences may be attributed to several influencing factors. After decellularization, there may be regional differences in protein retainment, possible damages to ECM structure or even DNA or cell remnants below the detectable threshold, yet still impeding repopulation. Additionally, seeding by pipette cannot guarantee uniform cell distribution onto the sample, which might also lead to the observed differences. Interestingly, the samples coated with Matrigel showed no improvement in adhesion behavior into the scaffold, which might indicate a preference of cells towards the inherently nutrient rich Matrigel when compared to bare ECM.

Based on the previously made observations that many cells grew on the bottom of the well itself and in the Matrigel, the seeding step was identified as crucial in ensuring cell adhesion into the actual scaffold. Therefore, the protocol where cells were sandwiched between layers of Matrigel (the mPm protocol) was excluded early on and the Pc and Pm seeding protocols were selected for comparative assessment of culture success in the subsequent experiments.

The observed differences in cell count, which showed significantly less growing cells in samples seeded according to the Pm-protocol when compared to those seeded according to the Pc-protocol after 14 days of culture may be attributable to several factors. Both a simple physical obstruction of cell adherence to the PCLS with increased runoff during the initial cell seeding, as well as preferential adhesion to the nutrient rich Matrigel are possible reasons. Based on these observations, Matrigel was excluded from the final recellularization protocol. An additional benefit of excluding Matrigel from the following experiments is the avoidance of potential interference in sample imaging. Additionally, the seeding volume restriction down to 50µl helped to ensure distribution of the lung cells into the scaffold, whilst averting excessive spread of cells in the well, and was a further step towards the final recellularization protocol.

5.3.2. Refined protocols for prolonged culture of a diverse cell population on previously decellularized ECM scaffolds

Cell growth and proliferation could be observed for up to 21 days of culture, which was the maximal experimental duration, after seeding according to our final protocol on previously decellularized PCLS (Fig 29). A significant increase in total cell number in a given area was documented from day 7 to day 21, while the amount of cells displaying proliferative activity declined. In relation to the scientific question posed under 2.2.2, a diverse range of cells could be readily identified by specific markers after 3 weeks of culture, including fibroblasts, macrophages, AECI and AECII. As expected, there was an abundance of (myo-)fibroblasts while other cell types were scarcer.

Additionally, there appeared to be a preference for cell adhesion to areas with good conservation of structure and ECM proteins (Fig. 31) This behavior was prominently displayed by AECI, identified by their shape and PDPN positivity. The covering of exposed ECM is a primary function of these epithelial cells and might indicate a reaction to that stimulus.

In the literature, the effects of different ECM composition and three-dimensional structure on cell survival and differentiation have been demonstrated to be immense, with significant differences in culture success between emphysematous and healthy lungs [168]. Similar effects have been described in models of fibrotic lung [17].

These observations are in line with the results in this study. Furthermore, experiments using mesenchymal cell lines and fibroblastic cell lines showed good adhesion of cells in decellularized grafts with preference for well-preserved areas, analogous to the heterogenous distribution and clustering of cells in this work [27, 190].

5.4. Summary

In conclusion, several crucial cell types were readily identified in the final experiments, suggesting that the final decellularization protocol generates PCLS that can be used to further study the regenerative and re-population capacity of different cell populations in the lung. Further experiments will need to establish optimal culture conditions for each cell type of interest, but so far, the collected data suggests that all cell types can attach and grow in the newly developed model.

One of the main goals of this work was to establish a decellularization protocol that would yield PCLS are suitable for recellularization, and the development of a protocol to facilitate this repopulation of the tissue. The cell composition of the samples was a secondary end point, and the results may serve as a first step into the complex world of efficient, anatomically and histologically correct recellularization. While it can be asserted with certitude that the decellularized PCLS generated with the new protocol are amenable to recellularization, quantitative conclusions related to the relative cell type distributions are beyond the scope of the current work. However, the fact that most important cell types present in the lung were successfully grown in culture, suggests that the newly developed model is a suitable stem assay to determine the regenerative capacity of various cell populations.

Quantitative analysis of marker proteins, cytokines and ECM-proteins might further illuminate the process of cell propagation and differentiation after seeding. However, the method developed in this study produces insufficient amounts of material at the small scale to be suitable for quantitative analysis. Full organ models may provide more sufficient quantities for further analysis. Therefore, this opens up a variety of possible future uses of the new model.

5.5. Future outlook

Working on PCLS provides unique opportunities due to the ease of live observation of the ongoing experiment. With the employment of lineage tracing techniques, the fate of individual cells and their descendants can be observed in the context of the three-dimensional graft. Thereby the individual behavior regarding cell propagation and differentiation may be examined and compared between differing sets of circumstances, e.g. healthy vs sick matrix. Additionally, modifications such as the introduction of pathway inhibitors, treatment agents or environmental stresses could be introduced to further illuminate the regenerative capabilities of lung cells in health and disease.

With the ulterior goal of bioengineering human organs in mind, the PCLS decellularization/recellularization model developed in this work provides the additional benefit of being able to utilize even small fragments of donor organs. Despite recent advances in biobanking and sample acquisition, human tissues remain a scarce commodity. With full organs or lung lobes being available for experiments being exceedingly rare, the proposition of using PCLS becomes even more enticing. Preliminary work not shown in detail suggests that the protocol developed on mouse PCLS successfully eliminates cells from donor and fibrotic PCLS. As per scientific question 2.2.3, this work therefore opens the door for the development of multiple other recellularization assays that would help answer important questions related to the pathophysiology of the normal and fibrotic human lung.

6. Abstract

Objective: Idiopathic lung fibrosis is a disease characterized by continuous injury and consequent repair of the distal epithelial lung compartment, which is facilitated by cells with regenerative capacity from the conducting airways and the alveolar compartment. The extent of this regenerative capacity, as well as possible stimuli inducing regeneration of tissue have yet to be extensively characterized. We therefore sought to establish a method for assessing the regenerative capability of diverse lung epithelial cell populations by using decellularized precision cut lung slices (PCLS) to offer a cell-free scaffold with similar mechanical properties, three-dimensional-structure and protein composition as the native lung.

Materials and methods: In this work we developed a method to generate extracellular lung matrix scaffolds for extended cell culture of unfractionated lung cells. To that end, we took a step-wise approach involving several detergents (SDS, TritonX, SDC and CHAPS) and decellularization regimens, to provide a reliable, optimized, and scalable method for efficiently generating high quality extracellular matrix scaffolds. Additionally, we developed a reseeding protocol to facilitate repopulation of the resultant ECM-scaffolds with unfractionated lung cells and study changes in the cellular composition as well as regenerative potential in decellularized PCLS.

Results: Detergent based protocols showed differences in both the efficacy of cell removal as well as the preservation of the histological appearance and protein composition of the scaffold. The final decellularization protocol was based on CHAPS and yielded completely decellularized extracellular matrix scaffolds with largely intact morphology and protein structure. These scaffolds were successfully used for extended culture of unfractionated lung cells for up to 3 weeks and supported the growth of different subpopulations including fibroblasts, macrophages, AEC I and AEC II. Both cell adhesion to the matrix as well as proliferative activity could be observed.

Conclusions: We conclude that our method of culture of unfractionated lung cells on decellularized extracellular matrix lung scaffolds described herein provides a feasible approach to enable and enhance translational research in regenerative medicine. The provided model is suited for extended research on the regenerative capability of various cell populations in the lung.

7. Zusammenfassung

Zielsetzung: Idiopathische pulmonale Fibrose ist ein durch kontinuierliche Verletzung und subsequente Reperatur des distalen epithelialen Lungenkompartimentes definiertes Krankheitsbild, welche durch Zellen des bronchialen und alveolären Kompartimentes geleistet wird. Das Ausmaß dieser Regenerationskapazität, sowie mögliche Stimuli, welche diese Reperaturvorgänge initiieren, sind bisher nicht vollends charakterisiert. Die Zielsetzung war daher, eine Methode zur Evaluation der regenerativen Kapazität verschiedener epithelialer Zellpopulationen auf der Basis von dezellularisierten PCLS zu entwickeln, welche eine zellfreie Matrix mit lungenähnlichen mechanischen Eigenschaften, dreidimensionaler Struktur und Proteinzusammensetzung bieten.

Material und Methoden: Im Rahmen dieser Arbeit wurde eine Methode zur Gewinnung von extrazellulären Lungenmatrix-Gerüsten (ELG) zur Kultur von unfraktionierten Lungenzellen entwickelt. Hierzu wurde ein schrittweises Herangehen mit Erprobung verschiedener Detergenzien (SDS, TritonX, SDC and CHAPS) und Dezellularisierungsregimes zur Entwicklung einer optimierten, skalierbaren Methode zur Generierung von ELG in hoher Qualität gewählt. Zusätzlich wurde ein Repopularisierungsregime der ELG mit unfraktionierten Lungenzellen entwickelt um das regenerative Potential sowie Veränderungen in der Zellkomposition zu untersuchen.

Ergebnisse: Detergenzien basierte Dezellularisierungsregimes zeigten Unterschiede hinsichtlich der Zellentfernung, sowie der Erhaltung der histologischen Struktur und Proteinerhaltung. Das finale Dezellularisierungsregime basierte auf CHAPS und liefert komplett dezellularisierte extrazelluläre Lungenmatrix-Gerüste mit weitgehend intakter Morphologie und Proteinstruktur. Diese extrazellulären Lungenmatrix-Gerüste wurden dann erfolgreich zur Kultur unfraktionierter Lungenzellen einschließlich Populationen von Fibroblasten, Makrophagen, AEC I und AEC II für bis zu 3 Wochen verwendet Sowohl Zelladhärenz zur Matrix als auch Proliferation konnten beobachtet werden.

Schlussfolgerung: Zusammenfassend ist die hier entwickelte Methode zur Kultur von unfraktionierten Lungenzellen auf extrazellulären Lungenmatrix-Gerüsten eine tragfähige Herangehensweise zur Erweiterung von translationaler Forschung im Gebiet der regenerativen Medizin. Das entwickelte Modell ist zur Untersuchung der regenerativen Kapazität verschiedener Zellpopulationen in der Lunge geeignet.

8. Abbreviations

PCLS – Precision cut lung slices

AB – Antibody

CHAPS - 3-[(3-cholamidopropyl) dimethylammonio]-1-propane sulfonate

Tr-X – Triton-X

SDS - Sodium dodecyl sulfate

SDC - sodium deoxycholate

IPF – Idiopathic pulmonary fibrosis

DPLD – Diffuse parenchymatoseous lung disease

NSIP – Non-specific interstitial pneumonia

UIP – usual interstitial pneumonia

ILD – interstitial lung disease

AEC I – Alveolar epithelial cell Type I

AEC II – Alveolar epithelial cell Type II

UK – United Kingdom

US, EU – United States (of America), European Union

MUC5B – Mucin 5B

DNA - Deoxyribonucleic acid

RNA - Ribonucleic acid

ERS – endoplasmatic reticulum stress, ER – Endoplasmatic reticulum

CHOP – C/EBP-homologous protein

EMT – Epithelial mesenchymal transition

ECM – Extracellular matrix

PI - propidium iodine

PCR – Polymerase chain reaction

ESCs - embryonic stem cells

MSCs - mesenchymal stem cells

iPSCs - induced pluripotent stem cells

PBS – Phosphate-buffered saline

DAPI - 4′,6-diamidino-2-phenylindole

EDTA - Ethylenediaminetetraacetic acid

DMEM – Dulbeccos modified Eagle's medium

FBS – Fetal bovine serum

HBSS – Hank's balanced salt solution

NDS – Normal donkey serum

SP-B/C - surfactant proteins B and C

HHV - human herpes virus family

UPR - unfolded protein response

CS - cigarette smoke

BLM – Bleomycin

AD - Amiodarone

9. Figure and Table Index

10. References

1. Akram KM, Patel N, Spiteri MA et al. (2016) Lung Regeneration: Endogenous and Exogenous Stem Cell Mediated Therapeutic Approaches. Int J Mol Sci 17. doi: 10.3390/ijms17010128

2. Arcasoy SM, Kotloff RM (1999) Lung transplantation. N Engl J Med 340:1081–1091. doi: 10.1056/NEJM199904083401406

3. Armanios M (2013) Telomeres and age-related disease: how telomere biology informs clinical paradigms. J Clin Invest 123:996–1002. doi: 10.1172/JCI66370

4. Azuma A, Nukiwa T, Tsuboi E et al. (2005) Double-blind, placebo-controlled trial of pirfenidone in patients with idiopathic pulmonary fibrosis. Am J Respir Crit Care Med 171:1040–1047. doi: 10.1164/rccm.200404-571OC

5. B Moore B, Lawson WE, Oury TD et al. (2013) Animal models of fibrotic lung disease. Am J Respir Cell Mol Biol 49:167–179. doi: 10.1165/rcmb.2013-0094TR

6. Badylak SF, Taylor D, Uygun K (2011) Whole-organ tissue engineering: decellularization and recellularization of three-dimensional matrix scaffolds. Annu Rev Biomed Eng 13:27–53. doi: 10.1146/annurev-bioeng-071910-124743

7. Bai Y, Krishnamoorthy N, Patel KR et al. (2016) Cryopreserved Human Precision-Cut Lung Slices as a Bioassay for Live Tissue Banking. A Viability Study of Bronchodilation with Bitter-Taste Receptor Agonists. Am J Respir Cell Mol Biol 54:656–663. doi: 10.1165/rcmb.2015-0290MA

8. Balestrini JL, Gard AL, Liu A et al. (2015) Production of decellularized porcine lung scaffolds for use in tissue engineering. Integr Biol (Camb) 7:1598–1610. doi: 10.1039/c5ib00063g

9. Balestrini JL, Gard AL, Gerhold KA et al. (2016) Comparative biology of decellularized lung matrix: Implications of species mismatch in regenerative medicine. Biomaterials 102:220–230. doi: 10.1016/j.biomaterials.2016.06.025

10. Banerjee A, Trivedi CM, Damera G et al. (2012) Trichostatin A abrogates airway constriction, but not inflammation, in murine and human asthma models. Am J Respir Cell Mol Biol 46:132–138. doi: 10.1165/rcmb.2010-0276OC

11. Barkauskas CE, Cronce MJ, Rackley CR et al. (2013) Type 2 alveolar cells are stem cells in adult lung. J Clin Invest 123:3025–3036. doi: 10.1172/JCI68782

12. Barratt SL, Creamer A, Hayton C et al. (2018) Idiopathic Pulmonary Fibrosis (IPF): An Overview. J Clin Med 7. doi: 10.3390/jcm7080201

13. Baumgartner KB, Samet JM, Stidley CA et al. (1997) Cigarette smoking: a risk factor for idiopathic pulmonary fibrosis. Am J Respir Crit Care Med 155:242–248. doi: 10.1164/ajrccm.155.1.9001319

14. Bernhard W (2016) Lung surfactant: Function and composition in the context of development and respiratory physiology. Ann Anat 208:146–150. doi: 10.1016/j.aanat.2016.08.003

15. Bertoncello I (2016) Properties of Adult Lung Stem and Progenitor Cells. J Cell Physiol 231:2582–2589. doi: 10.1002/jcp.25404

16. Betensley A, Sharif R, Karamichos D (2016) A Systematic Review of the Role of Dysfunctional Wound Healing in the Pathogenesis and Treatment of Idiopathic Pulmonary Fibrosis. J Clin Med 6. doi: 10.3390/jcm6010002

17. Booth AJ, Hadley R, Cornett AM et al. (2012) Acellular normal and fibrotic human lung matrices as a culture system for in vitro investigation. Am J Respir Crit Care Med 186:866–876. doi: 10.1164/rccm.201204-0754OC

18. Burri PH (1985) Morphology and respiratory function of the alveolar unit. Int Arch Allergy Appl Immunol 76 Suppl 1:2–12. doi: 10.1159/000233728

19. Burri PH (2006) Structural aspects of postnatal lung development - alveolar formation and growth. Biol Neonate 89:313–322. doi: 10.1159/000092868

20. Calle EA, Petersen TH, Niklason LE (2011) Procedure for Lung Engineering. J Vis Exp. doi: 10.3791/2651

21. Calle EA, Hill RC, Leiby KL et al. (2016) Targeted proteomics effectively quantifies differences between native lung and detergent-decellularized lung extracellular matrices. Acta Biomater 46:91–100. doi: 10.1016/j.actbio.2016.09.043

22. Cartmell JS, Dunn MG (2000) Effect of chemical treatments on tendon cellularity and mechanical properties. J Biomed Mater Res 49:134–140. doi: 10.1002/(SICI)1097-4636(200001)49:1<134:AID-JBM17>3.0.CO;2-D

23. Christie JD, Edwards LB, Kucheryavaya AY et al. (2010) The Registry of the International Society for Heart and Lung Transplantation: twenty-seventh official adult lung and heart-lung transplant report--2010. J Heart Lung Transplant 29:1104–1118. doi: 10.1016/j.healun.2010.08.004

24. Crabbé A, Liu Y, Sarker SF et al. (2015) Recellularization of decellularized lung scaffolds is enhanced by dynamic suspension culture. PLoS ONE 10:e0126846. doi: 10.1371/journal.pone.0126846

25. Crapo JD, Barry BE, Gehr P et al. (1982) Cell number and cell characteristics of the normal human lung. Am Rev Respir Dis 126:332–337. doi: 10.1164/arrd.1982.126.2.332

26. Crapo PM, Gilbert TW, Badylak SF (2011) An overview of tissue and whole organ decellularization processes. Biomaterials 32:3233–3243. doi: 10.1016/j.biomaterials.2011.01.057

27. Daly AB, Wallis JM, Borg ZD et al. (2012) Initial binding and recellularization of decellularized mouse lung scaffolds with bone marrow-derived mesenchymal stromal cells. Tissue Eng Part A 18:1–16. doi: 10.1089/ten.TEA.2011.0301

28. Dartsch RC, Fink L, Breithecker A et al. (2019) Chronisch-fibrosierende Lungenerkrankungen : Die idiopathische pulmonale Fibrose im Spiegel ihrer Differenzialdiagnosen (Chronic fibrosing lung diseases : Idiopathic pulmonary fibrosis from the perspective of its differential diagnosis). Internist (Berl) 60:345–361. doi: 10.1007/s00108-019-0571-1

29. Degryse AL, Tanjore H, Xu XC et al. (2010) Repetitive intratracheal bleomycin models several features of idiopathic pulmonary fibrosis. Am J Physiol Lung Cell Mol Physiol 299:L442-52. doi: 10.1152/ajplung.00026.2010

30. Desai TJ, Brownfield DG, Krasnow MA (2014) Alveolar progenitor and stem cells in lung development, renewal and cancer. Nature 507:190–194. doi: 10.1038/nature12930

31. Design of peripheral airways for efficient gas exchange. https://www.sciencedirect.com/science/article/pii/S1569904805000935?via%3Dihub. Accessed 17 Oct 2019

32. Dietl P, Haller T, Mair N et al. (2001) Mechanisms of surfactant exocytosis in alveolar type II cells in vitro and in vivo. News Physiol Sci 16:239–243

33. Doi R, Tsuchiya T, Mitsutake N et al. (2017) Transplantation of bioengineered rat lungs recellularized with endothelial and adipose-derived stromal cells. Sci Rep 7:8447. doi: 10.1038/s41598-017-09115-2

34. Donaldson JG (2015) Immunofluorescence Staining. Curr Protoc Cell Biol 69:4.3.1-4.3.7. doi: 10.1002/0471143030.cb0403s69

35. Evans CM, Fingerlin TE, Schwarz MI et al. (2016) Idiopathic Pulmonary Fibrosis: A Genetic Disease That Involves Mucociliary Dysfunction of the Peripheral Airways. Physiol Rev 96:1567–1591. doi: 10.1152/physrev.00004.2016

36. Fahim A, Crooks M, Hart SP (2011) Gastroesophageal reflux and idiopathic pulmonary fibrosis: a review. Pulm Med 2011:634613. doi: 10.1155/2011/634613

37. Faulk DM, Carruthers CA, Warner HJ et al. (2014) The effect of detergents on the basement membrane complex of a biologic scaffold material. Acta Biomater 10:183–193. doi: 10.1016/j.actbio.2013.09.006

38. Faverio P, Giacomi F de, Sardella L et al. (2018) Management of acute respiratory failure in interstitial lung diseases: overview and clinical insights. BMC Pulm Med 18:70. doi: 10.1186/s12890-018-0643-3

39. Fingerlin TE, Murphy E, Zhang W et al. (2013) Genome-wide association study identifies multiple susceptibility loci for pulmonary fibrosis. Nat Genet 45:613–620. doi: 10.1038/ng.2609

40. Fisher RL, Smith MS, Hasal SJ et al. (1994) The use of human lung slices in toxicology. Hum Exp Toxicol 13:466–471. doi: 10.1177/096032719401300703

41. Flaherty KR, Andrei A-C, Murray S et al. (2006) Idiopathic pulmonary fibrosis: prognostic value of changes in physiology and six-minute-walk test. Am J Respir Crit Care Med 174:803–809. doi: 10.1164/rccm.200604-488OC

42. Frank DB, Peng T, Zepp JA et al. (2016) Emergence of a Wave of Wnt Signaling that Regulates Lung Alveologenesis by Controlling Epithelial Self-Renewal and Differentiation. Cell Rep 17:2312–2325. doi: 10.1016/j.celrep.2016.11.001

43. Funamoto S, Nam K, Kimura T et al. (2010) The use of high-hydrostatic pressure treatment to decellularize blood vessels. Biomaterials 31:3590–3595. doi: 10.1016/j.biomaterials.2010.01.073

44. Gehr P, Bachofen M, Weibel ER (1978) The normal human lung: ultrastructure and morphometric estimation of diffusion capacity. Respiration Physiology 32:121–140. doi: 10.1016/0034-5687(78)90104-4

45. Ghaedi M, Le AV, Hatachi G et al. (2018) Bioengineered lungs generated from human iPSCs-derived epithelial cells on native extracellular matrix. J Tissue Eng Regen Med 12:e1623-e1635. doi: 10.1002/term.2589

46. Gilbert TW, Sellaro TL, Badylak SF (2006) Decellularization of tissues and organs. Biomaterials 27:3675–3683. doi: 10.1016/j.biomaterials.2006.02.014

47. Gilpin A, Yang Y (2017) Decellularization Strategies for Regenerative Medicine: From Processing Techniques to Applications. Biomed Res Int 2017:9831534. doi: 10.1155/2017/9831534

48. Gilpin SE, Charest JM, Ren X et al. (2016) Regenerative potential of human airway stem cells in lung epithelial engineering. Biomaterials 108:111–119. doi: 10.1016/j.biomaterials.2016.08.055

49. Gilpin SE, Guyette JP, Gonzalez G et al. (2014) Perfusion decellularization of human and porcine lungs: bringing the matrix to clinical scale. J Heart Lung Transplant 33:298–308. doi: 10.1016/j.healun.2013.10.030

50. Glanville AR, Estenne M (2003) Indications, patient selection and timing of referral for lung transplantation. Eur Respir J 22:845–852. doi: 10.1183/09031936.03.00039003

51. Goss RJ (1966) Hypertrophy versus hyperplasia. Science 153:1615–1620. doi: 10.1126/science.153.3744.1615

52. Grauss RW, Hazekamp MG, Oppenhuizen F et al. (2005) Histological evaluation of decellularised porcine aortic valves: matrix changes due to different decellularisation methods. Eur J Cardiothorac Surg 27:566–571. doi: 10.1016/j.ejcts.2004.12.052

53. Guenther A, Krauss E, Tello S et al. (2018) The European IPF registry (eurIPFreg): baseline characteristics and survival of patients with idiopathic pulmonary fibrosis. Respir Res 19:141. doi: 10.1186/s12931-018-0845-5

54. Günther A, Korfei M, Mahavadi P et al. (2012) Unravelling the progressive pathophysiology of idiopathic pulmonary fibrosis. Eur Respir Rev 21:152–160. doi: 10.1183/09059180.00001012

55. Guseh JS, Bores SA, Stanger BZ et al. (2009) Notch signaling promotes airway mucous metaplasia and inhibits alveolar development. Development 136:1751–1759. doi: 10.1242/dev.029249

56. Hansen KC, Kiemele L, Maller O et al. (2009) An in-solution ultrasonication-assisted digestion method for improved extracellular matrix proteome coverage. Mol Cell Proteomics 8:1648–1657. doi: 10.1074/mcp.M900039-MCP200

57. Hansen NUB, Karsdal MA, Brockbank S et al. (2016) Tissue turnover of collagen type I, III and elastin is elevated in the PCLS model of IPF and can be restored back to vehicle levels using a phosphodiesterase inhibitor. Respir Res 17:76. doi: 10.1186/s12931-016-0394-8

58. Hashimoto Y, Funamoto S, Sasaki S et al. (2010) Preparation and characterization of decellularized cornea using high-hydrostatic pressurization for corneal tissue engineering. Biomaterials 31:3941–3948. doi: 10.1016/j.biomaterials.2010.01.122

59. Herzog EL, Brody AR, Colby TV et al. (2008) Knowns and unknowns of the alveolus. Proc Am Thorac Soc 5:778–782. doi: 10.1513/pats.200803-028HR

60. Higuchi S, Lin Q, Wang J et al. (2013) Heart extracellular matrix supports cardiomyocyte differentiation of mouse embryonic stem cells. J Biosci Bioeng 115:320–325. doi: 10.1016/j.jbiosc.2012.10.004

61. Hilberg F, Roth GJ, Krssak M et al. (2008) BIBF 1120: triple angiokinase inhibitor with sustained receptor blockade and good antitumor efficacy. Cancer Res 68:4774–4782. doi: 10.1158/0008-5472.CAN-07-6307

62. Hill RC, Calle EA, Dzieciatkowska M et al. (2015) Quantification of extracellular matrix proteins from a rat lung scaffold to provide a molecular readout for tissue engineering. Mol Cell Proteomics 14:961–973. doi: 10.1074/mcp.M114.045260

63. Hinz B (2012) Mechanical aspects of lung fibrosis: a spotlight on the myofibroblast. Proc Am Thorac Soc 9:137–147. doi: 10.1513/pats.201202-017AW

64. Hirano A, Kanehiro A, Ono K et al. (2006) Pirfenidone modulates airway responsiveness, inflammation, and remodeling after repeated challenge. Am J Respir Cell Mol Biol 35:366–377. doi: 10.1165/rcmb.2005-0452OC

65. Hsia CCW, Hyde DM, Weibel ER (2016) Lung Structure and the Intrinsic Challenges of Gas Exchange. Compr Physiol 6:827–895. doi: 10.1002/cphy.c150028

66. Huang X, Yang N, Fiore VF et al. (2012) Matrix stiffness-induced myofibroblast differentiation is mediated by intrinsic mechanotransduction. Am J Respir Cell Mol Biol 47:340–348. doi: 10.1165/rcmb.2012-0050OC

67. Hughes CS, Postovit LM, Lajoie GA (2010) Matrigel: a complex protein mixture required for optimal growth of cell culture. Proteomics 10:1886–1890. doi: 10.1002/pmic.200900758

68. Hutchinson J, Fogarty A, Hubbard R et al. (2015) Global incidence and mortality of idiopathic pulmonary fibrosis: a systematic review. Eur Respir J 46:795–806. doi: 10.1183/09031936.00185114

69. Hutchinson JP, McKeever TM, Fogarty AW et al. (2014) Increasing global mortality from idiopathic pulmonary fibrosis in the twenty-first century. Ann Am Thorac Soc 11:1176–1185. doi: 10.1513/AnnalsATS.201404-145OC

70. Isakson BE, Lubman RL, Seedorf GJ et al. (2001) Modulation of pulmonary alveolar type II cell phenotype and communication by extracellular matrix and KGF. Am J Physiol , Cell Physiol 281:C1291-9. doi: 10.1152/ajpcell.2001.281.4.C1291

71. Iyer SN, Margolin SB, Hyde DM et al. (1998) Lung fibrosis is ameliorated by pirfenidone fed in diet after the second dose in a three-dose bleomycin-hamster model. Exp Lung Res 24:119–132. doi: 10.3109/01902149809046058

72. Izbicki G, Segel MJ, Christensen TG et al. (2002) Time course of bleomycin-induced lung fibrosis. Int J Exp Pathol 83:111–119. doi: 10.1046/j.1365-2613.2002.00220.x

73. Jackson DW, Grood ES, Arnoczky SP et al. (1987) Cruciate reconstruction using freeze dried anterior cruciate ligament allograft and a ligament augmentation device (LAD). An experimental study in a goat model. Am J Sports Med 15:528–538. doi: 10.1177/036354658701500602

74. Jain R, Barkauskas CE, Takeda N et al. (2015) Plasticity of Hopx(+) type I alveolar cells to regenerate type II cells in the lung. Nat Commun 6:6727. doi: 10.1038/ncomms7727

75. Janssens S, Pulendran B, Lambrecht BN (2014) Emerging functions of the unfolded protein response in immunity. Nat Immunol 15:910–919. doi: 10.1038/ni.2991

76. January CT, Wann LS, Alpert JS et al. (2014) 2014 AHA/ACC/HRS guideline for the management of patients with atrial fibrillation: executive summary: a report of the American College of Cardiology/American Heart Association Task Force on practice guidelines and the Heart Rhythm Society. Circulation 130:2071–2104. doi: 10.1161/CIR.0000000000000040

77. Jenkins RG, Moore BB, Chambers RC et al. (2017) An Official American Thoracic Society Workshop Report: Use of Animal Models for the Preclinical Assessment of Potential Therapies for Pulmonary Fibrosis. Am J Respir Cell Mol Biol 56:667–679. doi: 10.1165/rcmb.2017-0096ST

78. Kapanci Y, Assimacopoulos A, Irle C et al. (1974) "Contractile interstitial cells" in pulmonary alveolar septa: a possible regulator of ventilation-perfusion ratio? Ultrastructural, immunofluorescence, and in vitro studies. J Cell Biol 60:375–392. doi: 10.1083/jcb.60.2.375

79. Kapuściński J, Skoczylas B (1978) Fluorescent complexes of DNA with DAPI 4',6-diamidine-2-phenyl indole.2HCl or DCI 4',6-dicarboxyamide-2-phenyl indole. Nucleic Acids Res 5:3775–3799. doi: 10.1093/nar/5.10.3775

80. Katzen J, Wagner BD, Venosa A et al. (2019) An SFTPC BRICHOS mutant links epithelial ER stress and spontaneous lung fibrosis. JCI Insight 4. doi: 10.1172/jci.insight.126125

81. Keane TJ, Londono R, Turner NJ et al. (2012) Consequences of ineffective decellularization of biologic scaffolds on the host response. Biomaterials 33:1771–1781. doi: 10.1016/j.biomaterials.2011.10.054

82. Keane TJ, Swinehart IT, Badylak SF (2015) Methods of tissue decellularization used for preparation of biologic scaffolds and in vivo relevance. Methods 84:25–34. doi: 10.1016/j.ymeth.2015.03.005

83. Kim KK, Kugler MC, Wolters PJ et al. (2006) Alveolar epithelial cell mesenchymal transition develops in vivo during pulmonary fibrosis and is regulated by the extracellular matrix. Proc Natl Acad Sci U S A 103:13180–13185. doi: 10.1073/pnas.0605669103

84. King TE, Pardo A, Selman M (2011) Idiopathic pulmonary fibrosis. The Lancet 378:1949–1961. doi: 10.1016/S0140-6736(11)60052-4

85. King TE, Bradford WZ, Castro-Bernardini S et al. (2014) A phase 3 trial of pirfenidone in patients with idiopathic pulmonary fibrosis. N Engl J Med 370:2083–2092. doi: 10.1056/NEJMoa1402582

86. Kistler KD, Nalysnyk L, Rotella P et al. (2014) Lung transplantation in idiopathic pulmonary fibrosis: a systematic review of the literature. BMC Pulm Med 14:139. doi: 10.1186/1471-2466-14-139

87. Kleinman HK, Martin GR (2005) Matrigel: basement membrane matrix with biological activity. Seminars in cancer biology 15. doi: 10.1016/j.semcancer.2005.05.004

88. Knudsen L, Ochs M (2018) The micromechanics of lung alveoli: structure and function of surfactant and tissue components. Histochem Cell Biol 150:661–676. doi: 10.1007/s00418-018-1747-9

89. Kochanek KD, Murphy SL, Xu J et al. (2016) Deaths: Final Data for 2014. Natl Vital Stat Rep 65:1–122

90. Korfei M, Ruppert C, Mahavadi P et al. (2008) Epithelial endoplasmic reticulum stress and apoptosis in sporadic idiopathic pulmonary fibrosis. Am J Respir Crit Care Med 178:838–846. doi: 10.1164/rccm.200802-313OC

91. Korfei M, Beck D von der, Henneke I et al. (2013) Comparative proteome analysis of lung tissue from patients with idiopathic pulmonary fibrosis (IPF), non-specific interstitial pneumonia (NSIP) and organ donors. J Proteomics 85:109–128. doi: 10.1016/j.jprot.2013.04.033

92. Kotton DN, Morrisey EE (2014) Lung regeneration: mechanisms, applications and emerging stem cell populations. Nat Med 20:822–832. doi: 10.1038/nm.3642

93. Kretschmer S, Dethlefsen I, Hagner-Benes S et al. (2013) Visualization of intrapulmonary lymph vessels in healthy and inflamed murine lung using CD90/Thy-1 as a marker. PLoS ONE 8:e55201. doi: 10.1371/journal.pone.0055201

94. Laporta Hernandez R, Aguilar Perez M, Lázaro Carrasco MT et al. (2018) Lung Transplantation in Idiopathic Pulmonary Fibrosis. Med Sci (Basel) 6. doi: 10.3390/medsci6030068

95. Lauenstein L, Switalla S, Prenzler F et al. (2014) Assessment of immunotoxicity induced by chemicals in human precision-cut lung slices (PCLS). Toxicol In Vitro 28:588–599. doi: 10.1016/j.tiv.2013.12.016

96. Lederer DJ, Martinez FJ (2018) Idiopathic Pulmonary Fibrosis. N Engl J Med 378:1811–1823. doi: 10.1056/NEJMra1705751

97. Leeman KT, Fillmore CM, Kim CF (2014) Lung stem and progenitor cells in tissue homeostasis and disease. Curr Top Dev Biol 107:207–233. doi: 10.1016/B978-0-12-416022-4.00008-1

98. Ley B, Collard HR (2013) Epidemiology of idiopathic pulmonary fibrosis. Clin Epidemiol 5:483–492. doi: 10.2147/CLEP.S54815

99. Ley B, Collard HR, King TE (2011) Clinical course and prediction of survival in idiopathic pulmonary fibrosis. Am J Respir Crit Care Med 183:431–440. doi: 10.1164/rccm.201006-0894CI

100. Liu Y-M, Nepali K, Liou J-P (2017) Idiopathic Pulmonary Fibrosis: Current Status, Recent Progress, and Emerging Targets. J Med Chem 60:527–553. doi: 10.1021/acs.jmedchem.6b00935

101. Loeh B, Drakopanagiotakis F, Bandelli GP et al. (2015) Intraindividual response to treatment with pirfenidone in idiopathic pulmonary fibrosis. Am J Respir Crit Care Med 191:110–113. doi: 10.1164/rccm.201406-1106LE

102. Lohmann-Matthes ML, Steinmüller C, Franke-Ullmann G (1994) Pulmonary macrophages. Eur Respir J 7:1678–1689

103. Loveman E, Copley VR, Scott DA et al. (2015) Comparing new treatments for idiopathic pulmonary fibrosis--a network meta-analysis. BMC Pulm Med 15:37. doi: 10.1186/s12890-015-0034-y

104. Maharaj S, Shimbori C, Kolb M (2013) Fibrocytes in pulmonary fibrosis: a brief synopsis. Eur Respir Rev 22:552–557. doi: 10.1183/09059180.00007713

105. Mahavadi P, Henneke I, Ruppert C et al. (2014) Altered surfactant homeostasis and alveolar epithelial cell stress in amiodarone-induced lung fibrosis. Toxicol Sci 142:285–297. doi: 10.1093/toxsci/kfu177

106. Mahavadi P, Knudsen L, Venkatesan S et al. (2015) Regulation of macroautophagy in amiodarone-induced pulmonary fibrosis. J Pathol Clin Res 1:252–263. doi: 10.1002/cjp2.20

107. Mahida RY, Wiscombe S, Fisher AJ (2012) Current status of lung transplantation. Chron Respir Dis 9:131–145. doi: 10.1177/1479972311435909

108. Maina JN, West JB (2005) Thin and strong! The bioengineering dilemma in the structural and functional design of the blood-gas barrier. Physiol Rev 85:811–844. doi: 10.1152/physrev.00022.2004

109. Malloy JL, Veldhuizen RAW, Thibodeaux BA et al. (2005) Pseudomonas aeruginosa protease IV degrades surfactant proteins and inhibits surfactant host defense and biophysical functions. Am J Physiol Lung Cell Mol Physiol 288:L409-18. doi: 10.1152/ajplung.00322.2004

110. Marshall DC, Salciccioli JD, Shea BS et al. (2018) Trends in mortality from idiopathic pulmonary fibrosis in the European Union: an observational study of the WHO mortality database from 2001-2013. Eur Respir J 51. doi: 10.1183/13993003.01603-2017

111. Martinez FJ, Andrade JA de, Anstrom KJ et al. (2014) Randomized trial of acetylcysteine in idiopathic pulmonary fibrosis. N Engl J Med 370:2093–2101. doi: 10.1056/NEJMoa1401739

112. Mason C, Dunnill P (2008) A brief definition of regenerative medicine. Regen Med 3:1–5. doi: 10.2217/17460751.3.1.1

113. Mason RJ, Voelker DR (1998) Regulatory mechanisms of surfactant secretion. Biochimica et Biophysica Acta (BBA) - Molecular Basis of Disease 1408:226–240. doi: 10.1016/S0925-4439(98)00070-2

114. Mazza G, Rombouts K, Rennie Hall A et al. (2015) Decellularized human liver as a natural 3D-scaffold for liver bioengineering and transplantation. Sci Rep 5:13079. doi: 10.1038/srep13079

115. Moeller A, Ask K, Warburton D et al. (2008) The bleomycin animal model: a useful tool to investigate treatment options for idiopathic pulmonary fibrosis? Int J Biochem Cell Biol 40:362–382. doi: 10.1016/j.biocel.2007.08.011

116. Moore BB, Hogaboam CM (2008) Murine models of pulmonary fibrosis. Am J Physiol Lung Cell Mol Physiol 294:L152-60. doi: 10.1152/ajplung.00313.2007

117. Morimoto M, Liu Z, Cheng H-T et al. (2010) Canonical Notch signaling in the developing lung is required for determination of arterial smooth muscle cells and selection of Clara versus ciliated cell fate. J Cell Sci 123:213–224. doi: 10.1242/jcs.058669

118. Navaratnam V, Fogarty AW, Glendening R et al. (2013) The increasing secondary care burden of idiopathic pulmonary fibrosis: hospital admission trends in England from 1998 to 2010. Chest 143:1078–1084. doi: 10.1378/chest.12-0803

119. Newton CA, Batra K, Torrealba J et al. (2016) Telomere-related lung fibrosis is diagnostically heterogeneous but uniformly progressive. Eur Respir J 48:1710–1720. doi: 10.1183/13993003.00308-2016

120. Niklason LE (2018) Understanding the Extracellular Matrix to Enhance Stem Cell-Based Tissue Regeneration. Cell Stem Cell 22:302–305. doi: 10.1016/j.stem.2018.02.001

121. Nkadi PO, Merritt TA, Pillers D-AM (2009) An overview of pulmonary surfactant in the neonate: genetics, metabolism, and the role of surfactant in health and disease. Mol Genet Metab 97:95–101. doi: 10.1016/j.ymgme.2009.01.015

122. Noble PW, Albera C, Bradford WZ et al. (2011) Pirfenidone in patients with idiopathic pulmonary fibrosis (CAPACITY): two randomised trials. The Lancet 377:1760–1769. doi: 10.1016/S0140-6736(11)60405-4

123. Noble PW, Albera C, Bradford WZ et al. (2016) Pirfenidone for idiopathic pulmonary fibrosis: analysis of pooled data from three multinational phase 3 trials. Eur Respir J 47:243–253. doi: 10.1183/13993003.00026-2015

124. Nogee LM, Dunbar AE, Wert SE et al. (2001) A mutation in the surfactant protein C gene associated with familial interstitial lung disease. N Engl J Med 344:573–579. doi: 10.1056/NEJM200102223440805

125. Noth I, Zhang Y, Ma S-F et al. (2013) Genetic variants associated with idiopathic pulmonary fibrosis susceptibility and mortality: a genome-wide association study. The Lancet Respiratory Medicine 1:309–317. doi: 10.1016/S2213-2600(13)70045-6

126. Nureki S-I, Tomer Y, Venosa A et al. (2018) Expression of mutant Sftpc in murine alveolar epithelia drives spontaneous lung fibrosis. J Clin Invest 128:4008–4024. doi: 10.1172/JCI99287

127. Obata T, Tsuchiya T, Akita S et al. (2019) Utilization of Natural Detergent Potassium Laurate for Decellularization in Lung Bioengineering. Tissue Eng Part C Methods 25:459–471. doi: 10.1089/ten.TEC.2019.0016

128. Ochs M, Nyengaard JR, Jung A et al. (2004) The number of alveoli in the human lung. Am J Respir Crit Care Med 169:120–124. doi: 10.1164/rccm.200308-1107OC

129. Oku H, Nakazato H, Horikawa T et al. (2002) Pirfenidone suppresses tumor necrosis factor-α, enhances interleukin-10 and protects mice from endotoxic shock. European Journal of Pharmacology 446:167–176. doi: 10.1016/S0014-2999(02)01757-0

130. Oku H, Shimizu T, Kawabata T et al. (2008) Antifibrotic action of pirfenidone and prednisolone: different effects on pulmonary cytokines and growth factors in bleomycin-induced murine pulmonary fibrosis. European Journal of Pharmacology 590:400–408. doi: 10.1016/j.ejphar.2008.06.046

131. Okunishi K, Sisson TH, Huang SK et al. (2011) Plasmin overcomes resistance to prostaglandin E2 in fibrotic lung fibroblasts by reorganizing protein kinase A signaling. J Biol Chem 286:32231–32243. doi: 10.1074/jbc.M111.235606

132. Olmeda B, Martínez-Calle M, Pérez-Gil J (2017) Pulmonary surfactant metabolism in the alveolar airspace: Biogenesis, extracellular conversions, recycling. Ann Anat 209:78–92. doi: 10.1016/j.aanat.2016.09.008

133. O'Neill JD, Anfang R, Anandappa A et al. (2013) Decellularization of human and porcine lung tissues for pulmonary tissue engineering. Ann Thorac Surg 96:1046-55; discussion 1055-6. doi: 10.1016/j.athoracsur.2013.04.022

134. Orens JB, Garrity ER (2009) General overview of lung transplantation and review of organ allocation. Proc Am Thorac Soc 6:13–19. doi: 10.1513/pats.200807-072GO

135. Ott HC, Matthiesen TS, Goh S-K et al. (2008) Perfusion-decellularized matrix: using nature's platform to engineer a bioartificial heart. Nat Med 14:213–221. doi: 10.1038/nm1684

136. Ott HC, Clippinger B, Conrad C et al. (2010) Regeneration and orthotopic transplantation of a bioartificial lung. Nat Med 16:927–933. doi: 10.1038/nm.2193

137. Peljto AL, Zhang Y, Fingerlin TE et al. (2013) Association between the MUC5B promoter polymorphism and survival in patients with idiopathic pulmonary fibrosis. JAMA 309:2232–2239. doi: 10.1001/jama.2013.5827

138. Petersen TH, Calle EA, Zhao L et al. (2010) Tissue-engineered lungs for in vivo implantation. Science 329:538–541. doi: 10.1126/science.1189345

139. Petersen TH, Calle EA, Colehour MB et al. (2012) Matrix composition and mechanics of decellularized lung scaffolds. Cells Tissues Organs (Print) 195:222–231. doi: 10.1159/000324896

140. Phillips RJ, Burdick MD, Hong K et al. (2004) Circulating fibrocytes traffic to the lungs in response to CXCL12 and mediate fibrosis. J Clin Invest 114:438–446. doi: 10.1172/JCI20997

141. Povedano JM, Martinez P, Flores JM et al. (2015) Mice with Pulmonary Fibrosis Driven by Telomere Dysfunction. Cell Rep 12:286–299. doi: 10.1016/j.celrep.2015.06.028

142. Price AP, England KA, Matson AM et al. (2010) Development of a decellularized lung bioreactor system for bioengineering the lung: the matrix reloaded. Tissue Eng Part A 16:2581–2591. doi: 10.1089/ten.TEA.2009.0659

143. Raghu G, Richeldi L (2017) Current approaches to the management of idiopathic pulmonary fibrosis. Respir Med 129:24–30. doi: 10.1016/j.rmed.2017.05.017

144. Raghu G, Weycker D, Edelsberg J et al. (2006) Incidence and prevalence of idiopathic pulmonary fibrosis. Am J Respir Crit Care Med 174:810–816. doi: 10.1164/rccm.200602-163OC

145. Raghu G, Chen S-Y, Yeh W-S et al. (2014) Idiopathic pulmonary fibrosis in US Medicare beneficiaries aged 65 years and older: incidence, prevalence, and survival, 2001–11. The Lancet Respiratory Medicine 2:566–572. doi: 10.1016/S2213-2600(14)70101-8

146. Raghu G, Rochwerg B, Zhang Y et al. (2015) An Official ATS/ERS/JRS/ALAT Clinical Practice Guideline: Treatment of Idiopathic Pulmonary Fibrosis. An Update of the 2011 Clinical Practice Guideline. Am J Respir Crit Care Med 192:e3-19. doi: 10.1164/rccm.201506-1063ST

147. Raghu G, Remy-Jardin M, Myers JL et al. (2018) Diagnosis of Idiopathic Pulmonary Fibrosis. An Official ATS/ERS/JRS/ALAT Clinical Practice Guideline. Am J Respir Crit Care Med 198:e44-e68. doi: 10.1164/rccm.201807-1255ST

148. Richeldi L, Cottin V, Du Bois RM et al. (2016) Nintedanib in patients with idiopathic pulmonary fibrosis: Combined evidence from the TOMORROW and INPULSIS(®) trials. Respir Med 113:74–79. doi: 10.1016/j.rmed.2016.02.001

149. Richeldi L, Collard HR, Jones MG (2017) Idiopathic pulmonary fibrosis. The Lancet 389:1941–1952. doi: 10.1016/S0140-6736(17)30866-8

150. Rieg AD, Rossaint R, Uhlig S et al. (2011) Cardiovascular agents affect the tone of pulmonary arteries and veins in precision-cut lung slices. PLoS ONE 6:e29698. doi: 10.1371/journal.pone.0029698

151. Rock JR, Barkauskas CE, Cronce MJ et al. (2011) Multiple stromal populations contribute to pulmonary fibrosis without evidence for epithelial to mesenchymal transition. Proc Natl Acad Sci U S A 108:E1475-83. doi: 10.1073/pnas.1117988108

152. Rock JR, Gao X, Xue Y et al. (2011) Notch-dependent differentiation of adult airway basal stem cells. Cell Stem Cell 8:639–648. doi: 10.1016/j.stem.2011.04.003

153. Rosmark O, Åhrman E, Müller C et al. (2018) Quantifying extracellular matrix turnover in human lung scaffold cultures. Sci Rep 8:5409. doi: 10.1038/s41598-018-23702-x

154. ROUGHTON FJ, FORSTER RE (1957) Relative importance of diffusion and chemical reaction rates in determining rate of exchange of gases in the human lung, with special reference to true diffusing capacity of pulmonary membrane and volume of blood in the lung capillaries. J Appl Physiol 11:290–302. doi: 10.1152/jappl.1957.11.2.290

155. Rozycki HJ (2014) Potential contribution of type I alveolar epithelial cells to chronic neonatal lung disease. Front Pediatr 2:45. doi: 10.3389/fped.2014.00045

156. Rubin AS, Nascimento DZ, Sanchez L et al. (2015) Functional improvement in patients with idiopathic pulmonary fibrosis undergoing single lung transplantation. J Bras Pneumol 41:299–304. doi: 10.1590/S1806-37132015000000057

157. Sanderson MJ (2011) Exploring lung physiology in health and disease with lung slices. Pulm Pharmacol Ther 24:452–465. doi: 10.1016/j.pupt.2011.05.001

158. Sarma, Pei, Venkataraman (1997) Role of Oxidative Stress in Amiodarone-induced Toxicity. J Cardiovasc Pharmacol Ther 2:53–60. doi: 10.1177/107424849700200107

159. Schaefer-Prokop C (2014) HRCT-Muster der wichtigsten interstitiellen Lungenerkrankungen (HRCT patterns of the most important interstitial lung diseases). Radiologe 54:1170–1179. doi: 10.1007/s00117-014-2734-3

160. Seddon AM, Curnow P, Booth PJ (2004) Membrane proteins, lipids and detergents: not just a soap opera. Biochim Biophys Acta 1666:105–117. doi: 10.1016/j.bbamem.2004.04.011

161. Seibold MA, Wise AL, Speer MC et al. (2011) A common MUC5B promoter polymorphism and pulmonary fibrosis. N Engl J Med 364:1503–1512. doi: 10.1056/NEJMoa1013660

162. Selman M, King TE, Pardo A (2001) Idiopathic pulmonary fibrosis: prevailing and evolving hypotheses about its pathogenesis and implications for therapy. Ann Intern Med 134:136–151. doi: 10.7326/0003-4819-134-2-200101160-00015

163. Sgalla G, Iovene B, Calvello M et al. (2018) Idiopathic pulmonary fibrosis: pathogenesis and management. Respir Res 19:32. doi: 10.1186/s12931-018-0730-2

164. Shammas MA (2011) Telomeres, lifestyle, cancer, and aging. Curr Opin Clin Nutr Metab Care 14:28–34. doi: 10.1097/MCO.0b013e32834121b1

165. Shimbori C, Gauldie J, Kolb M (2013) Extracellular matrix microenvironment contributes actively to pulmonary fibrosis. Curr Opin Pulm Med 19:446–452. doi: 10.1097/MCP.0b013e328363f4de

166. Shin J-S, Hong A, Solomon MJ et al. (2006) The role of telomeres and telomerase in the pathology of human cancer and aging. Pathology 38:103–113. doi: 10.1080/00313020600580468

167. Sirianni FE, Chu FSF, Walker DC (2003) Human alveolar wall fibroblasts directly link epithelial type 2 cells to capillary endothelium. Am J Respir Crit Care Med 168:1532–1537. doi: 10.1164/rccm.200303-371OC

168. Sokocevic D, Bonenfant NR, Wagner DE et al. (2013) The effect of age and emphysematous and fibrotic injury on the re-cellularization of de-cellularized lungs. Biomaterials 34:3256–3269. doi: 10.1016/j.biomaterials.2013.01.028

169. Spira A, Beane J, Shah V et al. (2004) Effects of cigarette smoke on the human airway epithelial cell transcriptome. Proc Natl Acad Sci U S A 101:10143–10148. doi: 10.1073/pnas.0401422101

170. Strongman H, Kausar I, Maher TM (2018) Incidence, Prevalence, and Survival of Patients with Idiopathic Pulmonary Fibrosis in the UK. Adv Ther 35:724–736. doi: 10.1007/s12325-018-0693-1

171. Structure and Development of Alveolar Epithelial Cells. https://www.sciencedirect.com/science/article/pii/B9780323352147000810. Accessed 18 Oct 2019

172. Sverzellati N, Lynch DA, Hansell DM et al. (2015) American Thoracic Society-European Respiratory Society Classification of the Idiopathic Interstitial Pneumonias: Advances in Knowledge since 2002. Radiographics 35:1849–1871. doi: 10.1148/rg.2015140334

173. Syed O, Walters NJ, Day RM et al. (2014) Evaluation of decellularization protocols for production of tubular small intestine submucosa scaffolds for use in oesophageal tissue engineering. Acta Biomater 10:5043–5054. doi: 10.1016/j.actbio.2014.08.024

174. Szegezdi E, Logue SE, Gorman AM et al. (2006) Mediators of endoplasmic reticulum stress-induced apoptosis. EMBO Rep 7:880–885. doi: 10.1038/sj.embor.7400779

175. Tang Y-W, Johnson JE, Browning PJ et al. (2003) Herpesvirus DNA is consistently detected in lungs of patients with idiopathic pulmonary fibrosis. J Clin Microbiol 41:2633–2640. doi: 10.1128/jcm.41.6.2633-2640.2003

176. Tanjore H, Xu XC, Polosukhin VV et al. (2009) Contribution of epithelial-derived fibroblasts to bleomycin-induced lung fibrosis. Am J Respir Crit Care Med 180:657–665. doi: 10.1164/rccm.200903-0322OC

177. Tashiro J, Rubio GA, Limper AH et al. (2017) Exploring Animal Models That Resemble Idiopathic Pulmonary Fibrosis. Front Med (Lausanne) 4:118. doi: 10.3389/fmed.2017.00118

178. Taskar VS, Coultas DB (2006) Is idiopathic pulmonary fibrosis an environmental disease? Proc Am Thorac Soc 3:293–298. doi: 10.1513/pats.200512-131TK

179. Teisanu RM, Lagasse E, Whitesides JF et al. (2009) Prospective isolation of bronchiolar stem cells based upon immunophenotypic and autofluorescence characteristics. Stem Cells 27:612–622. doi: 10.1634/stemcells.2008-0838

180. Todd NW, Luzina IG, Atamas SP (2012) Molecular and cellular mechanisms of pulmonary fibrosis. Fibrogenesis Tissue Repair 5:11. doi: 10.1186/1755-1536-5-11

181. Travis WD, Costabel U, Hansell DM et al. (2013) An official American Thoracic Society/European Respiratory Society statement: Update of the international multidisciplinary classification of the idiopathic interstitial pneumonias. Am J Respir Crit Care Med 188:733–748. doi: 10.1164/rccm.201308-1483ST

182. Tsao P-N, Matsuoka C, Wei S-C et al. (2016) Epithelial Notch signaling regulates lung alveolar morphogenesis and airway epithelial integrity. Proc Natl Acad Sci U S A 113:8242–8247. doi: 10.1073/pnas.1511236113

183. Tsuchiya T, Sivarapatna A, Rocco K et al. (2014) Future prospects for tissue engineered lung transplantation: decellularization and recellularization-based whole lung regeneration. Organogenesis 10:196–207. doi: 10.4161/org.27846

184. Valapour M, Skeans MA, Smith JM et al. (2016) Lung. Am J Transplant 16 Suppl 2:141–168. doi: 10.1111/ajt.13671

185. van Moorsel CHM, van Oosterhout MFM, Barlo NP et al. (2010) Surfactant protein C mutations are the basis of a significant portion of adult familial pulmonary fibrosis in a dutch cohort. Am J Respir Crit Care Med 182:1419–1425. doi: 10.1164/rccm.200906-0953OC

186. Vancheri C, Kreuter M, Richeldi L et al. (2018) Nintedanib with Add-on Pirfenidone in Idiopathic Pulmonary Fibrosis. Results of the INJOURNEY Trial. Am J Respir Crit Care Med 197:356–363. doi: 10.1164/rccm.201706-1301OC

187. Veldhuizen EJA, Haagsman HP (2000) Role of pulmonary surfactant components in surface film formation and dynamics. Biochimica et Biophysica Acta (BBA) - Biomembranes 1467:255–270. doi: 10.1016/S0005-2736(00)00256-X

188. Wagner DE, Bonvillain RW, Jensen T et al. (2013) Can stem cells be used to generate new lungs? Ex vivo lung bioengineering with decellularized whole lung scaffolds. Respirology 18:895–911. doi: 10.1111/resp.12102

189. Wagner DE, Bonenfant NR, Parsons CS et al. (2014) Comparative decellularization and recellularization of normal versus emphysematous human lungs. Biomaterials 35:3281–3297. doi: 10.1016/j.biomaterials.2013.12.103

190. Wallis JM, Borg ZD, Daly AB et al. (2012) Comparative Assessment of Detergent-Based Protocols for Mouse Lung De-Cellularization and Re-Cellularization. Tissue Eng Part C Methods 18:420–432. doi: 10.1089/ten.tec.2011.0567

191. Wang Z, Li Y, Kong D et al. (2010) The Role of Notch Signaling Pathway in Epithelial-Mesenchymal Transition (EMT) During Development and Tumor Aggressiveness. Curr Drug Targets 11:745–751

192. Wells AU (2013) Managing diagnostic procedures in idiopathic pulmonary fibrosis. Eur Respir Rev 22:158–162. doi: 10.1183/09059180.00001213

193. Wells AU, Brown KK, Flaherty KR et al. (2018) What's in a name? That which we call IPF, by any other name would act the same. Eur Respir J 51. doi: 10.1183/13993003.00692-2018

194. White LJ, Taylor AJ, Faulk DM et al. (2017) The impact of detergents on the tissue decellularization process: A ToF-SIMS study. Acta Biomater 50:207–219. doi: 10.1016/j.actbio.2016.12.033

195. Williams MC (2003) Alveolar type I cells: molecular phenotype and development. Annu Rev Physiol 65:669–695. doi: 10.1146/annurev.physiol.65.092101.142446

196. Wolters PJ, Collard HR, Jones KD (2014) Pathogenesis of idiopathic pulmonary fibrosis. Annu Rev Pathol 9:157–179. doi: 10.1146/annurev-pathol-012513-104706

197. Wongkarnjana A, Yanagihara T, Kolb MR (2019) Treatment of idiopathic pulmonary fibrosis with Nintedanib: an update. Expert Rev Respir Med. doi: 10.1080/17476348.2019.1673733

198. Woods T, Gratzer PF (2005) Effectiveness of three extraction techniques in the development of a decellularized bone-anterior cruciate ligament-bone graft. Biomaterials 26:7339–7349. doi: 10.1016/j.biomaterials.2005.05.066

199. Wright JR (1997) Immunomodulatory functions of surfactant. Physiol Rev 77:931–962. doi: 10.1152/physrev.1997.77.4.931

200. Wright JR (2004) Host defense functions of pulmonary surfactant. Biol Neonate 85:326–332. doi: 10.1159/000078172

201. Wu H, Kuzmenko A, Wan S et al. (2003) Surfactant proteins A and D inhibit the growth of Gram-negative bacteria by increasing membrane permeability. J Clin Invest 111:1589–1602. doi: 10.1172/JCI16889

202. Wu W, Booth JL, Duggan ES et al. (2010) Innate immune response to H3N2 and H1N1 influenza virus infection in a human lung organ culture model. Virology 396:178–188. doi: 10.1016/j.virol.2009.10.016

203. Yang J, Hernandez BJ, Martinez Alanis D et al. (2016) The development and plasticity of alveolar type 1 cells. Development 143:54–65. doi: 10.1242/dev.130005

204. Yang IV, Fingerlin TE, Evans CM et al. (2015) MUC5B and Idiopathic Pulmonary Fibrosis. Ann Am Thorac Soc 12 Suppl 2:S193-9. doi: 10.1513/AnnalsATS.201503-110AW

205. Zacharias WJ, Frank DB, Zepp JA et al. (2018) Regeneration of the lung alveolus by an evolutionarily conserved epithelial progenitor. Nature 555:251–255. doi: 10.1038/nature25786

206. Zhang K, Kaufman RJ (2004) Signaling the unfolded protein response from the endoplasmic reticulum. J Biol Chem 279:25935–25938. doi: 10.1074/jbc.R400008200

207. Zhang Y, Noth I, Garcia JGN et al. (2011) A variant in the promoter of MUC5B and idiopathic pulmonary fibrosis. N Engl J Med 364:1576–1577. doi: 10.1056/NEJMc1013504

208. Zhu Y, Chen X, Yang X et al. (2018) Stem cells in lung repair and regeneration: Current applications and future promise. J Cell Physiol 233:6414–6424. doi: 10.1002/jcp.26414

209. Zoz DF, Lawson WE, Blackwell TS (2011) Idiopathic pulmonary fibrosis: a disorder of epithelial cell dysfunction. Am J Med Sci 341:435–438. doi: 10.1097/MAJ.0b013e31821a9d8e

A. Honorary Declaration

Erklärung zur Dissertation

„Hiermit erkläre ich, dass ich die vorliegende Arbeit selbständig und ohne unzulässige Hilfe oder Benutzung anderer als der angegebenen Hilfsmittel angefertigt habe. Alle Textstellen, die wörtlich oder sinngemäß aus veröffentlichten oder nichtveröffentlichten Schriften entnommen sind, und alle Angaben, die auf mündlichen Auskünften beruhen, sind als solche kenntlich gemacht. Bei den von mir durchgeführten und in der Dissertation erwähnten Untersuchungen habe ich die Grundsätze guter wissenschaftlicher Praxis, wie sie in der „Satzung der Justus-Liebig-Universität Gießen zur Sicherung guter wissenschaftlicher Praxis“ niedergelegt sind, eingehalten sowie ethische, datenschutzrechtliche und tierschutzrechtliche Grundsätze befolgt. Ich versichere, dass Dritte von mir weder unmittelbar noch mittelbar geldwerte Leistungen für Arbeiten erhalten haben, die im Zusammenhang mit dem Inhalt der vorgelegten Dissertation stehen, oder habe diese nachstehend spezifiziert. Die vorgelegte Arbeit wurde weder im Inland noch im Ausland in gleicher oder ähnlicher Form einer anderen Prüfungsbehörde zum Zweck einer Promotion oder eines anderen Prüfungsverfahrens vorgelegt. Alles aus anderen Quellen und von anderen Personen übernommene Material, das in der Arbeit verwendet wurde oder auf das direkt Bezug genommen wird, wurde als solches kenntlich gemacht. Insbesondere wurden alle Personen genannt, die direkt und indirekt an der Entstehung der vorliegenden Arbeit beteiligt waren. Mit der Überprüfung meiner Arbeit durch eine Plagiatserkennungssoftware bzw. ein internetbasiertes Softwareprogramm erkläre ich mich einverstanden.“

_____ _____

Ort, Datum Unterschrift

B. Acknowledgements

Firstly, I want to express my deep gratitude towards my supervising professor, Prof. Dr. med Andreas Günther, for the opportunity to conduct this work and his constant support and critical insight towards my scientific endeavors.

A heartfelt thank you goes out to my direct supervisor Mrs. MD PhD Roxana Wasnick, who inspired me with her tremendous passion for science and who provided extensive support for which I cannot thank her enough.

I also want to thank every single person in the AG-Lungenfibrose team for their kindness, their patience and their support in all my time in the laboratory.

These persons include but are not limited to Ms. Dr. rer. nat. Martina Korfei, Mr. Dr. Clemens Ruppert, Mrs. Dr. rer. nat. Poornima Mahavadi, Ms. Cand. PhD Irina Shalashova, Simone Becker, Silke Händel and many others.

I want to thank my wife for her unrelenting support, her endless capability to cheer me up in countless ingenious ways and most importantly for her tremendous kindness and extraordinary strength and grace with which she handles the recent start of our little family.

Finally, I want to thank my parents for their enduring support and constant belief in me. Without them none of this would have been possible.